MANUFACTURING OF MgB_2 POWDER USING MECHANICAL ALLOYING AND CHARACTERIZATION OF SUPERCONDUCTING WIRE DRAWN BY POWDER-IN-TUBE AND POWDER-IN-POWDER METHODS

by

Engin YAZICI

A dissertation submitted to

the Graduate Institute of Science

of

Melikşah University

in partial fulfillment of the requirements for the degree of

Doctor of Philosophy

in

Material Science and Mechanical Engineering

June 2015
Kayseri, Turkey

APPROVAL PAGE

I certify that this dissertation satisfies all the requirements as a dissertation for the degree of Doctor of Philosophy.

_____(Signature)_____
(Title and Name)
Head of Department

This is to certify that I have read this dissertation and that in my opinion it is fully adequate, in scope and quality, as a dissertation for the degree of Doctor of Philosophy.

Asst. Prof. Dr. A. Esad OZMETIN
Supervisor

Examining Committee Members

Asst. Prof. Dr. A. Esad OZMETIN (Signature)_____

Assoc. Prof. Dr. Fehmi NAIR (Signature)_____

Asst. Prof. Dr. Ercan SEVKAT (Signature)_____

Assoc. Prof. Dr. Murat CITIR (Signature)_____

Asst. Prof. Dr. Fatih AY (Signature)_____

It is approved that this thesis/dissertation has been written in compliance with the formatting rules laid down by the Graduate Institute of Sciences and Engineering.

_____(Signature)_____
(Title and Name)
Director

June 2015

MANUFACTURING OF MgB_2 POWDER USING MECHANICAL ALLOYING AND CHARACTERIZATION OF SUPERCONDUCTING WIRE DRAWN BY POWDER-IN-TUBE AND POWDER-IN-POWDER METHODS

Engin YAZICI

PhD Dissertation – Material Science and Mechanical Engineering
June 2015

Supervisor: Asst. Prof. Dr. A. Esad ÖZMETIN

ABSTRACT

MgB_2 powder produced by mechanical alloying was manufactured using the superconducting cable. Firstly, MgB_2 powders filled in copper rods with using Powder-in-Tube method and then Powder-in-Powder method. Later on copper billets were pressed by hot extrusion technique. Extended copper rods at approximately 20 times to obtain a very thin superconductor cables by a wire drawing machine. Electrical and magnetic characterization was performed in a cryogenic environment. T_c, I_c and H_{c2} measurements of MgB_2 wires were obtained. Then some mechanical tests for mechanical characterization were performed.

Keywords: Superconductor Wires, MgB_2, Mechanical Alloying, Extrusion, Powder-in-Powder Method.

MEKANİK ALAŞIMLAMA İLE MgB_2 TOZ ÜRETİMİ VE POWDER-IN-TUBE VE POWDER-IN-POWDER METODLARI KULLANILARAK YAPILAN SÜPERİLETKEN KABLONUN KARAKTERİZASYONU.

Engin YAZICI

Doktora Tezi – Malzeme Bilimi ve Makine Mühendisliği
Haziran 2015

Tez Yöneticisi: Yrd. Doç. Dr. A. Esad ÖZMETİN

ÖZ

Mekanik alaşımlama ile üretilen MgB_2 tozu kullanılarak süperiletken kablo imal edildi. MgB_2 tozu önce Powder-in-Tube metodu ile daha sonra da Powder-in-Powder metodu kullanılarak bakır çubuklara doldurduldu. Daha sonra bakır kovanlar sıcak ekstrüzyon tekniği ile preslendi. Uzatılmış bakır çubuklar, kablo çekme makinesi ile yaklaşık olarak 20 kat uzatılarak çok ince süperiletken kablolar elde edildi. Elektriksel ve manyetik ölçümler krayojenik ortamda yapıldı. Üretilen MgB_2 kabloların I_c T_c ve H_{c2} ölçümleri elde edildi. Daha sonra kabloların bazı mekanik testleri yapıldı.

Anahtar Kelimeler: Süperiletken kablolar, MgB_2, Mekanik Alaşımlama, Ekstrüzyon, Toz içinde Toz Metodu.

To my wonderful parents

ACKNOWLEDGEMENT

I would like to thank to Ministry of Science, Industry and Technology that supported this dissertation under the SANTEZ project number STZ.1138-2011.2.

I would like to express sincere appreciation to my supervisor Dr. A. Esad Ozmetin for his guidance, stimulating suggestions, encouragement helped me during the research period and his tolerance throughout my research.

Thanks go to the Erciyes University member, Dr. Fehmi Nair for his valuable contributions, suggestions and comments.

I also want to thank Research Assistant Mehmet Cengil and Master Student Emre Ciminli for their significant contributions to my research endeavors.

I express my thanks and appreciation to my wife for her understanding, motivation and patience.

TABLE OF CONTENTS

LIST OF TABLES

TABLE

LIST OF FIGURES

FIGURE

LIST OF SYSMBOLS AND ABBREVIATIONS

SYMBOL / ABBREVIATION

A	:	Cross sectional area of a superconductor wire
K	:	Kelvin
T	:	Tesla
HTS	:	High T_c Superconductors
LTS	:	Low T_c Superconductors
MA	:	Mechanical Alloying
MN	:	Mega Newton
B	:	Magnetic Field
I_c	:	Critical current
J_c	:	Critical current density
T_c	:	Critical transition temperature
H_{c2}	:	Upper critical magnetic field
mA	:	Mili Amper
PIT	:	Powder-in-Tube
PIP	:	Powder-in-Powder
PM	:	Powder Metallurgy
SEM	:	Scanning Electron Microscopy

: : :

CHAPTER 1

SUPERCONDUCTOR WIRES AND TECHNOLOGY

1.1 INTRODUCTION

In the last 30 years, we have seen incredible developments relevant to the superconducting technology in the world**.** Especially in studies after 1987, a huge energy transport systems, very large capacity electromagnets, very strong electric motors etc. were presented to the people. All of these technologies were made possible thanks to superconductivity.

1.2 SUPERCONDUCTIVITY

Superconductivity phenomenon was discovered in 1911 by Heike Onnes while he was studying on electrical properties of some metals at low temperatures. Onnes sighted the electrical resistance of mercury suddenly down to zero when the sample cooled below 4.2 K. Onnes explained this event as superconductivity [72]. Major innovations were made over 100 years thanks to the studies in this field, superconductors are used in many various engineering areas such as electrical transmission systems , motors and generators, energy storages and transportation vehicles [70]. Superconducting materials can carry huge amount of current without any loss of energy. But the realization of this condition, it is basically by standing below a certain temperature defined as the critical temperature T_c. It is considered characteristic transition temperature value. All the superconductor materials reveal zero resistance behavior under the critical temperatures [71]. The following chart (Figure 1.2.1) shows the relationship between the normal and superconducting conductors.

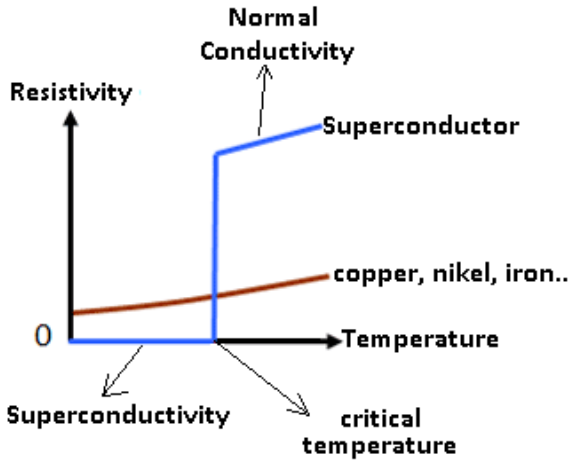

Figure 1.2.1 : Normal conductor and superconductor behavior.

With the discovery by Abrikosov in 1958 superconductors were divided into two groups. Type I and Type II superconductors according to their behaviors in magnetic fields sensitivity [73]. One of the most important studies in recent years the discovery of the high-Tc superconductors (abbreviated HTS) in 1986 [74]. Thanks to the present invention was achieved on the boiling temperature of liquid nitrogen (77K). To obtain the superconductivity at 77 kelvin, lots of electronic devices in more economical when compared to low temperature conventional superconductors and using in industry spread out rapidly after this time.

One of the most important phenomena is applying magnetic field to a superconductor. High magnetic fields destroy superconductivity and restore the normal conducting state. Depending on the character of this transition, two different types of superconductor can be mentioned in existence and they are into two, type I and II superconductors. Most of the pure elements in Figure 2-a tend to be type I superconductors. Type II superconductors, respond differently to an applied magnetic field (in Figure 1.2.2). An increasing magnetic field from zero results in two critical fields, H_{c1} and H_{c2}. At H_{c1} the applied field begins to partially penetrate the interior of the superconductor. But the superconductivity is maintained at this point. The superconductivity vanishes above the second, much higher, critical field, H_{c2}. For applied fields between B_{c1} and B_{c2}, the applied field is able to partially penetrate the superconductor [76].

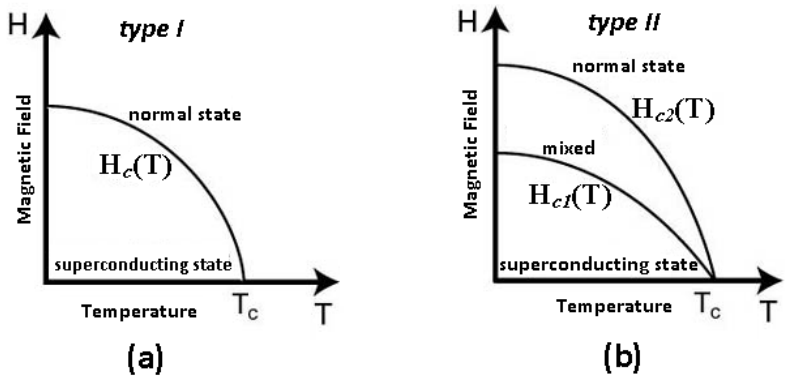

Figure 1.2.2 : Type I and type II superconductors behavior.

Type II superconductors are the most preferred in technological applications, because the second critical field can have truly high values. This useful feature makes building high field electromagnets possible using superconducting wires.

1.2.1 Critical Current (I_c) and Critical Magnetic Field (H_c)

Superconductor materials can carry very high currents up to the point where it loses its superconductivity. A threshold value for the current density though the material stays below its transition temperature. This threshold is explained as the critical current (I_c).

The superconductor current density has a limit J_c. When external magnetic field is applied with superconductor, a current is generated so as to maintain the perfect diamagnetism. If the current density needed to screen the field exceeds J_c, the material will lose its superconductivity. This limit of the field strength is called the critical magnetic field (H_c). The critical magnetic field at any temperature below the critical temperature is given by the relationship :

$$H_C(T) = H_C(0)\left[1-\left(T/T_C\right)^2\right] \tag{1.1}$$

where $H_c(0)$ indicates the critical field at zero temperature and T_c is the transition temperature of the superconductor. In addition to the requirement that the

temperature and magnetic field must be below some certain value, there is also a limit on the current density in a superconducting material. Hereby the three critical values H_c, T_c, and J_c, which are all interdependent are shown in Figure 1.2.3, and a material will only remain in the superconducting state within a volume [77].

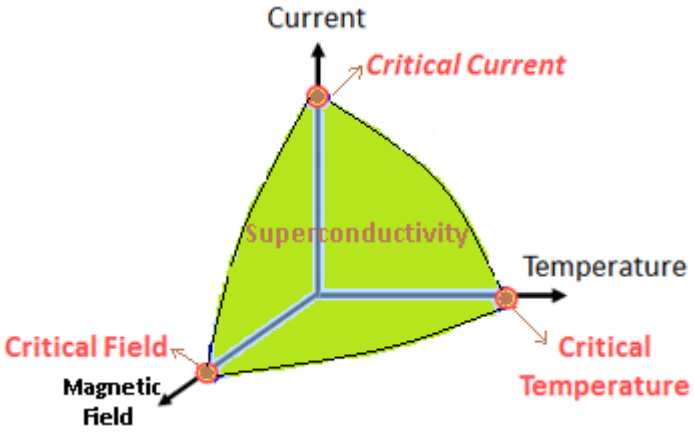

Figure 1.2.3: Schematic of the regions of current density, magnetic field and critical temperature within that is a material remains superconducting.

1.3 CONVENTIONAL SUPERCONDUCTING WIRES

When considering today's technology, the superconducting wires and tapes produced until the discovery [74] of the High T_c Superconductors (abbreviated as HTS) produced in the period up to 1986, we can accept as conventional superconductors. These superconductors within the lower temperatures group and require expensive liquid Helium to cool them to 4K temperature. Moreover, extra cost is required to transfer liquid Helium from one container to another without freezing component [79]. Most low temperature superconductor wires (LTS) that are in use today were made from Nb_3Sn (niobium-tin) and NbTi (niobium-titanium).

1.3.1 Structure of a Superconducting Wire

A superconductor wire can transmit very high electrical currents which is more than 100 times of a standard copper cable. Several studies have revealed that more than 10 kA/cm^2 [30]. Since their first development, the superconductor wires have jackets and dielectrics that provide the prevention of electromagnetic field leakage outside of cable and it also can eliminate eddy current loss from electromagnetic field [31]. A standart conductive wire and superconductor wire structure are shown in Figure 1.3.1.1.

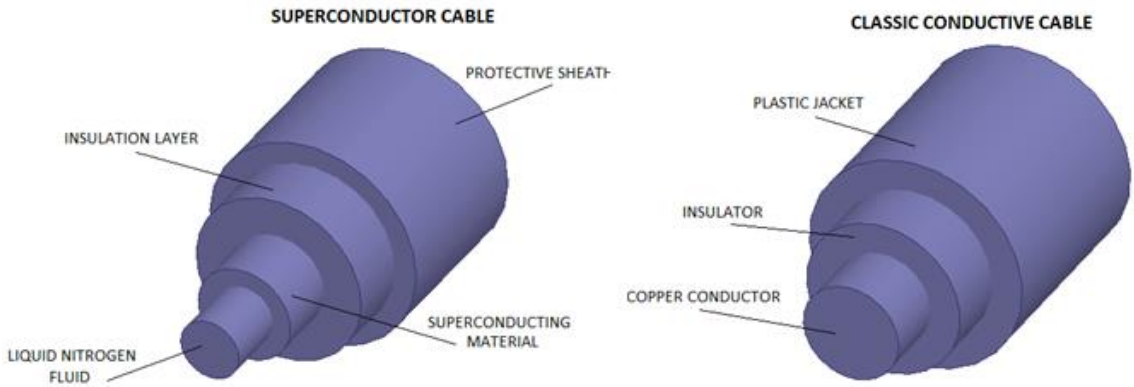

Figure 1.3.1.1: Structure of a conductive cable and typical superconductor cable.

Today's most widely used cable structure in superconductor technology (in Figure 1.3.1.2) contains in its own cryostat mechanism. The superconductor cables can be several km long which are liquid nitrogen cooled through inside the length [80].

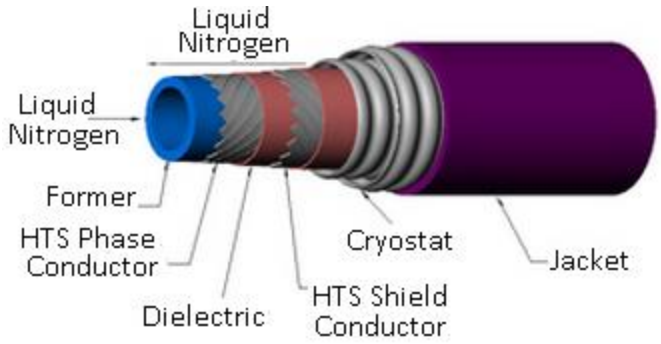

Figure 1.3.1.2: Modern single phase superconductor cable (courtesy of Htstriax comp.) [96].

Superconducting tapes (in Figure 1.3.1.3) are used in compact electric motor technology which needs megawatt level of power [81].

Figure 1.3.1.3: Hundreds of meters superconductor tape [81].

1.3.2 Multicore - Multilayer Superconductor Wires

The structure of a multicore superconducting cable is shown in Fig.1.3.2.1. The conductor is formed by laying the Bi-based superconducting wires in a spiral on a former. Polypropylene Laminated Paper (PPLP) is used for the electrical insulation due to its good insulation strength and low dielectric loss at low temperatures, and liquid nitrogen works as a compound insulation in addition to coolant. On the outside of the insulation layer, a super-conducting wire of the same conductor material is wound in a spiral to form a shield layer. Each shield layer of each core is connected to each other at both end of the cable, so that an electrical current of the same magnitude as that in the conductor is induced in the shield layer in the reverse direction, thus reducing the electro-magnetic field leakage outside the cable to zero. Three cores are stranded together, and this is placed inside a double-layered SUS corrugated piping. Thermal insulation is placed between the inner and outer SUS corrugated pipings, where a vacuum state is maintained to improve the thermal insulation performance [82]. A multicore superconductor schema is shown in Figure 1.3.2.1.

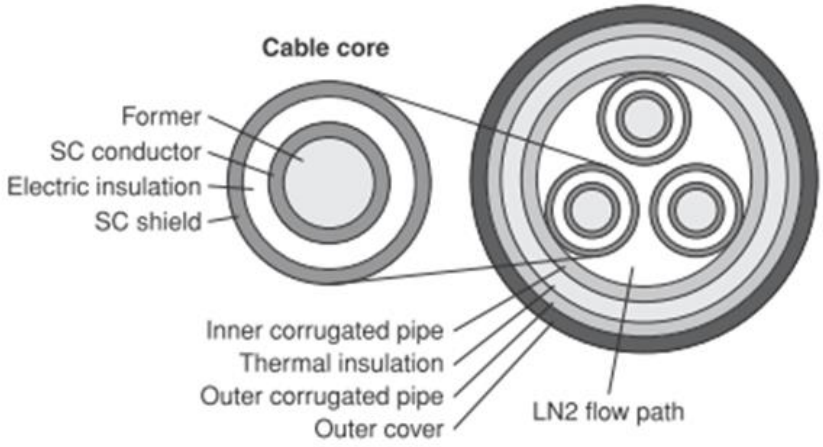

Figure 1.3.2.1: Typical Multicore Superconducting Cable Structure [82].

The structure of a superconducting wire is such that multiple superconducting tapes are spirally wound on the center core called former, which is covered by an electric insulation layer, and then by a superconducting shielding layer and a protection layer which constitute a cable core, and the three cores are accommodated in a thermal insulation pipe in which liquid nitrogen flows as shown in Figure 1.3.2.2.

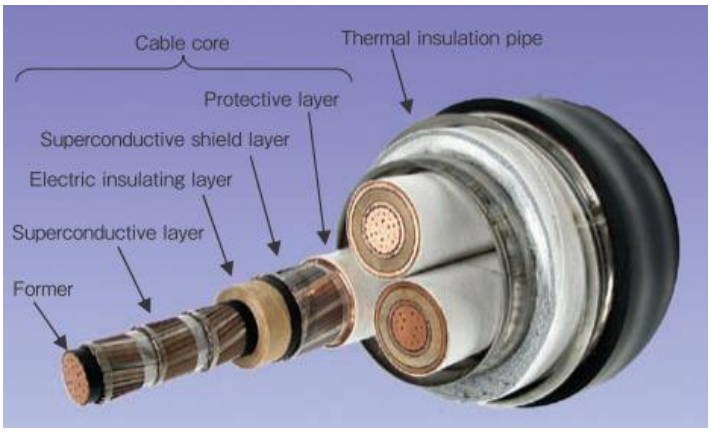

Figure 1.3.2.2: 66/77-kV HTS triplex type power cable [84].

In addition to high critical magnetic field sensitivity characteristics, one of the biggest advantages of multi-core superconducting cables can reach the very high critical current density in Figure 1.3.2.3.

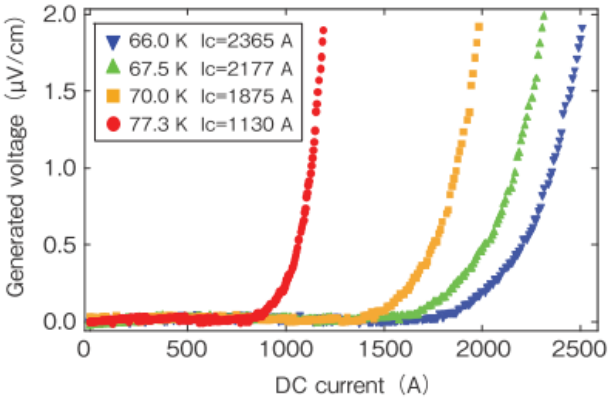

Figure 1.3.2.3: Measurement results of critical current (Ic) of 10-m long YBCO superconductor [84].

Stranded and nested multi layer superconductor (in Figure 1.3.2.4) cables used in power transport system. This type of superconductors has a big current carrying capacity and it can carry about 3000 Amper current [84].

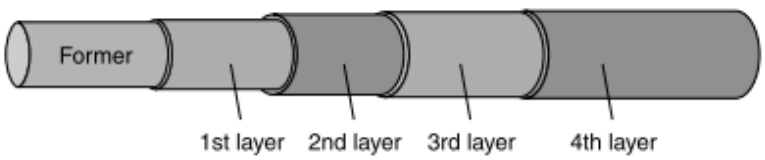

Figure 1.3.2.4: Multi-layer conductor [84].

1.4 SECOND GENERATION HIGH T_c SUPERCONDUCTOR WIRES

High T_c (or HTS) metallic superconductors usually have transition temperatures below 30 K (i.e. LaFeAs, NbTi, Nb_3Sn, Hg). But lots of HTS have been found with transition temperatures more than 110 K [32-35]. In recent years many high T_c superconductors have been discovered in laboratories over the temperature of 77 K liquid nitrogen boiling point. These include 93 K YBCO group, 110 K Bi-based BSCCO group and 134 K Hg-based HBCCO group can be counted. Basically a conventional superconductor has the same mechanism of a HTS. The biggest major difference is that the conventional superconductors have strong phonon interaction mechanism but there is also a strong electron spin density waves mechanism in high T_c superconductors according to RVB (Resonating Valence Bond) theory [36-39]. A typical and modern HTS wire model is shown in Figure 1.4.1.

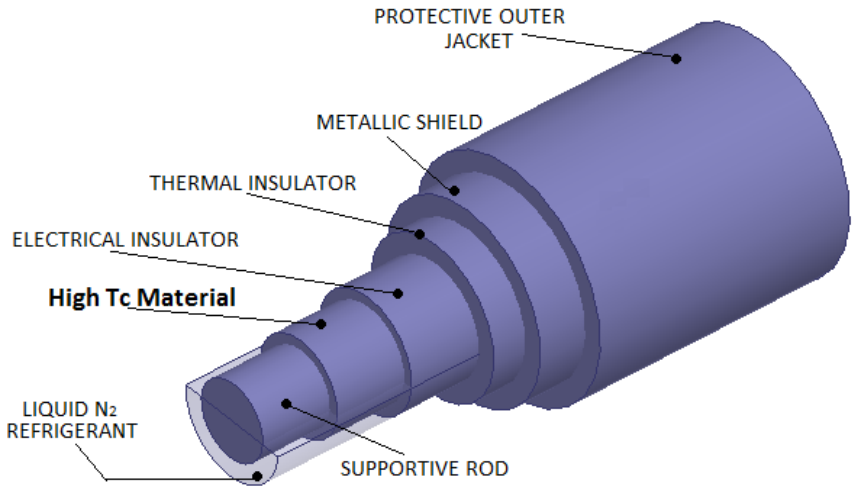

Figure 1.4.1: Typical High T_c Superconductor Cable.

Between conventional low temperature superconductors, superconductors which value less than 77 K T_c and HTS types are shown in a comparative table below [Table 1.4.1].

Table 1.4.1: Transition temperatures of well-known superconductors.

Transition Temperature (K)	*Material*	*Class*
133	$HgBa_2Ca_2Cu_3O_x$	Copper-Oxide Superconductors
110	$Bi_2Sr_2Ca_2Cu_3O_{10}$ (BSCCO)	
90	$YBa_2Cu_3O_7$ (YBCO)	
77	Boiling point of liquid nitrogen	
55	SmFeAs(O,F)	Iron based Superconductors
41	CeFeAs(O,F)	
26	LaFeAs(O,F)	
20	Boiling point of liquid hydrogen	
18	Nb_3Sn	Metallic – Low Temperature Superconductors
10	NbTi	
9,2	Nb	
4,2	Hg	

1.4.1 YBCO Tapes and Wires

YBaCuO (abbreviated YBCO) was the first discovered high Tc superconducting material and YBCO attains superconductive behavior at much higher than 77 K temperature of liquid nitrogen. M.Wu, P.Chu and their students discovered as a first superconductor material above 77 K (boiling point of liquid nitrogen) at Huntsville Unv. of Alabama and at University of Houston laboratories in 1987 [1]. YBCO has a critical temperature of 93 K. The general formula of YBCO is $YBa_2Cu_3O_y$ or Y123. In addition $YBa_2Cu_4O_y$ (Y124) and $Y_2Ba_4Cu_7O_y$ (Y247) alloys are common in literature. Single crystal structure YBCO superconductors have very high critical current density (J_c) and it's measured nearly 2 MA/cm^2 at 77 K [45]. A typical YBCO tape structure is given in Figure 1.4.1.1.

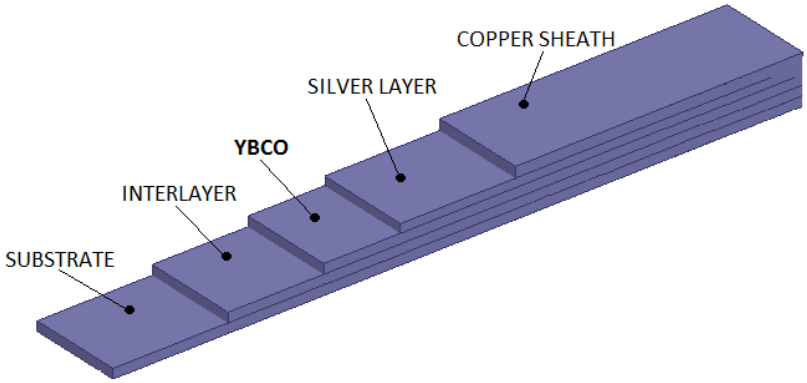

Figure 1.4.1.1: YBCO tapes Structure

Joint of the YBCO tapes wrap over a 1.5 or 2 inches mandrell mechanism in Figure 1.4.1.2 [46].

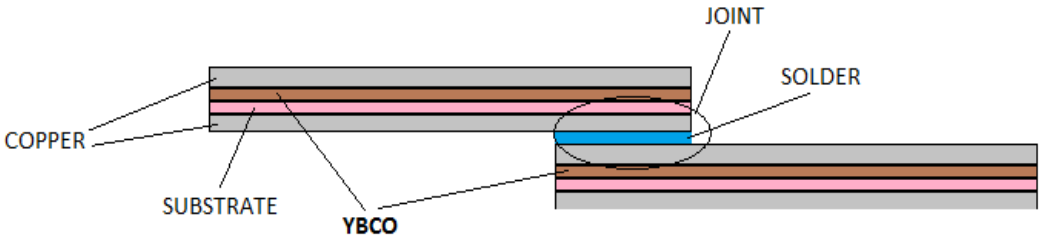

Figure 1.4.1.2: A joint structure of the YBCO tape.

YBCO superconductors are preferably in some commercial applications instead of BSCCO groups for that more difficult fabrication process.

1.4.2 BSCCO Wires

A Type II superconductor Bi-Sr-Ca-Cu-O (abbreviated BSCCO) was discovered in 1988 by H. Maeda and his group in Japan as the first component of BSCCO family [40]. $Bi_2Sr_2Ca_xCu_yO_z$ family has three different phase forms can be expressed as Bi-2201, Bi-2212 and Bi-2223. But only these last two have over liquid nitrogen transition temperature, 85 and 110 K respectively [41]. Most of studies have revealed that BSCCO wires fabricated as joint tapes form [42-44]. Today industry can produce long length Bi-2223 superconductor wires in kilometer level. After the tapes joint process the jointed form transformed to the wires by wrapping in Figure 1.4.2.1 [43].

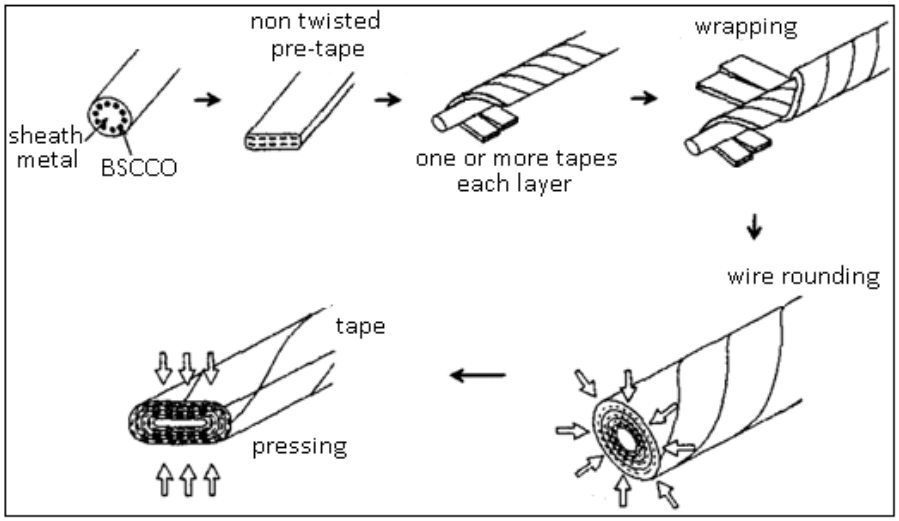

Figure 1.4.2.1: A BSCCO wire manufacturing process [43].

1.5 MgB_2 WIRES

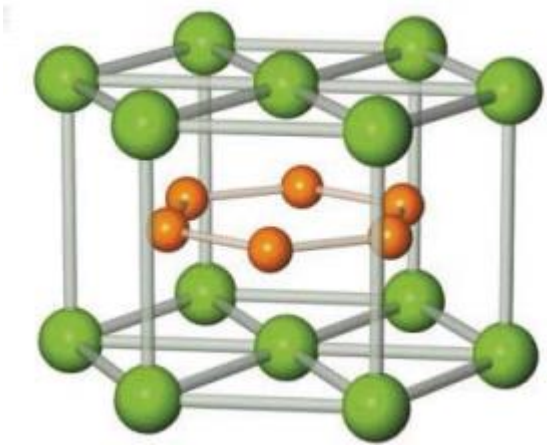

Figure 1.5.1: Crystal Structure of MgB_2 [75].

The MgB_2 material which has hexagonal crystal structure (in Figure 1.5.1) was synthesized first in 1953 [7] and was discovered a superconductor material by Akimitsu group in 2001 [3]. The measured highest superconducting transition temperature (T_c) of MgB_2 is 39 K. MgB_2 is accepted as a Type II superconductor and the measured maximum critical current density (J_c) is ~10^9 A/m^2 at 5 T [4]. In recent years, laboratory studies have attempted to improve the upper critical field (H_{c2}) and the maximum current density (J_c) by some doping materials [5,6].

Depending on the coupling of electron-phonon major components, a high superconducting transition temperature of 39.5 K can be reached [3,8]. The strong

bonding between grain boundaries in MgB_2 [9-12] and this intermetallic has powerful upper critical field (H_{c2}) compared to the conventional superconductor wire materials (NbS_3 and NbTi) [13,14].

The discovery of superconductivity in MgB_2 within a few years following the varying lengths of superconducting wire manufacturing was carried out by several different groups [22-24].

Today MgB_2 based superconducting cable alternative methods [25,26] although mainly in the production of powder in tube (PIT) method has been adopted as the overall.

Additionally in this dissertation study "powder in powder" method information will be described in the next section. MgB_2 powder or compressed into Mg and B precursors alternative materials selected for the metal tubes of copper (Cu) [25,27], Aluminum (Al) [28], Titanium (Ti) [29], Silver (Ag) [25] and Nickel (Ni) [25,27] stands out. Pure copper tube as well as a method to include titanium composite sheath [29]. The most successful of these choices indicating superconducting electric properties is Cu-Ti composite usage. Likely reason for this is the combination of the outer part of the copper tube superior heat transmission and mechanical properties of titanium inner sheath. A typically multicore MgB_2 wire picture is given in Figure 1.5.2.

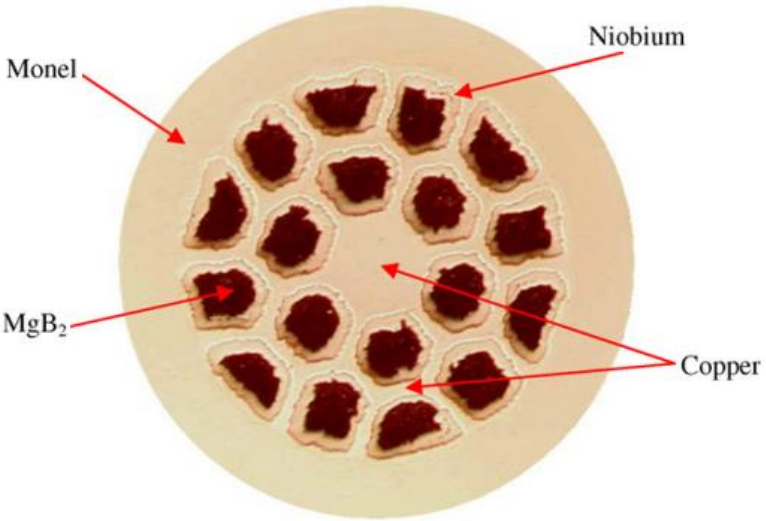

Figure 1.5.2: Cross section of typical multicore MgB_2 wire [78].

1.5.1 Comparison of MgB_2 Wires with Others

Today's industry mainly uses Nb_3Sn and NbTi cable runs at the temperature of about 4.2 K in magnets. Due to the fact that near this temperature and in environments that are not cryogenic system is very expensive to run these cables made of magnets runs in liquid helium. Whereas magnets made from MgB_2 wires can be run easily around 20-30 K [15,16] because depends on basic components of the electron-phonon pairing, such as high superconductivity transition temperature of 39.5 [3,8]. This means that the magnets in a dry environment can provides cooling by a cryo-cooler pump without cryogenic environment [17]. The features mentioned without cryogenic environment running in the 0.5 Tesla experimental MRI magnet in 2010 as the first company in partnership with Paramed Medical System and Columbus Superconductors Inc. was produced with the name "OpenSky" [18].

At present, superconducting magnet industry predominantly uses NbTi and Nb_3Sn cables rolling and wire drawing processes are common in contrast to the rolling tube containing MgB_2 powder processing is more complex and more difficult to control [19]. The formation of cracks in the wires [20] or heterogeneity of the powder density in filaments are frequently encountered obstacles [21].

Additionally, the strong bonds between the grain boundaries [9,10], the higher upper critical field (H_{c2}) values compared the conventional superconducting cable materials ($NbSn_3$ and NbTi) [4,13] and low manufacturing costs are caused high interest in this MgB_2 material [14].

1.6 SUPERCONDUCTING APPLICATIONS

1.6.1 Transmissions Cables

When analyzed throughout the world, BSCCO-2223 superconducting material is used in almost all of the HTS transmission cable projects and all of these projects current type are AC. In developed countries (USA, Japan, France, etc.) between 1992 and 2006 both state institutions and the private industries supported by a very large

cable projects have been carried out. The transmission cables operating temperature is 110 K since the cables were made with BSCCO HTS material. This temperature range is useful for low magnetic field applications [58]. Two main types transmission cable project were conducted. One of them the warm dielectric material cable form is located a conductor made from BSCCO HTS wire is wrapped around a flexible hollow core. Liquid nitrogen flows through the core, cooling the HTS material cable to the zero resistance condition. The conductor is surrounded by conventional dielectric insulation. This design also has to minimize productivity losses [59]. The following table (Table 1.6.1.1) is the largest HTS projects carried out worldwide in recent years.

Table 1.6.1.1: HTS Power Transmission Cable Projects

Corporation	Location	System	Parameters
Pirelli-DOE SPI	USA	Flexible and Warm Dielectric	120 m , 24 kV , 2.4 kA , Single Phase
Tokyo Electric Power Cor.	Japan	Flexible and Cold Dielectric	100 m , 66 kV , 1.25 kA 3 Phase
Pirelli-EDF	France	Flexible and Cold Dielectric	50 m , 225 kV , 2.6 kA , 3 Phase
Southwire Cor.	USA	Flexible and Cold Dielectric	30 m , 12.5 kV , 1.25 kA 3 Phase
Furukawa , CRIEPI METI	Japan	Single-Core and Cold Dielectric	500 m , 77 kV , 1 kA

Some system advantages can be mentioned : HTS transformers have potential advantages over conventional transformers in the following areas: about 30% reduction in total losses, about 45% lower weight, and about 20% reduction in total cost of ownership. These advantages are based on a 100 MVA transformer with HTS wire providing a critical current density of 10 kA/cm 2 and AC losses of 0.25 mW/A-m in a parallel field of 0.1 tesla. Additional benefits include: unprecedented fault current limiting functionality which is expected to protect and reduce the cost of utility system components, and reduced operating impedance which will improve network voltage regulation.

In addition to greater efficiency than conventional transformers, HTS transformers eliminate oil cooling, thus reducing fire and environmental hazards associated with oil-based systems. These benefits enable HTS transformers to have higher power densities so they can be sited in high-density urban areas and inside buildings [85].

1.6.2 Motors and Generators

From the 20th century, electric propulsion systems were allowed new and more flexible arrangement. These systems have enabled more efficient operation of transportation. However, conventional electrical drive motors and generators were large copper based and they covered very large place. This problem was solved more easily thanks to the discovery of HTS wires. Because HTS wire based superconducting motors and generators are smaller and lighter volume. Compared superconducting motor with the same capacity conventional opponent is about the half size and volume.

The working principle of the superconducting wire based motor can be explained as follows : Consists of large magnetic fields when excessive current is passed through the loop formed of superconducting wires. And this magnetic field enables to rotate the flywheels without friction at high speeds. This rotational movement is transferred to a shaft. Thanks to the obtained mechanical power, huge fans, compressors and pumps are operated in big plants and vessels [62].

The superconducting generator technologies enable a valuable reduction for size and weight. HTS generators for wind turbine systems reduce the cost of clean energy. Compact and light-weight 10 MW-class HTS generators and high power wind turbine systems enable practical and low maintenance operations. Under a program funded by the NIST-Advanced Technology Program, key generator technologies for a 10 MW class generator have been developed [60].

The working principle of a superconducting generator as follows : Superconducting AC synchronous generators work by electromagnetic induction principle. According to Faraday's law, rotating electric machines provide power. When electromotive force induced from magnetic fields the AC voltage generated. It is occurred in between the fitting (rotor) coils and the magnetic field (excitation) coils. A

superconducting generator can be divided into three major subcomponents: the rotor, the stator, and the cooling system in Figure 1.6.2.1 [61].

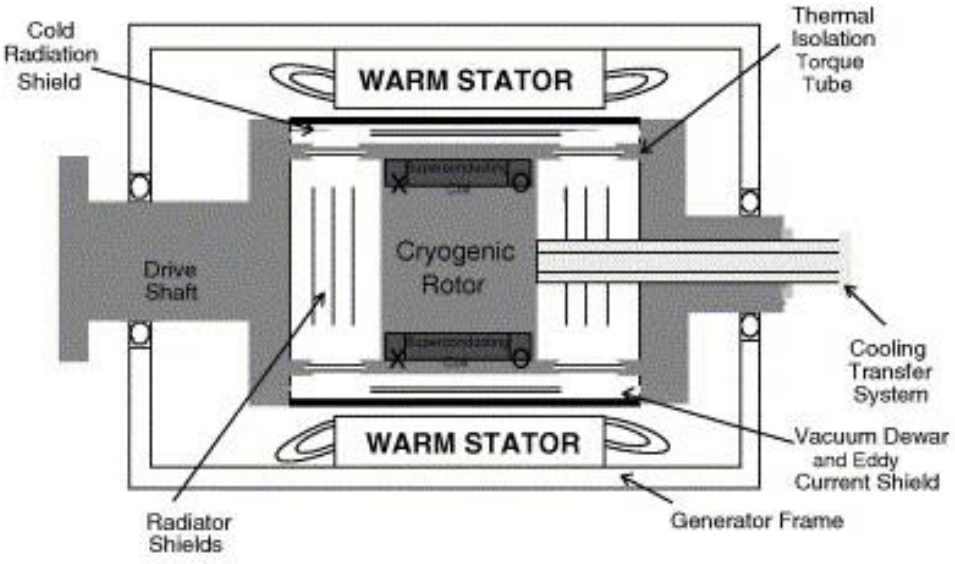

Figure 1.6.2.1: Basics of a classic superconducting generator [61].

1.6.3 Energy Storage with Superconductors

Basic operating principles of the superconducting magnetic energy storage (SMES) system as described by the general principles of electrodynamics. Energy storage operation is done in the following way: A superconducting coil which is kept below the superconducting critical transition temperature can store energy in a magnetic field that is created by very high current passing through. The main components of this storage system are a coil made of superconducting material and include power conditioning equipment, in addition a cryogenic cooling refrigeration system.

There are many advantages of SMES systems over the conventional storage systems. The faster response time is one of them. The required amount of electrical power can be supplied immediately in these systems.The SMES systems have got high overall round-trip efficiency (~90 %) and very high power output.The SMES system can be stored on condition that the cooling system is open.

Currently in use in the world, with a large capacity (more than 10 MW power) SMES systems generally are used in nuclear fusion units and high-energy particle

dedectors. Also small capacity SMES systems are used in some commercial applications, for instance a power quality control in manufacturing plant is used SMES system [63]. A SMES system block diagram is given in Figure 1.6.3.1.

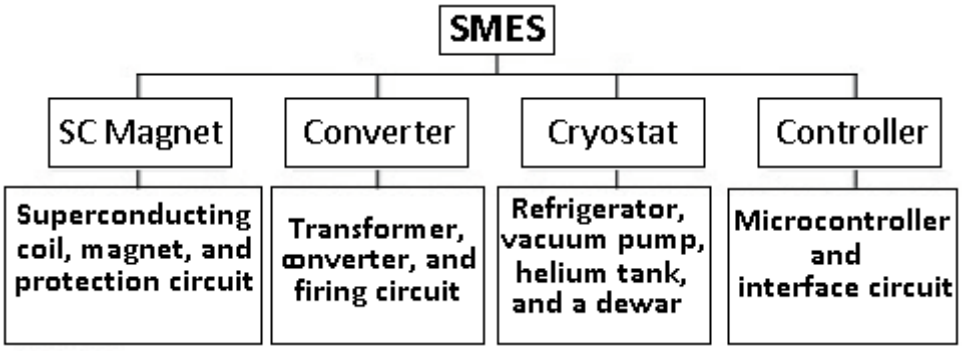

Figure 1.6.3.1: Block diagram of a SMES [107].

1.6.4 High-Field Magnets

Recent technological developments show that in superconducting materials and cryogenic systems the requirement is increased. High field (HF) magnets mainly are used in research, health, industrial and energy application. Superconducting magnets at high field are enabled the improvement of new generation of HF magnets for research applications. Both LTS and HTS wires are used in the manufacturing of the new generation HF magnets. New tin Nb_3Sn wires used as an advanced low temperature superconducting (LTS) materials for HF magnets. Advanced coil structure solutions are used in effective magnet quench management. The new generation HF magnets present the innovative studies for research and industry. Some new HF magnets are undergoing development enabling high field magnets greater than 22 T using high temperature superconductors (HTS) [65]. A high field superconductor magnet design is given in Figure 1.6.4.1.

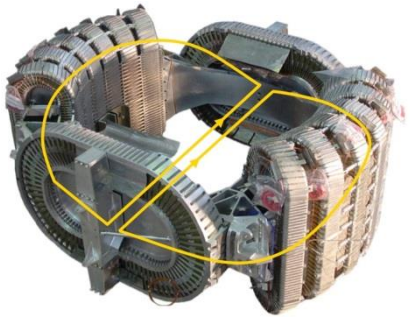

Figure 1.6.4.1: A High Field Superconductor Magnet (AMS Project) [91].

CHAPTER 2

POWDER METALLURGY

2.1 POWDER METALLURGY

Powder metallurgy (PM) is the method known as the fabrication of shaped components or semi-finished metal products from metal powders. A lot of reasons are available to technical and economic advantages. It is one of the best ways of sintered hard metal production. Processing of powder materials begins with consideration of the powder properties and characteristics, such as shape, size, structure and composition. According to H. Kuhn (86), these powder features affect response of subsequent compaction and sintering processes. Actually, powder properties and characteristics are related to the method and situation of fabrication and affect the calculation of these processes directly [86].

In 60's Hirschhorn classified the different way of the powder metallurgy process : Atomization, mechanical alloying, electrolysis and chemical reduction. Atomization is a melting operation for some metal-alloys, electrolysis used for high purity powder deposition and chemical reduction used for iron oxidation can be listed [86].

Some advantages of powder metallurgy: Various metal or nonmetal powder can be operated, good material utilization, very low quantity of loss metal, good control of physical properties and very good surface features obtained. Also some limitations are available: initial machine and system costs can be very high, some powder material costs, low fracture toughness and limited part size.

The process steps sequence is extremely important in the powder metallurgy process. Flow chart in the Figure 2.1.1 summarizes the powder metallurgy process.

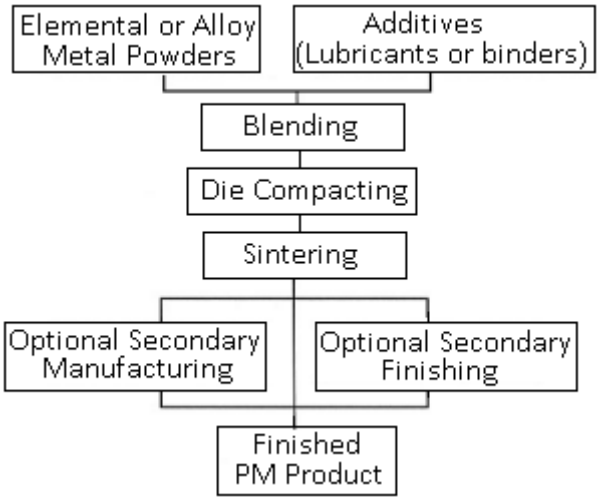

Figure 2.1.1: The flowchart of PM Process [87].

When a conventional PM process sequence is described schematically, situation of steps and powder products situation is such as in the Figure 2.1.2 [87].

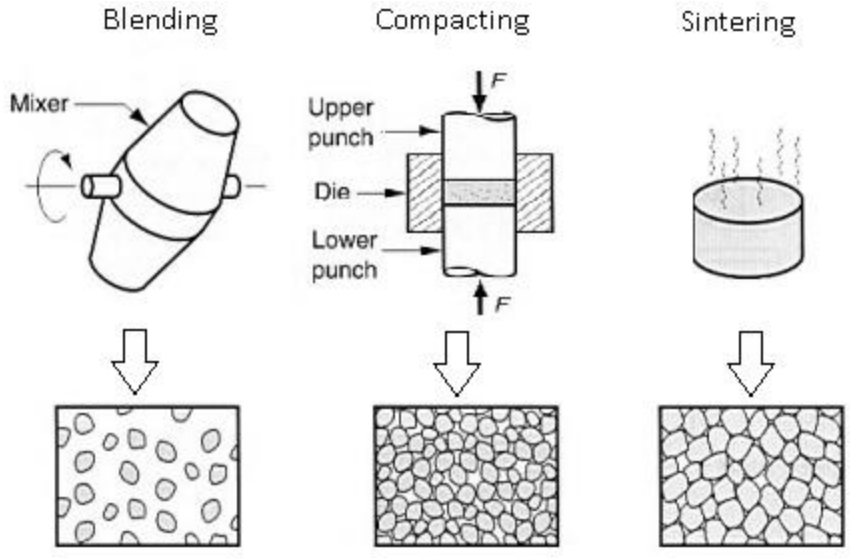

Figure 2.1.2: PM Schematic [87].

In the whole of powder metallurgy process, the last operation is sintering and a result product is obtained. In literature [88-89], the main purpose of sintering process, reducing the surface energy, to improve the porous structure by providing the merge between the grains. As a result of sintering process, provided pores decreasing and finally shrinkage will occur. This shrinkage will cause good electrical conductivity as well as mobility. In the same time, sintering process helps for mechanical hardness and strengthening of material [90]. A 3D simulation is given in Figure 2.1.3 for explaining sintering mechanism.

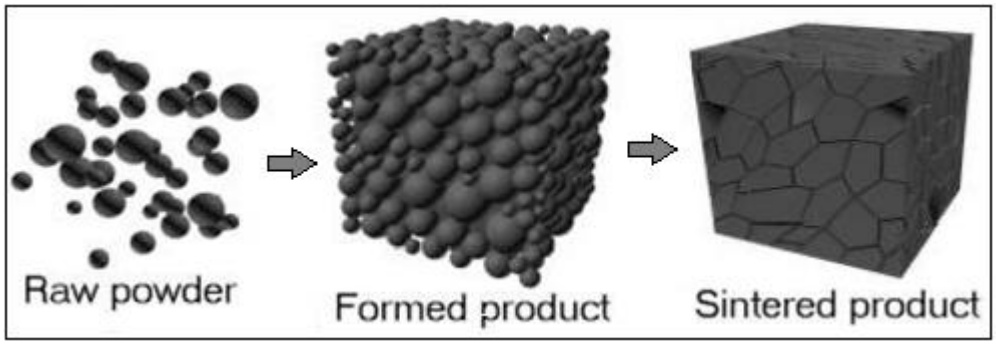

Figure 2.1.3: A 3D modelling of sintering mechanism [109].

2.2 MECHANICAL ALLOYING

The mechanical alloying (MA) method was developed and contributed to the improvement by J.S. Benjamin at the end of 1960's [51-54]. The mechanical alloying operation is an effective and versatile method for producing composite metal powders with controlled microstructures at room temperatures [2]. While getting powder alloys in powder metallurgy to prevent clumping problems developed mechanical alloying method [48]. In this technique, the solid-state welding powders are provided periodically to each other, and welded by providing powders again breakage and uniform microstructure with finer, high strength and high corrosion resistance composite materials are produced [49]. The purpose of this technique is the more fine-grained and uniform microstructure obtaining. Thereby mechanical alloyed powders can withstand to exposed high temperature environments. After the MA process they become strengthened for oxidation and creep deformation [50]. Mechanical alloyed materials suitable for the fabrication of high-tech materials, high thermal stable amorphous alloys, nanocomposite materials [51] and a large number of small particles is a technology for economical production.

Mechanical alloying (MA) has provided the benefits as a result of use at powder metallurgy in recent years and usage area has expanded in technology. MA process is a kind of solid state reaction and this procedure is evenly carried out uniformly dispersed.

Many commercial products can be manufactured by mechanical alloying method. Some of these products are current applications , while some others in design phase : Magnetic materials, sensors, catalysts, hydrogen storage, ODS superalloys,

nanostructured materials, PVD targets, pure metal productions and superconducting alloy materials can be listed [55]. A mechanical alloying process is given in Figure 2.2.1.

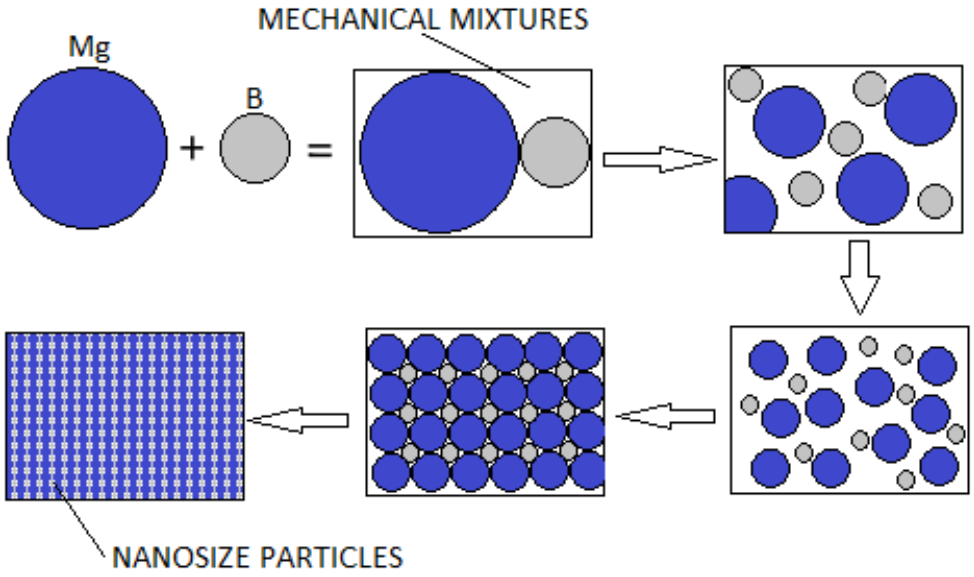

Figure 2.2.1: A mechanical alloying application with Mg + B powders.

2.3 POWDER – IN – TUBE METHOD (PIT)

Basically, it is a technique which consists of a metal tube filled with powders for the preparation of wire drawing process. For the last 40 years, it has been recognized as one of the most effective methods for produced superconducting cable technology. Obtaining the experimental environment of alloys (in-situ) and externally available as getting synthesized (ex-situ) are two fundamental PIT parameters. Method of pressing and heat treatment step is very important.

Main advantage of this method is to enable development of such samples that are able to carry high critical current density. A schematic view is given in Figure 2.3.1.

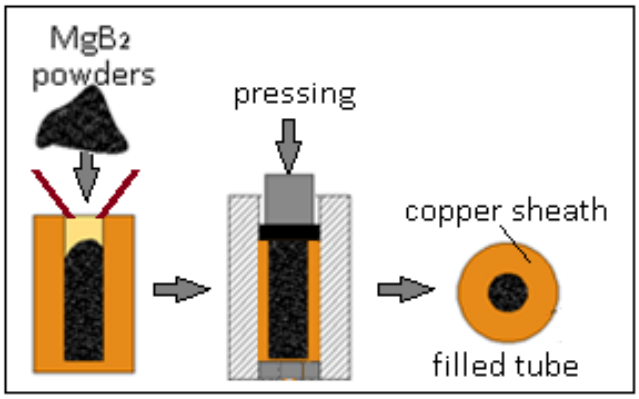

Figure 2.3.1: Powder-in-Tube process.

2.4 POWDER – IN – POWDER METHOD (PIP)

Substantially, powder-in-powder method can be called as forming (compression) compact or briquetting [92]. The most common forming process is filling the powder mixture to the mold with the help of a staple and pressing in a hydraulic or mechanical press [93]. The compact shape of the pressed powder called raw compact or briquettes. Density of the mixture is "raw intensity" and the strength to have raw strength is called, the word “raw” is used because the item is not yet sintered [94].

Pressing process is the most important part during the manufacturing. For the following reasons : Giving required form to the powder mixture, required size to the powder mixture and bring in required strength further treatments [92-93]. Repacked powder during pressing process, eliminate the mounds that occurred during filling up and pores are reduced as the contact points increase between the powder grains. When pressure increases, grains undergo plastic deformation, and re-increased contact areas. Raw density and raw strength increases with increasing pressure [92-94]. Between the pressing pressure and true density graph is give in Figure 2.4.1.

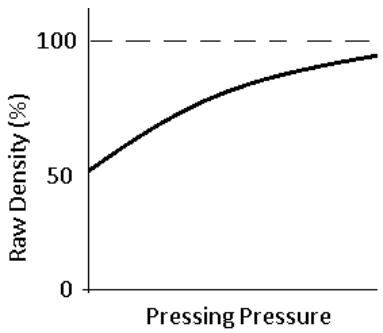

Figure 2.4.1: Raw Density vs. pressing pressure graph.

Heating is another parameter for powder-in-powder method. The applying temperature to the Powder in the mold and pressing speed will affect the realization of the powder compacting. A schematic illustration is shown about PIP method in Figure .

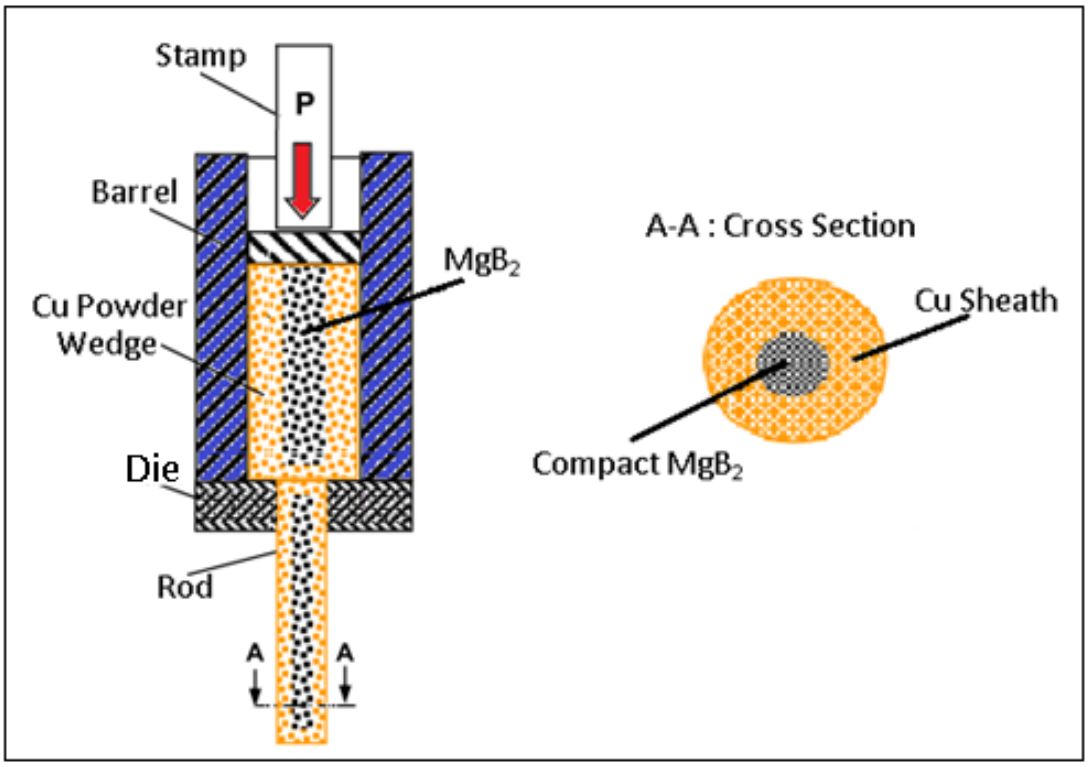

Figure 2.4.2: Schematic view of Cu sheathed MgB_2 rod manufacturing by Powder-in-Powder method

2.5 EXTRUSION

A liquid, powder or paste form into an appropriate volume of material in rod or wire form by compressing the preparation procedure is called extrusion. The material is drawn through a die of the desired cross-section fixed to create a profile by pressing [47]. Substantially extrusion which is forming process some slight metals (Cu, Al, Ag etc.) by passing through a matrix pattern. An illustration of a standart extrusion mechanism is given in Figure 2.5.1.

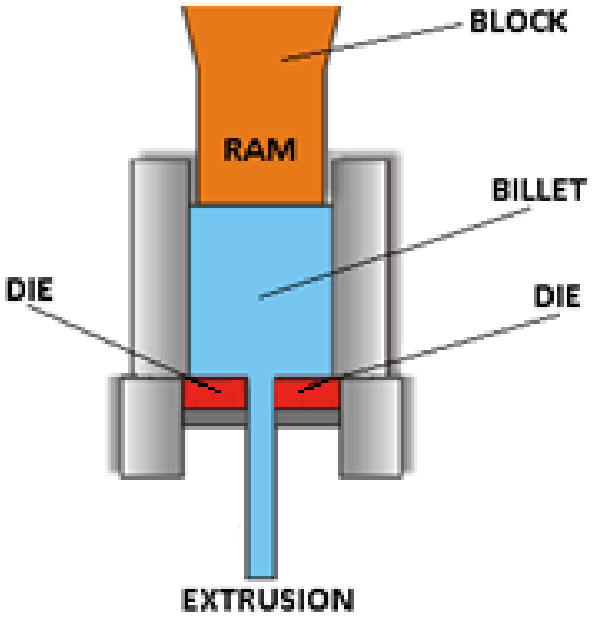

Figure 2.5.1: Standart extrusion mechanism.

As a result of extrusion in order to obtain the products properly, extrusion rate and the magnitude of the externally applied temperature is very important. Required equations are as follows :

$$R = \frac{A_i}{A_f} \tag{2.1}$$

$$P = kA_i \ln \frac{A_i}{A_f} \tag{2.2}$$

$$T_a = T + T_d + T_f \tag{2.3}$$

where R is the extrusion ratio, A_i is the initial cross-sectional area, A_f is the final cross-sectional are in equation 2.1. P is the extrusion force and k is the extrusion constant in equation 2.2. Other significant expression is given in equation 2.3 for calculation of the final average material temperature (T_a) where T is the average instantaneous temperature, T_d is the temperature for frictionless deformation temperature, T_f is the temperature of increasing due to friction.

2.5.1 Direct - Indirect Extrusion

In a direct extrusion system, a metal billet is placed in a barrel, driven through the die by the ram and is passed through the matrix. An extra pressure plate is inserted at the end part of the ram in contact with the billet due to needing extra force. Friction becomes too much in the last part of extrusion at the die in Figure 2.5.1.1.

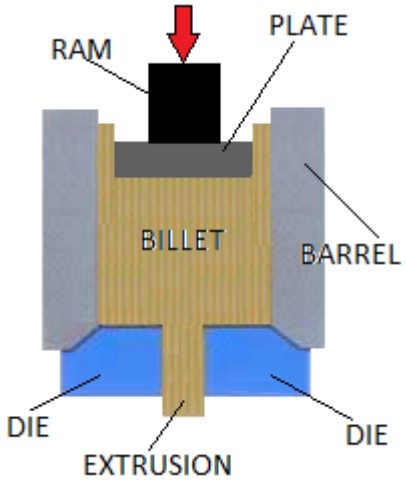

Figure 2.5.1.1: Direct Extrusion.

In the indirect extrusion mechanism which is similar to the direct method, there is a small mechanic difference: the barrel with the metal billet to move when die is keeping fixed position like in Figure 2.5.1.2. Friction at the die only requires approximately constant pressure.

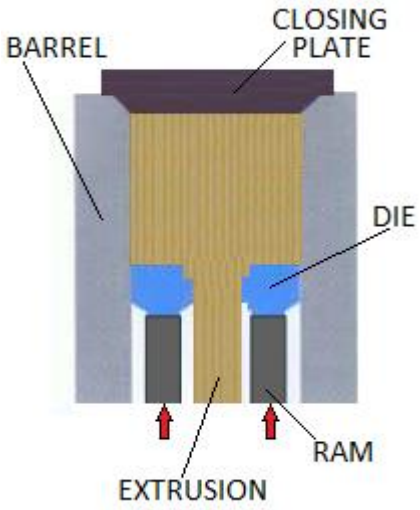

Figure 2.5.1.2: Indirect Extrusion.

2.5.2 Hot - Cold Extrusion

Most of metal materials are not ductile in room temperature. Hence, hot extrusion process is performed in the melting temperature of the material up to about 75% at temperatures relatively higher. The thrust exerted pressure can range from 50 to 750 MPa. Lubrication procedure is extremely necessary while hot extrusion process performing, because the high temperatures and pressures and its harmful effect on the dies and other extrusion components [57]. An abrasive oxide layer can occur on the surface of the metal billet. Oxide problem can be solved by decreasing the diameter. Lubricant material is glass powder in hot extrusion process.

In cold extrusion process, relatively small diameter metal billets are used. Even cold extrusion process, hardening improves the mechanical properties of extrusion if friction heat does not reach the temperature of the recrystallization. Oxide usually does not occur on the surface. Less energy is consumed since there is no heating process. Examples of the metals can be extruded are Al, Cu, Ti, Pb and some steels and of which the cylinders, aluminum cans and collapsible tubes can be manufactured.

2.5.3 Vertical - Horizontal Extrusion

There are some extrusion types corresponding to geometrical orientations. Vertical extrusion technique is commonly used in industrial thin-walled tubes. Easier alignment between the press ram and tools, higher rate of production are known advantages. Besides, vertical extruders take up less floor space. In this technique, uniform deformation consists due to uniform cooling of the billet in the container [56,69]. Up to 20 MN extrusion press can be reached at industrial applications.

Other geometrical types that the horizontal extrusion technique uses for most commercial products are bars and rod shapes. In excess of 100 MN forces are applied in industry [57].

2.5.4 Hydrostatic Extrusion

The most significant feature of this process is that there is no friction between the billet and the container walls and thus the length of the billet is not any limited like it is in conventional extrusion applications. Furthermore, the frictional forces between die and the billet tend to be lower in hydrostatic since the lubricant acts as a force by the high fluid pressure to flow into the interface. A low frictional stress on the die surface permits a smaller die angle, pan out more uniform shape in the extruded product. From another point of view, the indirect driving of the billet through the compressible fluid sometimes makes it difficult to control the motion of the billet [68]. A hydrostatic extrusion mechanism is given in Figure 2.5.4.1.

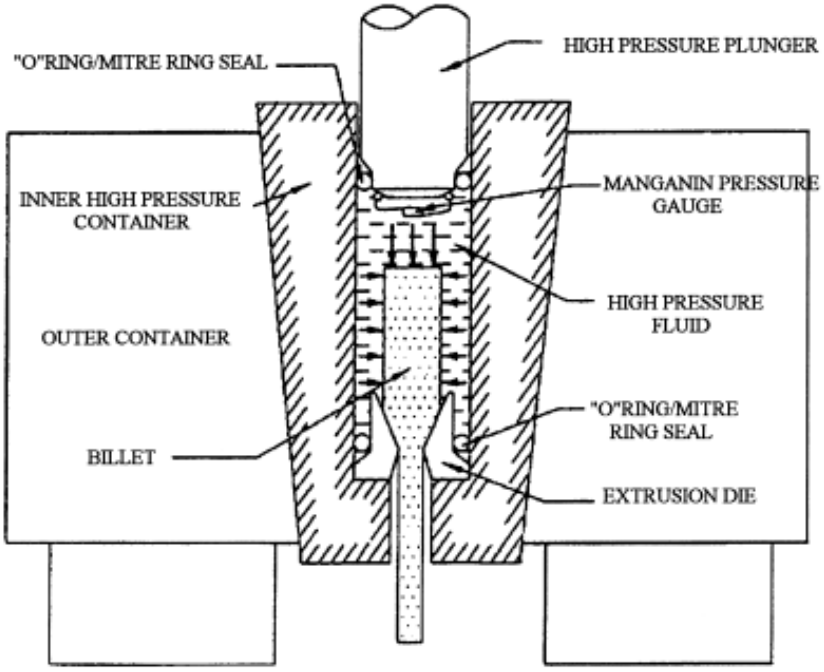

Figure 2.5.4.1: A modern hydrostatic extrusion contrivance [67].

2.6 DRAWING

A wire drawing mechanism covers reducing the diameter of a rod or wire with passing through a series of drawing dies or plates. The drawing mechanism of rods and bars are basically the same in principle, although the equipment that is used is different for the varying-sized products [56]. A classic wire drawing mechanism is given in Figure 2.6.1.

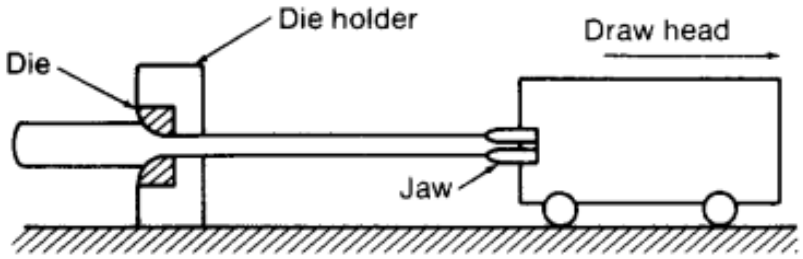

Figure 2.6.1: A basic wire drawing mechanism.

When studying tube drawing the mechanism works by reducing the cross section and wall thickness through a draw die. The cross-section can be in different geometrical shapes. Circular, square, hexagonal or any required shapes can be used. A circular shape product of a wire drawing design is given in Figure 2.6.2.

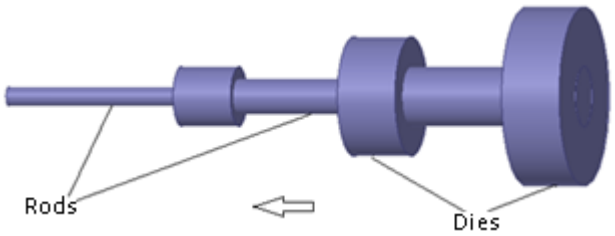

Figure 2.6.2: Wire drawing dies with reduced diameters

Drawing operations involve pulling the material through a die, it means of applying a tensile force to the exit part of the die. When the drawing process a plastic flow behavior is caused by compression force, rise up from the response of the metal with the die [69]. It is essential to have some significant features while drawing the materials. The main ones including have high ductility and enough tensile strength [57]. When the rods are concerned, reducing the diameter rod through plastic deformation while the volume of the rod remains the same. The ideally capacity of the wire drawing machine should be as follows: 1 MN drawbench, 30 m of runout and 150-1000 mm/s draw speed [56-57]. A reference sample of draw machine design is in Figure 2.6.3.

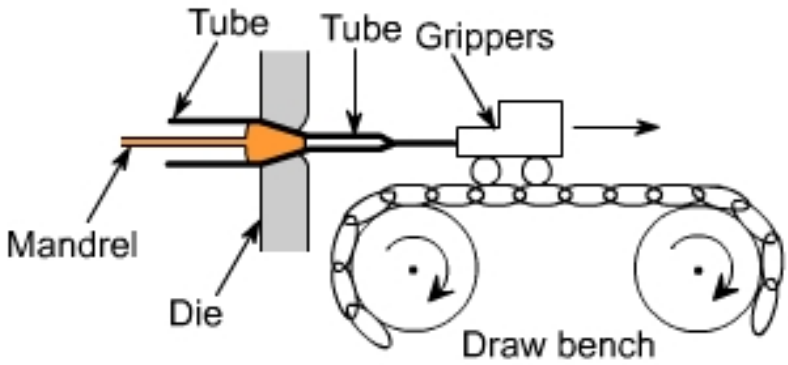

Figure 2.6.3: A design of wire drawing machine [95].

Knowledge about the force of the die pull is a major calculation in a wire drawing machine for preventing the rupture of wire. The follow expression provide it :

$$F = \sigma_{avg} . A_f . \ln\left(\frac{A_i}{A_f}\right) \tag{2.4}$$

where σ_{avg} is the average true stress of the material in the die side and A_o - A_f initial – final areas of the cross-section of material respectively.

CHAPTER 3

MATERIALS AND MANUFACTURING METHODS

3.1 MECHANICAL ALLOYED MgB_2 POWDERS

In this study, MgB2 intermetallic powders was produced by Mechanical Alloying (MA) method. At the start of the experiments were available from Merck KGaA Company, amorphous boron (B) and magnesium (Mg) powders were used.

Figure 3.1.1: Retsch PM200 Planetary Mills MA Device

The average sizes of Mg – B powders 2 µm and 300 µm respectively. MA experiments at "Retsch PM200" branded device was performed in different time periods. There are some different parameters in first and second production. Parameter differents is given in Table 3.1.1.

Table 3.1.1: MA parameters of first and second production

Operation	1st Product	2nd Product
BPR (Ball to Powder Ratio)	1/20	1/10
Container volume (ml)	450	500
MA process time (hour)	10	20
Turning speed (rpm)	600	800
Steel balls diameter (mm)	8	50

The device was operated at 600-800 rpm during the experiments and hardened steel containers at 450-500 ml volume were used in Figure 2.2. In stoichiometric proportions at containers 10-5 sensitive precision scales weighed elemental Mg + B powder mixtures which had been done in a total of 10-20 hours were performed with MA. The steel balls (diameter 8 – 50 mm) and ball to powder ratio (BPR) as 1/10 and 1/20 has been selected as alloying parameters for MA processing.

The powder sample obtained 4 in 10 mm diameter steel mold at a pressure of 575 MPa is pressed separately and 10x2 mm size block specimens were revealed out. Then the block shaped specimens were heat treated for 2 hours at 600 ^{o}C.

All of these actions, the elemental form of test samples into block shape specimen, and the step of applying heat treatment to the whole of the process was carried out in high purity (99.996%) Argon (Ar) atmosphere. An imaginative mechanic alloying of MgB_2 is given in Figure 3.1.2.

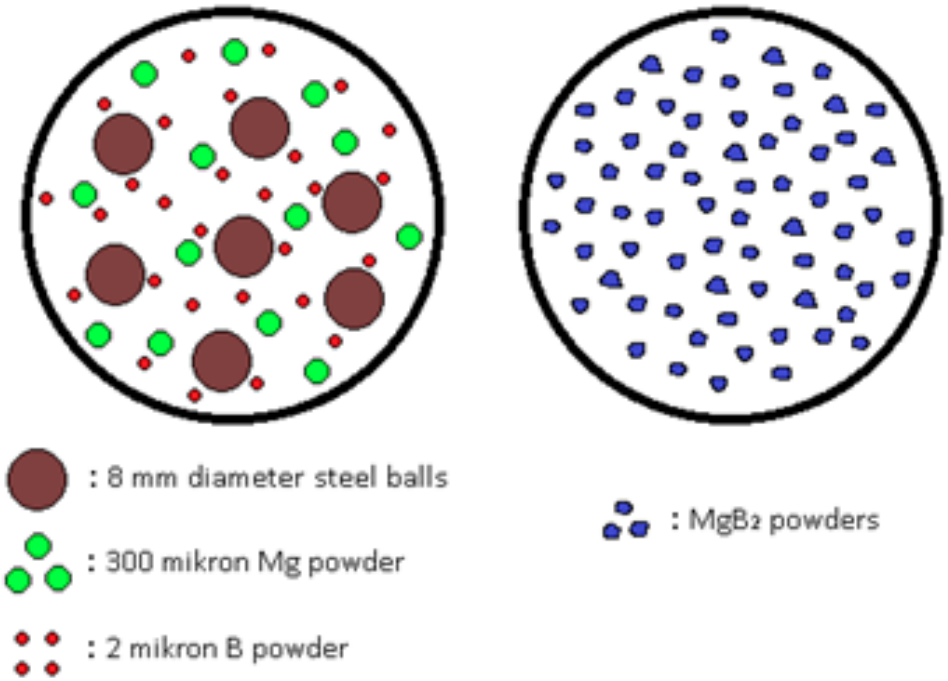

Figure 3.1.2: Mg + B powders mixing and final MgB_2 product.

Some features of MgB_2 powder, which has an intermetallic structure, are given in the Table 3.1.2. As can be seen from the table, the density and the melting temperature of MgB_2 are quite different characteristics from the forming mixture of pure Mg and B elements.

Table 3.1.2: MgB_2 properties.

Molar Mass	45.93 g mol^{-1}
Density	4.52 g cm^{-3}
Melting Point	2970 °C
Crystal Structure	Hexagonal
Poisson Ratio	0.10 – 0.15
Knoop Hardness	1800

Commercial powder grain size is 40 micron according to the Alfa Easer company calculations which received from commercial MgB_2 powders. But in this study, mechanical alloyed powder grain size was not calculated exactly accurate because this calculation needs a micro-size jig component.

Finally, the XRD measurement was performed to understand the accuracy of mixed powders obtained by mechanical alloying process. The result is shown in Figure 3.1.3. XRD measurements were done by a Bruker device in Erciyes Unv. Research Center (in Figure 3.1.4).

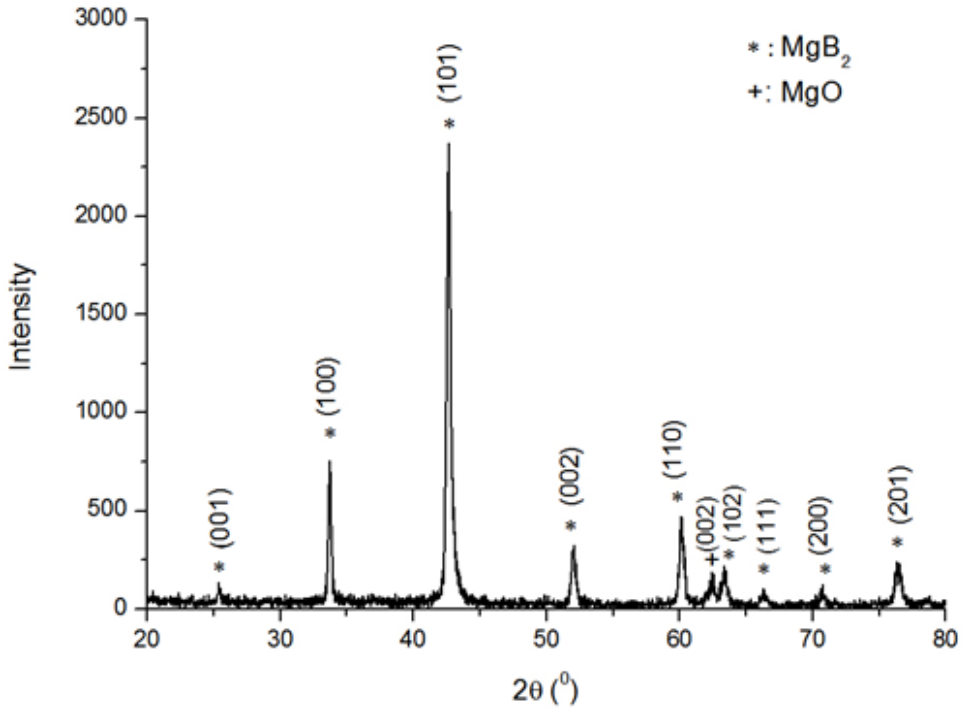

Figure 3.1.3: XRD result of mechanical alloyed MgB_2 powder.

Figure 3.1.4: Bruker AXS-D8 Advance Model XRD System at Erciyes Unv. Tamu.

3.2 IN–SITU AND EX–SITU SYNTHESIZED OF MgB_2 WIRE BY PIT METHOD

10mm and 20mm inner diameter of copper billets are used in this experimental study. The depth of the billet hole is 20mm. Length of the billet is 35mm. MgB_2 powder is filled into the billet (in Figure 3.2.1) with using the following equation:

$$N = V_H \times D \times (60\%) \tag{2.1}$$

where N is the amount of powder, V_H is volume of the barrel hole and D is density of MgB_2. Since MgB_2 powder grain size cannot be clearly known, the powder compaction ratio is used as %60 while calculating the powder compaction rate.

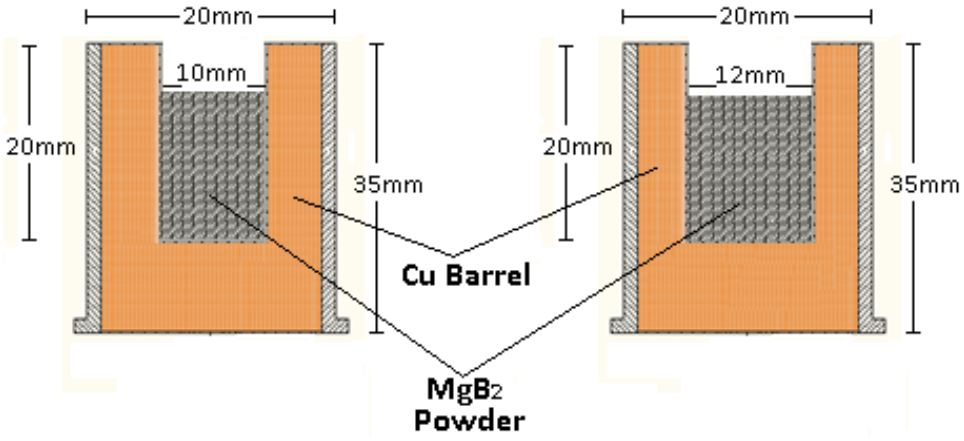

Figure 3.2.1: Cu billets which are inner diameter 10mm and 12 mm.

A final billet product with stopper stamp shown in Figure 3.2.2. The billet size is 50 mm length, 35 mm depth for powder and 10 mm (in Figure 3.2.2).

Figure 3.2.2: Cu billet by using PIT method.

After the experimental trials, different length of Cu rods were obtained in Figure 3.2.3 and cross-sectional area picture is shown in Figure 3.2.4

.

Figure 3.2.3: Cu sheath material for multicore manufacturing

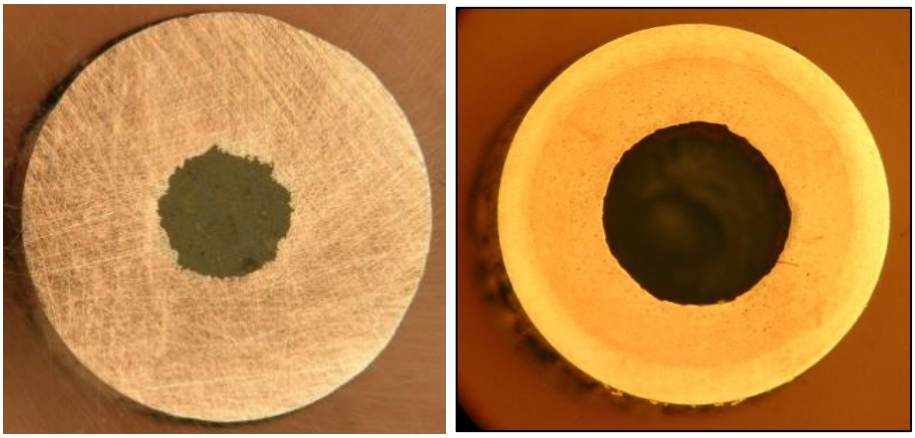

Figure 3.2.4: Cross-section of a Cu rod.

3.2 EX – SITU SYNTHESIZED OF MgB_2 BY PIP METHOD

Copper powder was used as the sheath material in the MgB_2 composite superconductor wire manufacturing due to its high formability and good thermal conduction properties. Used -100 mesh copper powder (max 150 micron in particle size) is provided from Alfa AESER® company in 99.996% purity (total metal impurities: 0.001% max.). Also MgB_2 -100 ~40 micron mesh ceramic powder is provided from the same company (in Figure 3.3.1) .

Figure 3.3.1: Cu powder on the left, commercial MgB_2 powder on the right.

General characteristics and some significant features of the copper powder are given in the Table 3.3.1.

Table 3.3.1: Copper powder features.

Melting Point	1083 °C
Density	8.94 g/cm^3 @ 20 C
Coef. Thermal Expansion	17.0 x 10^6 /C (20-100 C)
Thermal Conductivity	0.934 cal/cm^2/cm/sec/C @ 20 C
Electrical Resistivity	1.71 microhm-cm @ 20 C
Electrical Conductivity*	0.586 megmho-cm @ 20 C
Specific Heat	0.092 cal/g/C @ 20 C
Modulus of Elasticity (Tension)	117,000 MPa
Modulus of Rigidity	44,000 MPa

Die diameters in the experiments shown in Figure 3.3.2, with conical and flat dies were manufactured to be used during the extrusion process. In the experiments, designed in different dies to provide the different extrusion ratios and wire rod produced in various diameters. Whether the product obtained according to the PIT method's products, the wires were manufactured in 0.5 and 1.0 mm diameters as the result of this process.

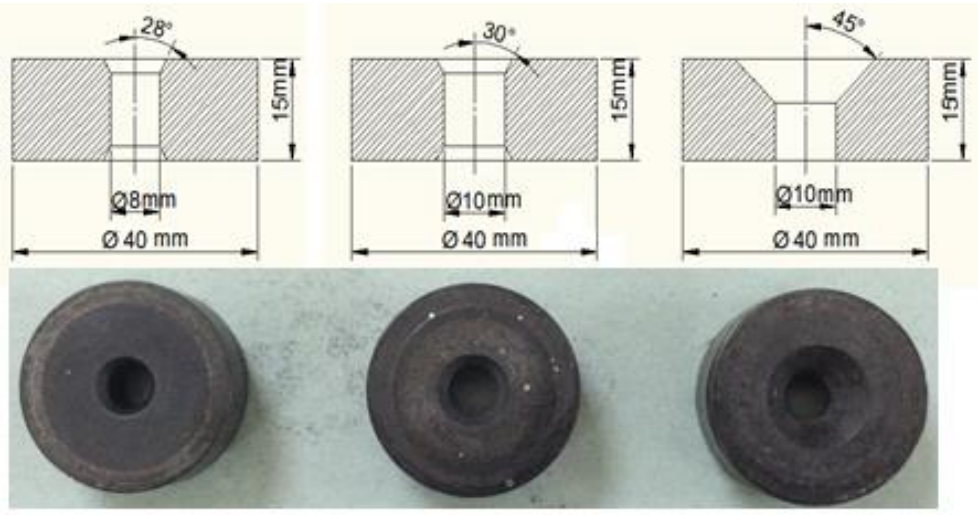

Figure 3.3.2: Three different dies which are made from AISI 2344 steels.

60 g of copper powder was filled into a barrel in Figure 3.3.3.a. Later on 5 gr MgB_2 powder was filled into the barrel cavity [in Figure 3.3.3.b). Then barrel was heated at 600 ^oC for 60 minutes. After completing the final case of this mechanism, finally pressed with a 150 ton hydraulic press. (All of the PIP process was performed by E. Ciminli [103] under the 1138.STZ.2011.2 project at Erciyes Unv. Composit Material Lab.)

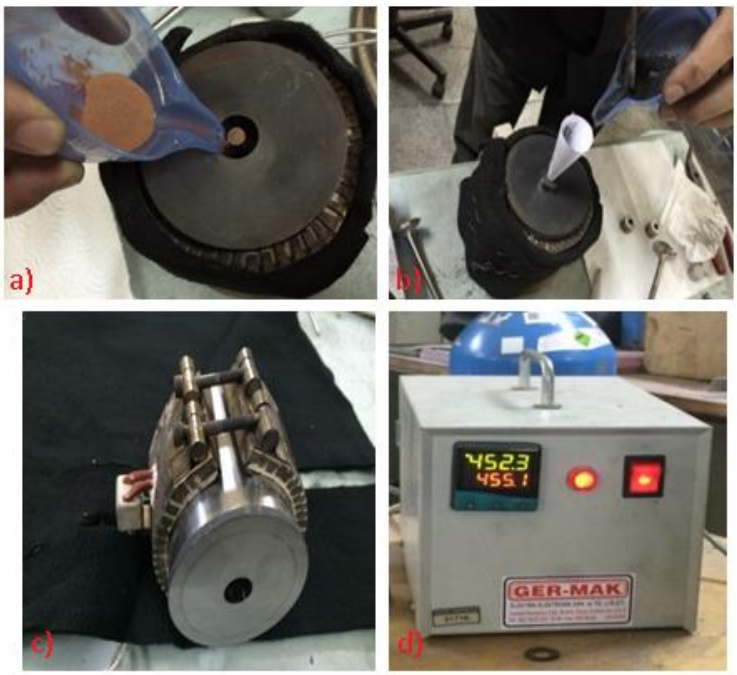

Figure 3.3.3: a) Copper powder filling into the mold, b) MgB_2 powder filling into the mold cavity, c) Mold heating unit of the die production, d) The mold heating control unit.

It resulted in failure in many pre-trial manufacturing. Usually due to the compact wires in the wire-drawing stage was broken to two pieces (in Figure 3.3.4).

Figure 3.3.4: Broken to pieces, unsuccessful trial.

After that, in many of trials superconductor wires were obtained by PIP method. 20 cm rods were produced from 5 cm length of a billet. According to extrusion ratio 5 in equation (xxx) 1mm diameter and 4 meter length superconductor wires were manufactured at one wire drawing operation (uninterrupted) (in Figure 3.3.5).

Figure 3.3.5: Single piece and 40 meters mono-core mechanical-alloyed MgB_2 powder made SC wire.

3.3 MANUFACTURING OF WIRE ROD WITH HOT EXTRUSION

Hot extrusion method was used in this study. MgB_2 powder filled into the billet with the PIT and PIP methods. The billets were annealed at 600 C for one hour before the extrusion procedure. The annealing process was performed at 5 $^{o}C.min^{-1}$ heating and cooling values. After the preheating procedure completion, the billets are pressed for the extrusion process with 150 tons of hydraulic presses (in Figure 3.4.1) under 600 MPa compressive force.

Figure 3.4.1: 150 tons of compressive force capacity hydraulic press in Erciyes Unv. Composit Lab.

The extrusion process temperature is 350 ^{o}C. The cooling down period lasted of approximately 3 hours and then 1/20 elongated wire rods (in Figure 3.4.2) removed from the extrusion die, finally Cu/MgB_2 rods have been made ready to wire drawing process.

Figure 3.4.2: Cu sheath MgB_2 mono-core extended rods by made hot extrusion method.

3.4 WIRE DRAWING MECHANISM

A machine was manufactured specifically for this study and it has 30-channel dies with an electric motor (speed adjustable) were used in a machine (in Figure 3.5.1). It provides square shape outputs in the cross-section when drawing machine rolling the wires.

Figure 3.5.1: 30 channel specific design wire drawing machine.

Firstly the diameter of the billets were reduced to 10-11 mm which are filled with MgB_2 powder by PIT and PIP methods. Later on, the wire drawing process was performed by 30 channels wire drawing machine in a controlled manner. Wire drawing speed was set to 3-4 $cm.s^{-1}$. A lubricant material was used to reduce friction and to prevent unexpected plastic deformation of material in wire drawing (in Figure 3.5.2).

Figure 3.5.2: Wire drawing process.

The dimensions of channels of the wire drawing machine are given in Table . Wire drawing process is made sequentially using each channel one by one. The sawdust of wire has been cleared by passing through previous two channels.

Table 3.5.1: Roll cylinder channel measures of drawing machine.

Channel number	Wire radius (mm)	Channel number	Wire radius (mm)
1	11,00	16	1,90
2	9,90	17	1,80
3	8,00	18	1,70
4	7,00	19	1,60
5	6,00	20	1,50
6	5,00	21	1,40
7	4,50	22	1,30
8	4,00	23	1,20
9	3,50	24	1,10
10	3,25	25	1,00
11	3,00	26	0,90
12	2,75	27	0,80
13	2,50	28	0,70
14	2,25	29	0,60
15	2,00	30	0,50

A 12 turns, 40 cm length and 0.5 mm diameter of MgB_2 superconductor wire picture is given in Figure 3.5.3.

Figure 3.5.3: 0.5 mm diameter – 30 cm long MgB_2 coil wire.

3.5 HEAT TREATMENTS

All of the heat treatments were done in Protherm Quartz Tube Vacuum Furnace in Figure 3.6.1. Furnace heating range was between 20-1100 ^{o}C. The different pieces of the wire samples were placed in quartz tube which is nearly 40 cm long. After placing and pre-vacuuming operation, the sample wires were heated rapidly to 300 ^{o}C and then down to room temperature. This pre-heating was inevitable due to the required coil shape. Wire samples were wrapped as coils without delay and sintered at different temperatures. Inspired by the pre-literature study [96-102], 500, 600, 700 and 800 ^{o}C temperatures were preferred. Before each heating, vacuum system has reduced to 10^{-4} Torr (mmHg) pressure inside for the tube free of particles. Then, the wire samples heat treated by supplying high purity Argon gas atmosphere for 60 minutes period. Only item of different wire product groups of PIP method sintering temperature were applied for 90 minutes.

During the entire heating process, the pressure was set to $2x10^{-1}$ Torr and Argon gas flow was continued. Though it has been investigated the sintering time period in the literature [108], only in different temperature but equal sintering time period was performed in this dissertation study.

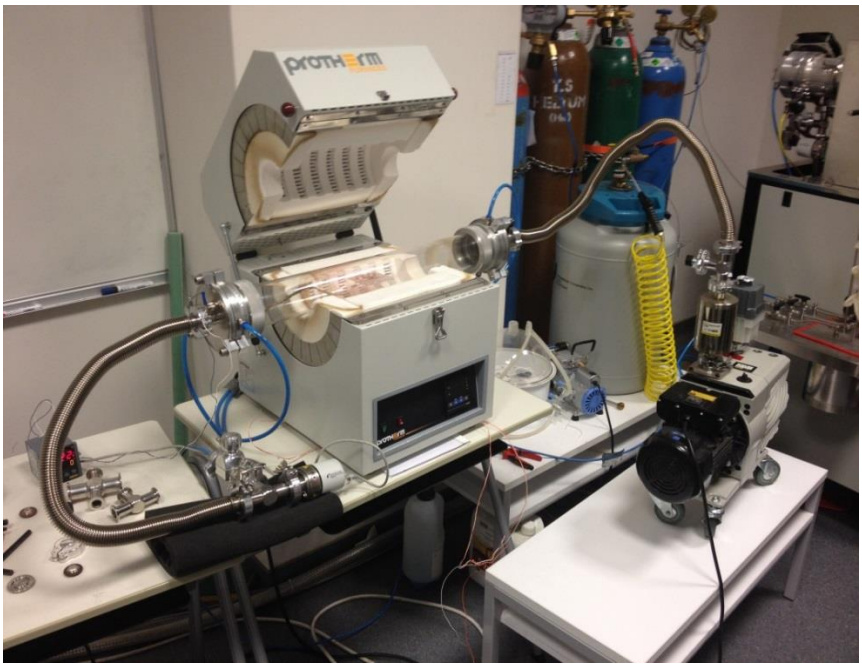

Figure 3.6.1: Vacuum furnace system with pump.

The oxygen control and backscattering thermal radiation control can not be made over 900 ^{o}C values, so the system could not be more heated. Superconductivity was not observed over 900 ^{o}C temperatures at several trials and this event proved that the furnace system wasn't controlled with sensitivity. The heat treatment and cooling rates of the average temperature were applied to be 4 ^{o}C min^{-1}.

CHAPTER 4

TESTS

4.1 MECHANICAL TESTS OF MgB_2 WIRES

4.1.1 Tensile Test

The tensile tests were executed by MTS tensile test machine. 15 cm length standard wire pieces used for measurements. Parts of a 5 cm length of wire attached to the gripping apparatus of the test device. In this case, it was only 5 cm length exposured for the tensile test. But this test system has no any special wire-cable holder apparatus. In literature, almost all of the wire tensile tests used a specific wire gripping mechanism. Thanks to this mechanism, all the measuring process gives more accurate results then without of this one. Due to the lack of specific gripping apparatus, the results are likely to be made when the statistical estimation margin of error between 5% and 10%. All of the tensile tests were performed by MTS Company Model 45 Tensile Test Machine (in Figure 4.1.1.1).

Figure 4.1.1.1: MTS Criterion Tensile Test System.

The Young's Modulus values of the MgB_2 superconductor wires were attained using the force-elongation data in the following equations. The results are given in chapter 5 in the respective table. The standard formulas used for calculation as follows:

$$\text{Engineering stress :} \quad s = \frac{F}{A_o} \tag{4.1}$$

$$\text{Engineering strain :} \quad \varepsilon = \frac{\Delta L}{L_o} \tag{4.2}$$

$$\Delta L = L - L_o \tag{4.3}$$

$$\text{Modulus of Elasticity :} \quad E = \frac{s}{\varepsilon} \tag{4.4}$$

where L_o is initial length of wire, L is elongation of wire and A_o is cross-sectional area of wire.

Tensile test results used for understanding the elastic region, the amount of elongation and the fracture points with the contribution of the following engineering stress-strain graph (in Figure 4.1.1.2).

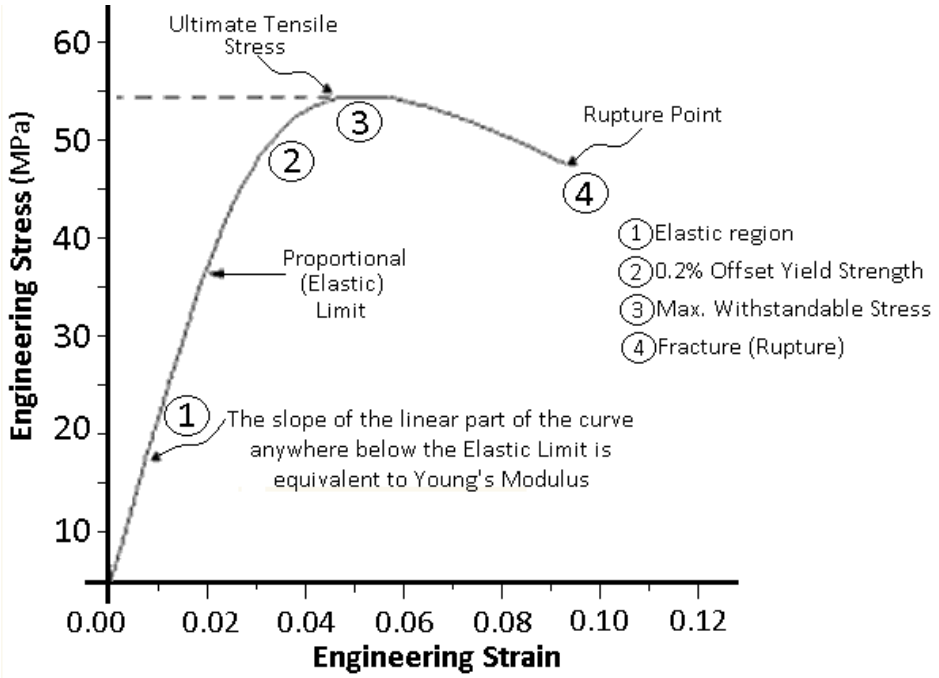

Figure 4.1.1.2: Stress-Strain Graph.

4.2 CRYOSTAT MEASUREMENTS

4.2.1 Measurement System

The superconducting transition temperature (T_c) measurements, critical current (I_c) measurements and upper critical field (H_{c2}) were executed by four-probe resistivity method using Keithley voltmeter (Model 2182A) and Current Source (Model 238) (in Figure 4.2.1.1) and a constant DC bias current of 40 mA between 4-50 K (Kelvin) temperatures.

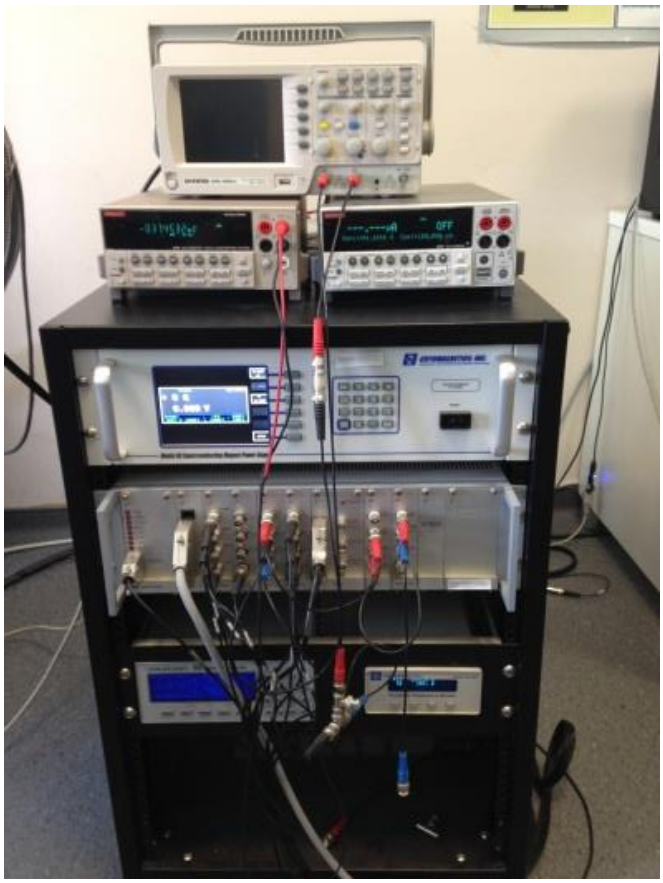

Figure 4.2.1.1: Keithley volmeter and current source with magnetic field controller.

All R-T and I-V measurements were applied in a closed Helium cycled dry cryostat system which is supplied from NanoMagnetics Company (in Figure 4.2.1.2).

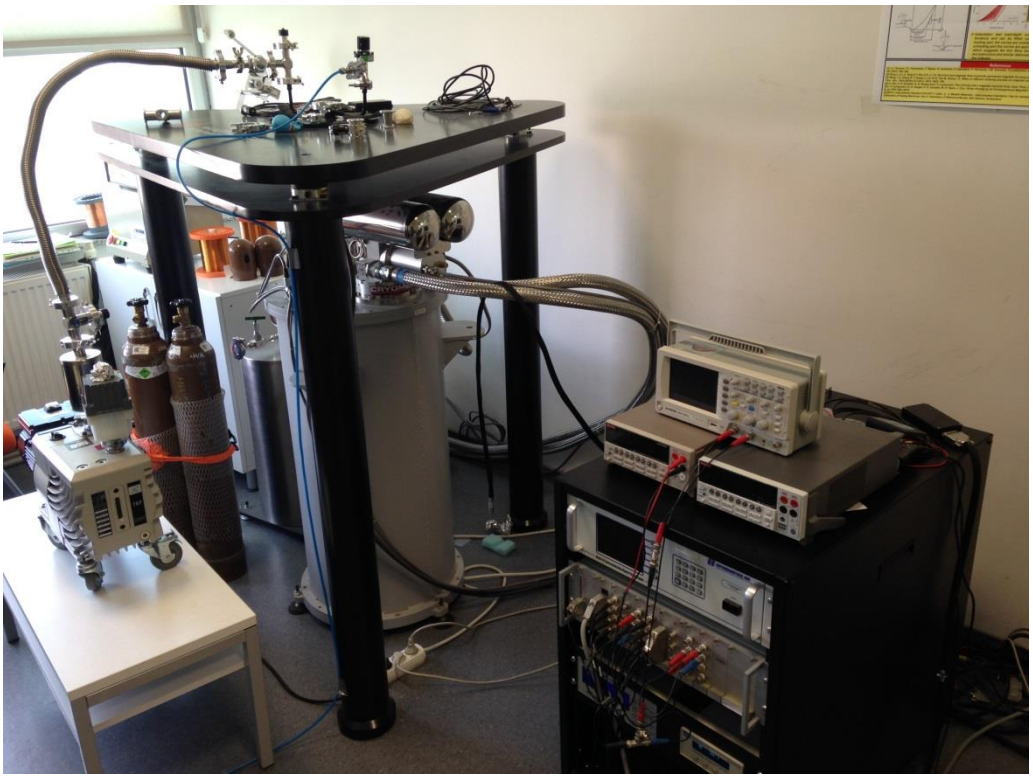

Figure 4.2.1.2: 9 Tesla Closed He Cycled Dry Cryostat System for electrical and magnetic resistivity measurements.

Closed cycle helium cooling system has a Chiller pump. It was used for the continuous water circulating operation in Figure 4.2.1.3. After 40 Kelvin is reached, a second helium pump reduces the temperature to 2 Kelvin.

Figure 4.2.1.3: a) Helium Cooler Unit , b) Water circulation Chiller System.

4.2.2 Electrical and Magnetic Resistivity Measurements.

All of the four-probe gold plated pucks are connected to the end of the thermal barrier bar (in Figure 4.2.2.1) and it's lowered into the cryostat.

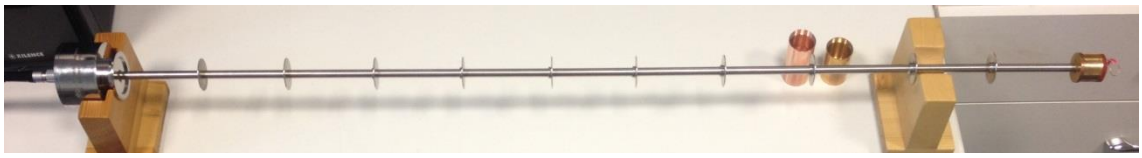

Figure 4.2.2.1: Thermal barrier insert bar.

Standard Pb-Sn (40/60) solder was used for forming the current and voltage contacts and a special design golden puck four-probe component as a connector is shown in Figure 4.2.2.2. Four-probe technique is applied as follows : Number of 1-4 pins for current connections and number of 2-3 pins for voltage connections.

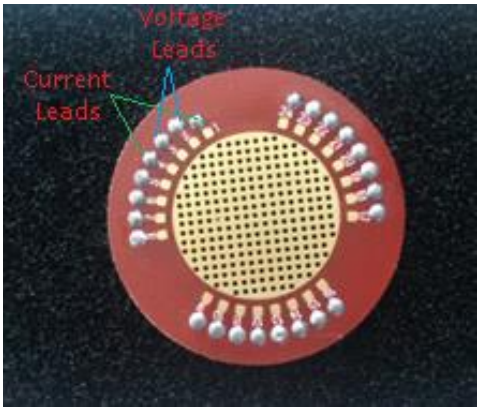

Figure 4.2.2.2: 4-probe voltage puck

Both of voltage contacts were directly soldered with solder to the copper sheath materials of the superconductor wires. All of the wire samples were insulated with vacuum grease and teflon tape for abstaining some short cuts (in Figure 4.2.2.3).

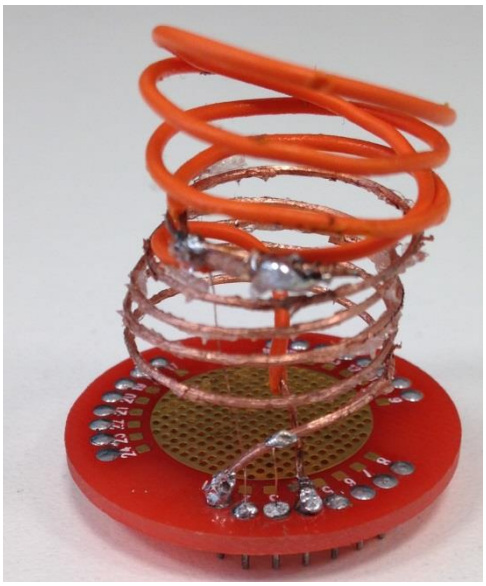

Figure 4.2.2.3: Extra copper wire bounding for preventing B_{in} flux pinning.

According to first experimental results, for accurate measurement of the sample wires must be at least 30 cm long for accurate measurements, because voltmeter can not detect less than 10^{-9} volt. But cryostat slot is not big enough to placing a vertical wire. So was required a coil geometry for wires. Another problem emerged when the coiled structures which is an extra magnetic flux (illustrated in Figure 4.2.2.4).

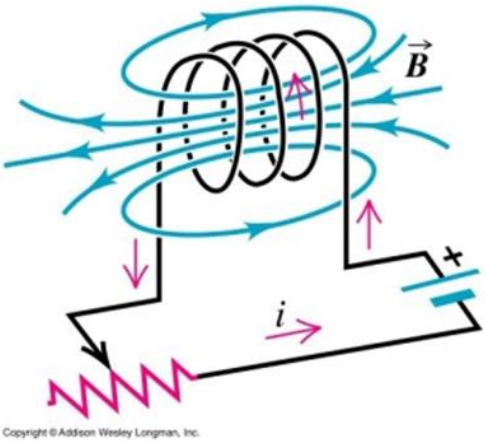

Figure 4.2.2.4: A coil that is certain current causes magnetic fluxes.

Due to the coiled form of sample, occurred magnetic fluxes over the 4-probe puck. The magnitude of this flux pinning calculation made as following Ampere Law :

$$\int_C B.dl = \mu_o.I_{enc} \quad \text{, (C represents the coil curved)} \tag{4.1}$$

$$B = \frac{\mu_o.N.I}{L} \tag{4.2}$$

$$\Phi_B = B.A \tag{4.3}$$

where $\mu_{o=4}\pi_{x10}^{-7}$, ***B*** is magnetic field, ***I*** is applied constant current, $\boldsymbol{\Phi}$ is magnitude of magnetic flux and $A = \pi r^2$ is solenoid cavity area of the wire sample. And about 400 Weber magnitude was emerged as a result of this calculation. Due to the constant current (40 mA) through the coils, the magnitude of 400 wb magnetic flux was marred the superconducting resistivity measurement. Two different methods were tried to avoid this problem. One of them, loop coil geometry in Figure . A loop was made middle of wire, it was reset the resulting extra inductance (in Figure 4.2.2.5).

.

Figure 4.2.2.5: 30 cm multicore loop wire.

The other method which is joined a second standard sheathed copper wire at the same length. This geometry also was prevented the corruptive inductance (in Figure 4.2.2.5).

Magnetic resistivity measurements were performed by using standard 4-probe contact method with DC current of 40 mA between 5-45 K temperatures under the constant magnetic field 1, 2, 3 and 4 Tesla respectively by electromagnet measurement system. DC electrical resistivity and magnetic resistivity measurement devices are shown in Figure 4.2.1. A He pump unit and a chiller mechanism was used

(in Figure 4.2.1.3) for system of cooling from room temperature to 40 Kelvin. After the reaching this value, an inner He pump system can reduce to 2 K.

The current was applied to the two outer electrical contacts and the voltage drop across the two inner electrical contacts was measured against temperature. The superconducting transition temperature (T_c) was defined as resistance equal to zero. In order to convert voltage to resistivity the calculation is made as following:

$$R = \rho \frac{L}{A} \tag{4.4}$$

$$V = I.R \tag{4.5}$$

$$\rho = R\frac{A}{L} = \frac{V.A}{I.L} \tag{4.6}$$

ρ is the resistivity, ***L*** is the length of superconductor wire, ***V*** is voltage, ***I*** is current and ***A*** is cross sectional area of wire.

Two different diameters were used while doing cross sectional area calculation :

A = 0,00049 cm^2 for 0.5 mm diameter

A = 0,00785 cm^2 for 1.0 mm diameter.

The wires used in tests 3-cores, 4-cores and powder-in-powder method one made with 1 mm diameter, while all the others were half mm.

CHAPTER 5

EXPERIMENTAL RESULTS

5.1 TENSILE TEST RESULTS

For that multiple powder forms, the names of the wire in the Table which are obtained as a result product in the experimental manufacturing.

Table 5.1.1: The title table of different wire products.

	Wire Type
W1	Commercial MgB_2 powder monocore wire
W2	Commercial MgB_2 powder multicore (7 cores) wire
W3	Mechanical Alloyed MgB_2 powder (1^{st} product) monocore wire
W4	Mechanical Alloyed MgB2 powder (1^{st} product) multicore (7 cores) wire
W5	Mechanical Alloyed MgB2 powder (2^{nd} product) monocore wire
W6	Mechanical Alloyed MgB2 powder (2^{nd} product) multicore (4 cores) wire
W7	Mechanical Alloyed MgB2 powder (2^{nd} product) multicore (3 cores) wire
W8	Commercial MgB_2 powder monocore wire (made with PIP Method)

The results obtained from the tensile tests (between the Figure 5.1.1 and Figure 5.1.5). As appears from the graphs, the vibration amplitude is emerged too much in the tensile tests. The reason for this, the presence of MgB_2 powder inside the copper sheath material can be accepted. Displacement vs. Force graphs are shown as following five graphs :

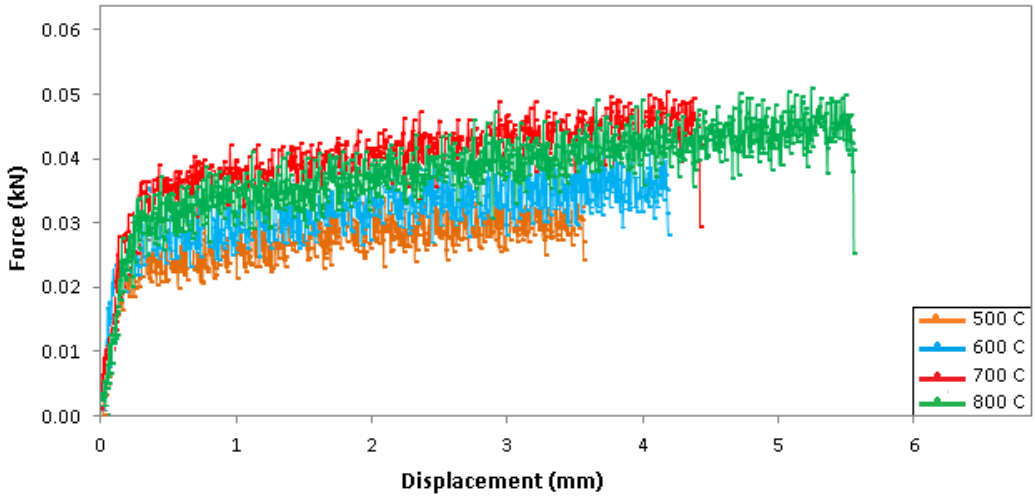

Figure 5.1.1: Force vs. Displacement graph of commercial MgB_2 powder monocore wire

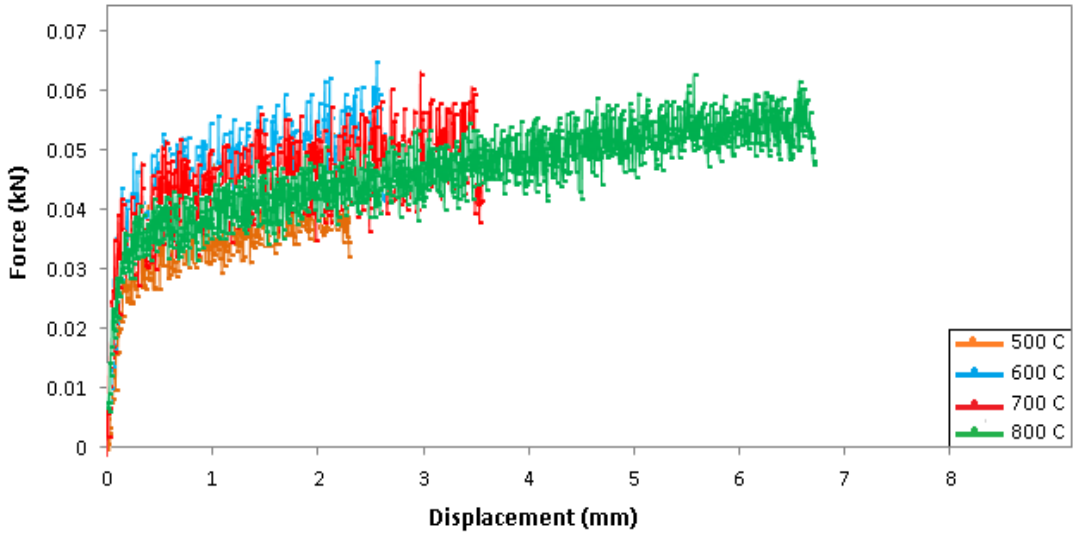

Figure 5.1.2: Force vs. Displacement graph of commercial MgB_2 powder multicore (7 cores) wire.

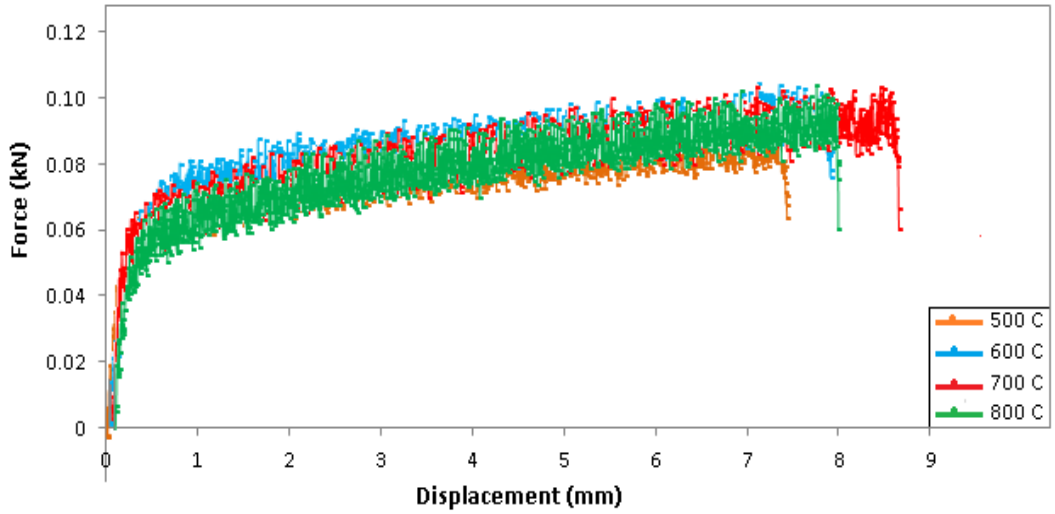

Figure 5.1.3: Force vs. Displacement graph of mechanical alloyed MgB_2 (2^{nd} group) powder monocore wire

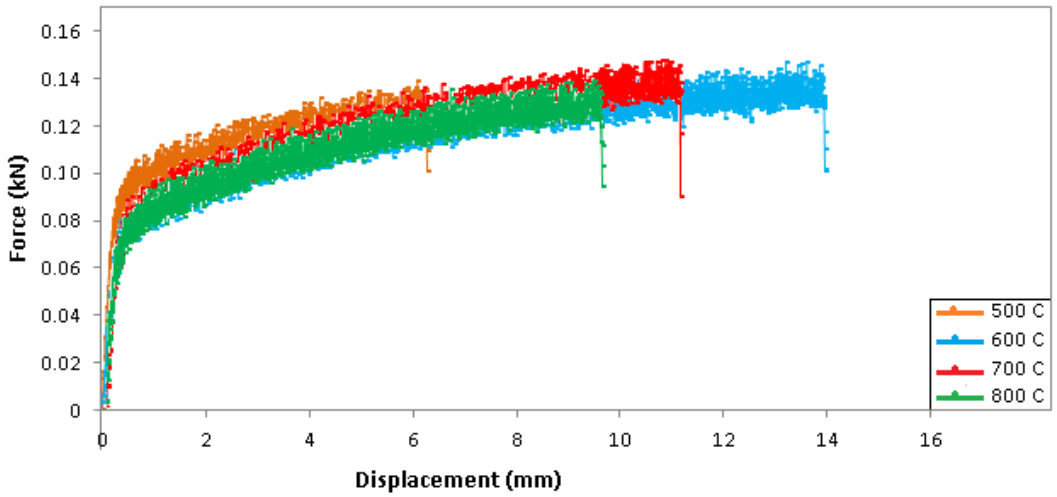

Figure 5.1.4: Force vs. Displacement graph of mechanical alloyed MgB_2 powder multicore (4 cores) wire.

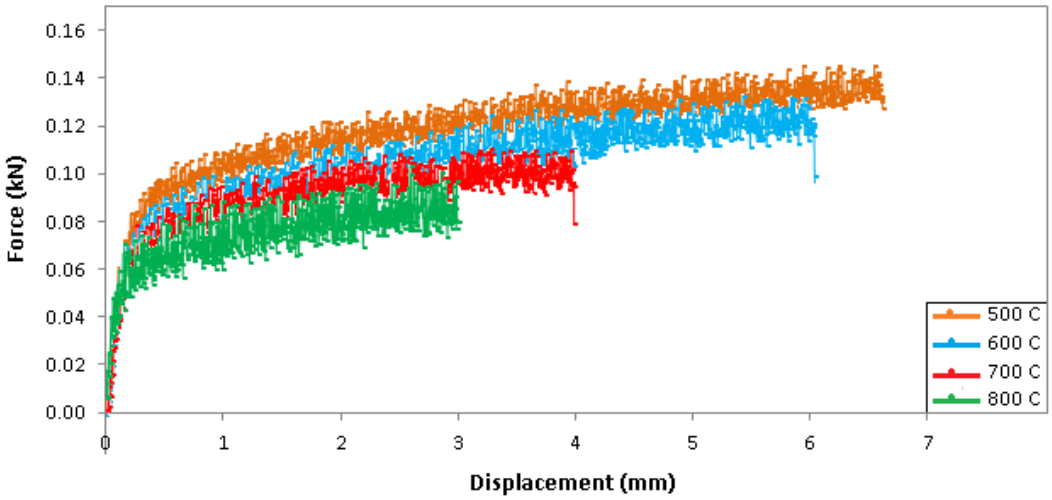

Figure 5.1.5: Force vs. Displacement graph of PIP method's monocore wire.

The Table 5.1.2 shows the amount of elongation some of the sample wires according to the sintering temperature. As seen in the table only for PIP method's wire, while the temperature increases, the elongation is reduced.

Table 5.1.2 : The elongations of some sample wires.

	Elongation (mm)				
Ann.Temp.	W1	W2	W5	W6	W8
500 C	3.75	2.32	7.45	6.25	6.72
600 C	4.27	2.74	7.94	14.05	6.12
700 C	4.48	3.52	8.65	11.25	4.05
800 C	5.61	6.78	8.02	9.75	3.02

5.2 I_c , T_c MEASUREMENTS

5.2.1 *R-T* Measurements

The first measurements were carried out for superconducting MgB_2 wires were made to understand the critical transition temperatures. Firstly received the R-T graphs without any external magnetic field (0 Tesla). Between the Figure 5.2.1.1 and Figure 5.2.1.8 are shown resistivity – temperature graphs of MgB_2 superconductor wires. R-T measurements were made between 45 K and 5 K temperatures.

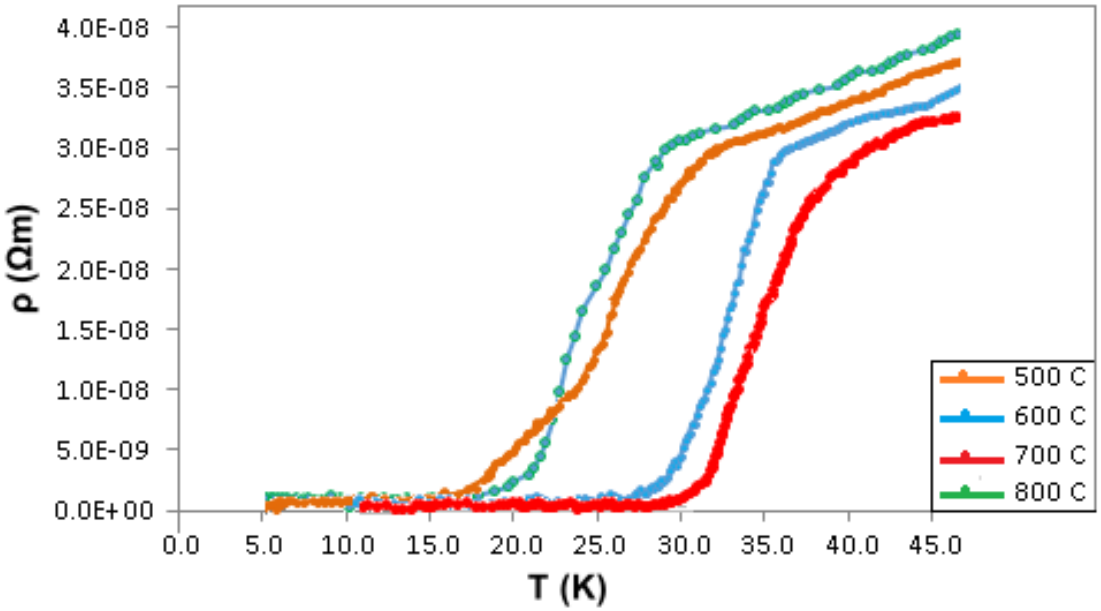

Figure 5.2.1.1: Resistivity vs. Temperature graph of the commercial MgB_2 powder monocore wire.

Table 5.2.1.1: R-T measurement values of the commercial MgB_2 powder monocore wire.

Annealing	T_c^{onset} (K)	T_c^{offset} (K)	ΔT_c (K)
500 °C-60 min.	31.3	23.8	7.5
600 °C-60 min.	35.4	29.2	6.2
700 °C-60 min.	37.2	32.6	4.6
800 °C-60 min.	28.4	22.3	6.1

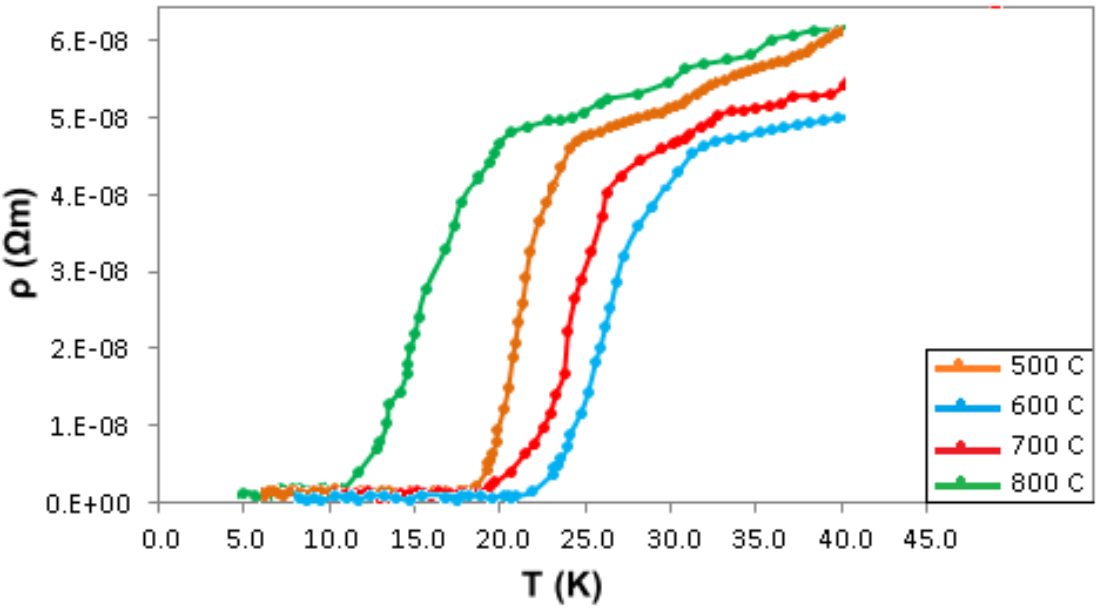

Figure 5.2.1.2 : Resistivity vs. Temperature graph of the commercial MgB_2 powder multicore (7 cores) wire.

Table 5.2.1.2: R-T measurement values of the commercial MgB_2 powder – multicore (7cores) wire.

Annealing	T_c^{onset} (K)	T_c^{offset} (K)	ΔT_c (K)
500°C-60 min.	24.2	19.3	4.9
600°C-60 min.	32.2	24.5	7.7
700°C-60 min.	26.9	20.8	6.1
800°C-60 min.	20.4	13.3	7.1

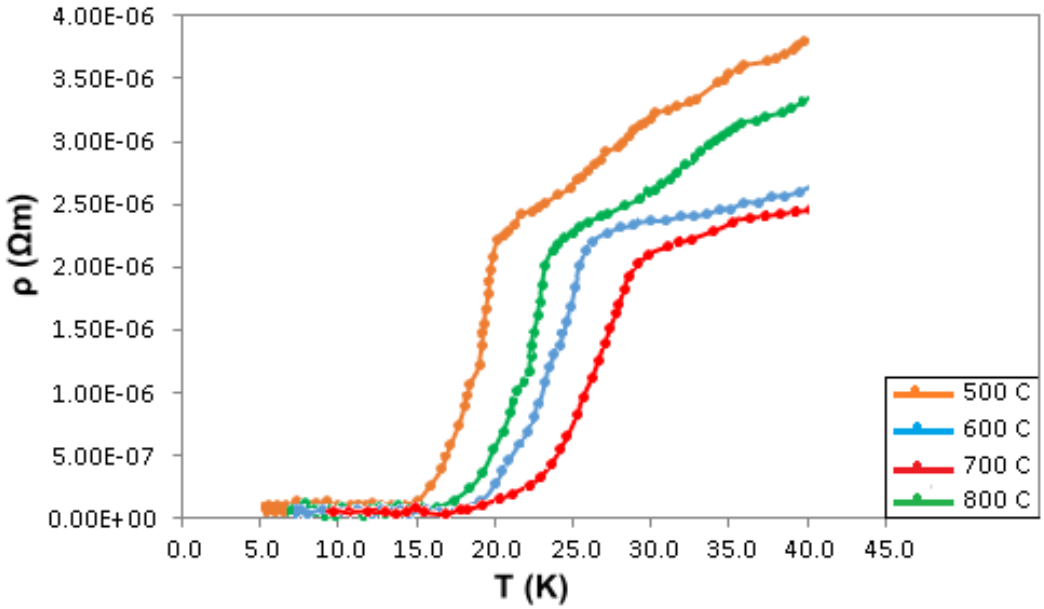

Figure 5.2.1.3: Resistivity vs. Temperature graph of the mechanical alloyed MgB_2 powder (1st product) monocore wire.

Table 5.2.1.3: R-T measurement values of the mechanical alooyed MgB_2 powder (1st product) – monocore wire.

Annealing	T_c^{onset} (K)	T_c^{offset} (K)	ΔT_c (K)
500°C-60 min.	20.2	15.7	4.5
600°C-60 min.	26.4	20.3	6.1
700°C-60 min.	30.2	23.8	6.4
800°C-60 min.	22.5	16.6	5.9

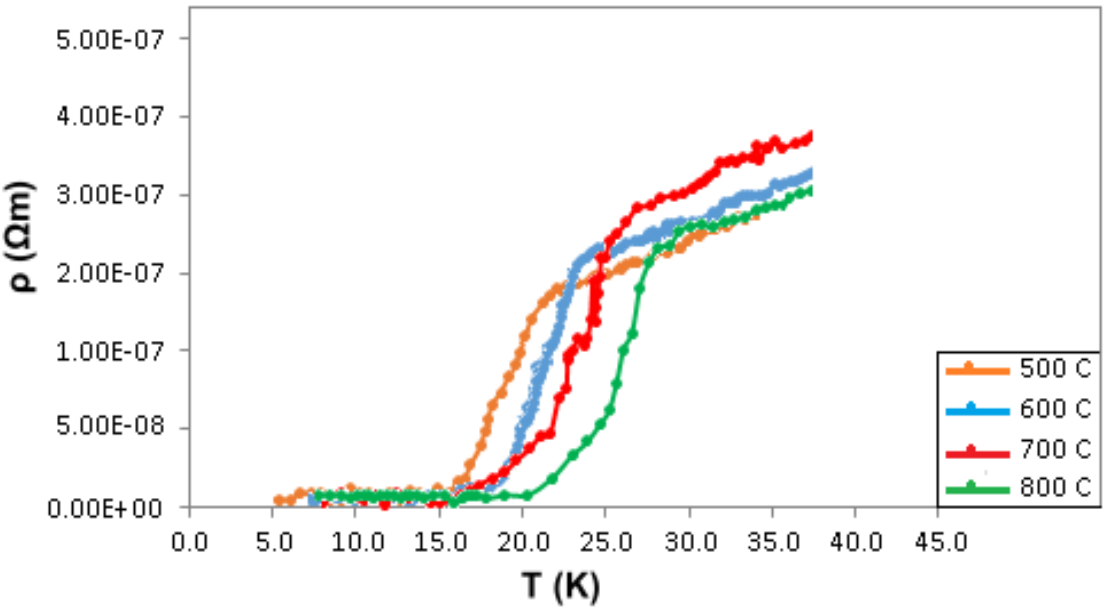

Figure 5.2.1.4: Resistivity vs. Temperature graph of the mechanical alloyed MgB_2 powder (2^{nd} product) monocore wire.

Table 5.2.1.4: R-T measurement values of the mechanical alooyed MgB_2 powder (2^{nd} product) – monocore wire.

Annealing	T_c^{onset} (K)	T_c^{offset} (K)	ΔT_c (K)
500°C-60 min.	20.3	17.1	3.2
600°C-60 min.	22.8	18.7	4.1
700°C-60 min.	26.4	19.6	6.8
800°C-60 min.	28.5	22.4	6.1

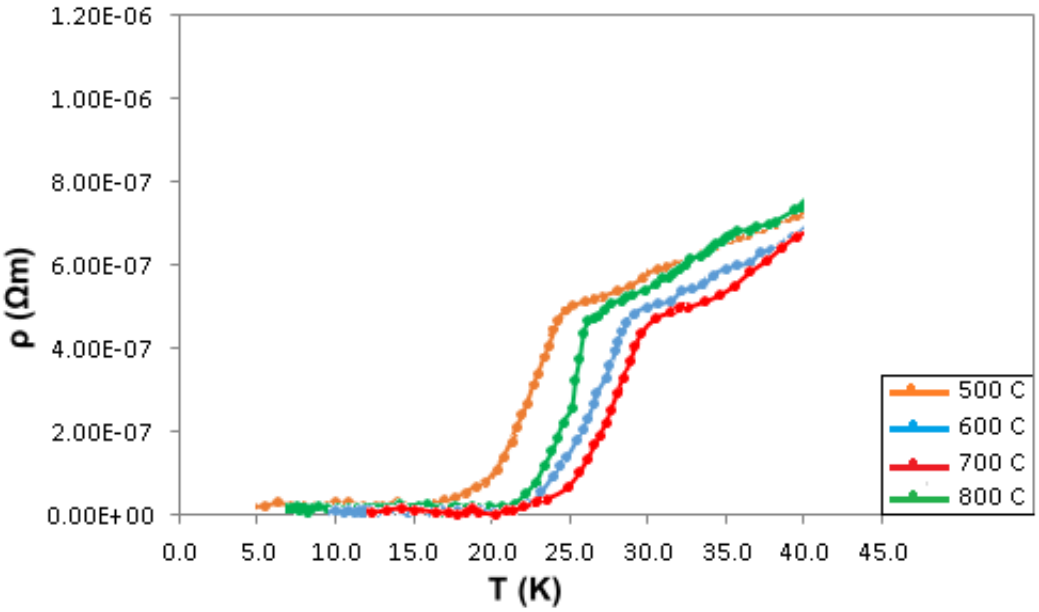

Figure 5.2.1.5: Resistivity vs. Temperature graph of the mechanical alloyed MgB_2 powder (1^{st} product) multicore (7 cores) wire.

Table 5.2.1.5: R-T measurement values of the mechanical alooyed MgB_2 powder (1^{st} product) – multicore (7 cores) wire.

Annealing	T_c^{onset} (K)	T_c^{offset} (K)	ΔT_c (K)
500°C-60 min.	22.8	18.6	4.2
600°C-60 min.	27.5	22.7	4.8
700°C-60 min.	29.4	23.9	5.5
800°C-60 min.	24.6	21.1	3.5

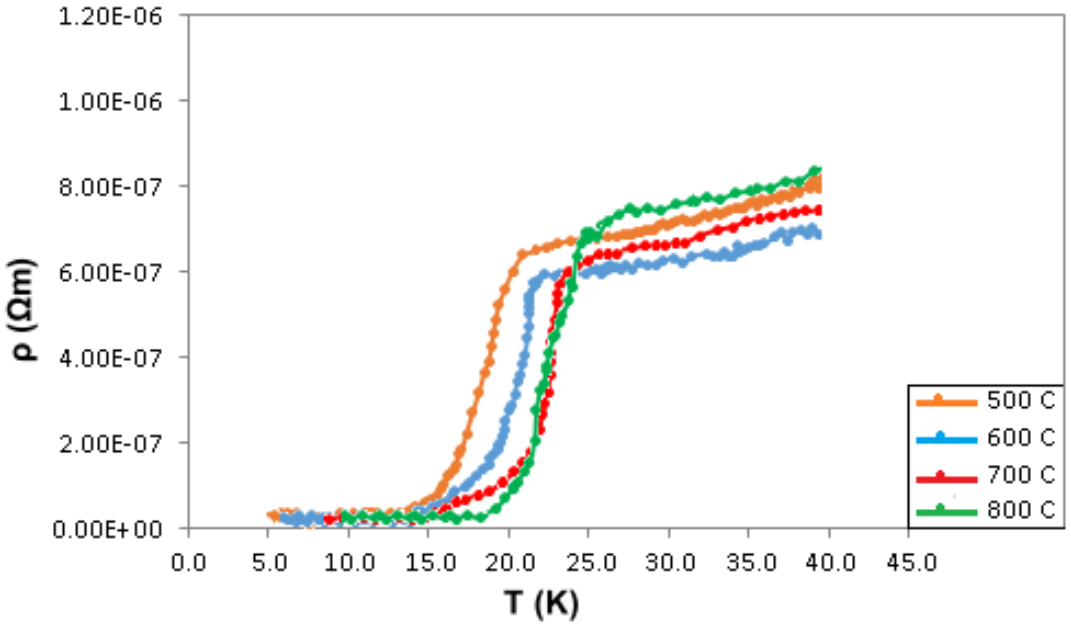

Figure 5.2.1.6: Resistivity vs. Temperature graph of the mechanical alloyed MgB_2 powder (2^{nd} product) multicore (3 cores) wire.

Table 5.2.1.6: R-T measurement values of the mechanical alooyed MgB_2 powder (2^{nd} product) – multicore (3 cores) wire.

Annealing	T_c^{onset} (K)	T_c^{offset} (K)	ΔT_c (K)
500°C-60 min.	20.2	15.8	4.4
600°C-60 min.	22.3	17.4	4.9
700°C-60 min.	24.5	17.9	6.6
800°C-60 min.	25.4	20.6	4.8

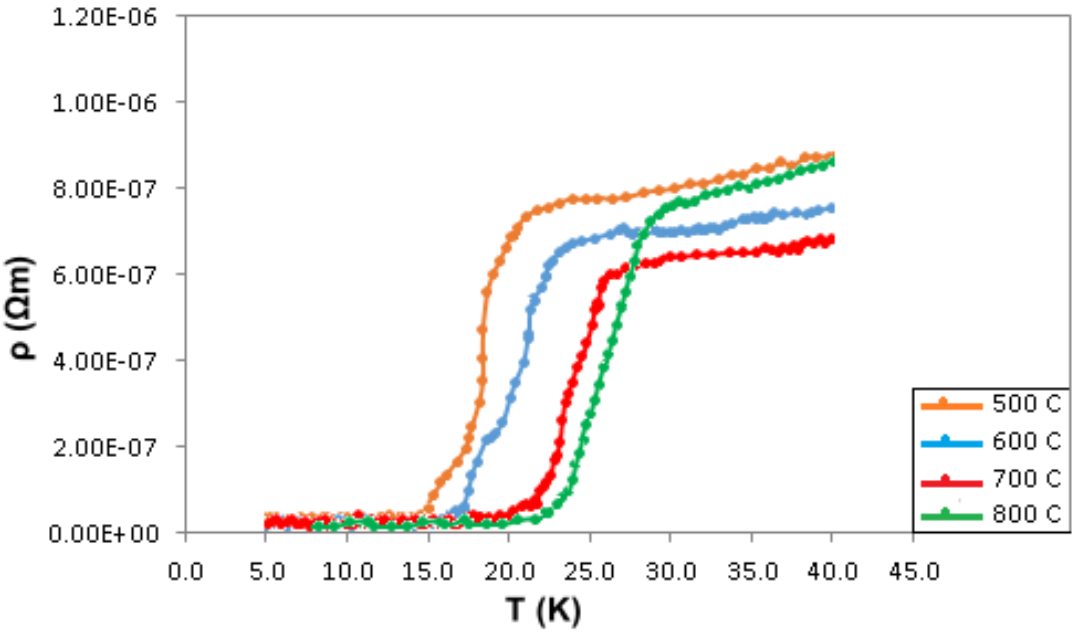

Figure 5.2.1.7: Resistivity vs. Temperature graph of the mechanical alloyed MgB_2 powder (2^{nd} product) multicore (4 cores) wire.

Table 5.2.1.7: R-T measurement values of the mechanical alooyed MgB_2 powder (2^{nd} product) – multicore (4 cores) wire.

Annealing	T_c^{onset} (K)	T_c^{offset} (K)	ΔT_c (K)
500 °C-60 min.	20.2	15.8	4.4
600 °C-60 min.	23.5	18.7	4.8
700 °C-60 min.	26.1	22.6	3.5
800 °C-60 min.	30.5	23.8	6.7

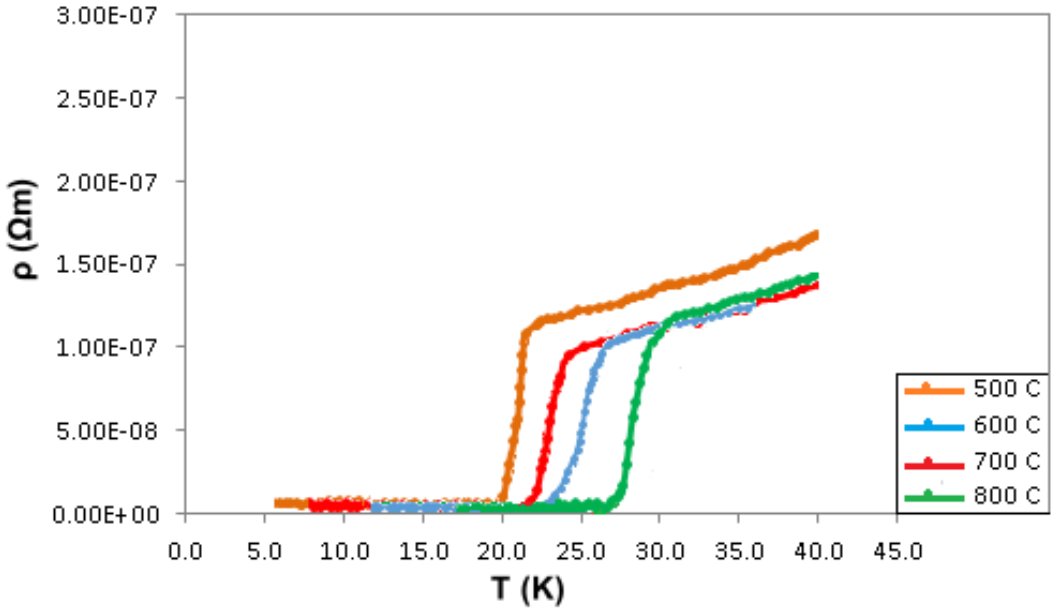

Figure 5.2.1.8: Resistivity vs. Temperature graph of the Powder-in-Powder Method's monocore wire.

Table 5.2.1.8: R-T table for PIP method's MgB_2 powder wire

Annealing	T_c^{onset} (K)	T_c^{offset} (K)	ΔT_c (K)
500°C-60 min.	21.5	18.4	3.1
600°C-60 min.	24.6	21.3	3.3
700°C-60 min.	22.7	18.8	3.9
800°C-60 min.	30.2	26.7	3.5

5.2.2 *I-V* Measurements

The current-voltage characteristic of the MgB_2 wire samples were measured at 10K, 15K, 20K, 25K and 30 K respectively. I-V measurements were performed with the standart four-probe (in Figure 4.2.2.2) technique and between the Figures 5.2.2.1 and 5.2.2.10 show I-V graphs. The system applying current range was applied as 0-40 mA. When the I_c graphs analysis, results show up the I_c values decrease as the temperature increased.

According to measurements, highest critical current values were taken for multicore (7 cores) wire of commercial MgB_2 powder at 600 ^oC annealing temperature and multicore (4 cores) wire of mechanical alloyed MgB_2 powder at 800 ^oC annealing temperature.

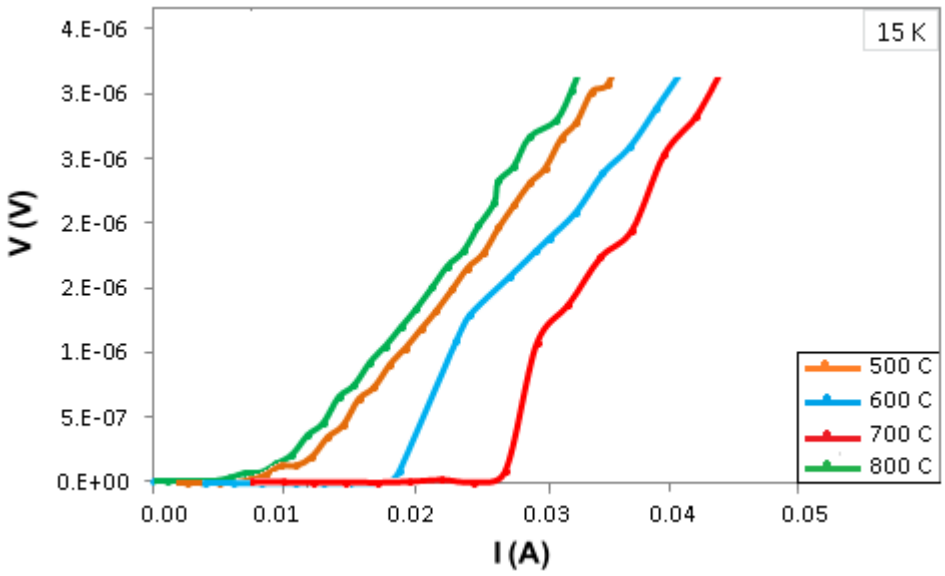

Figure 5.2.2.1: I-V measurement graph of the commercial MgB_2 powder monocore wire (at 15K).

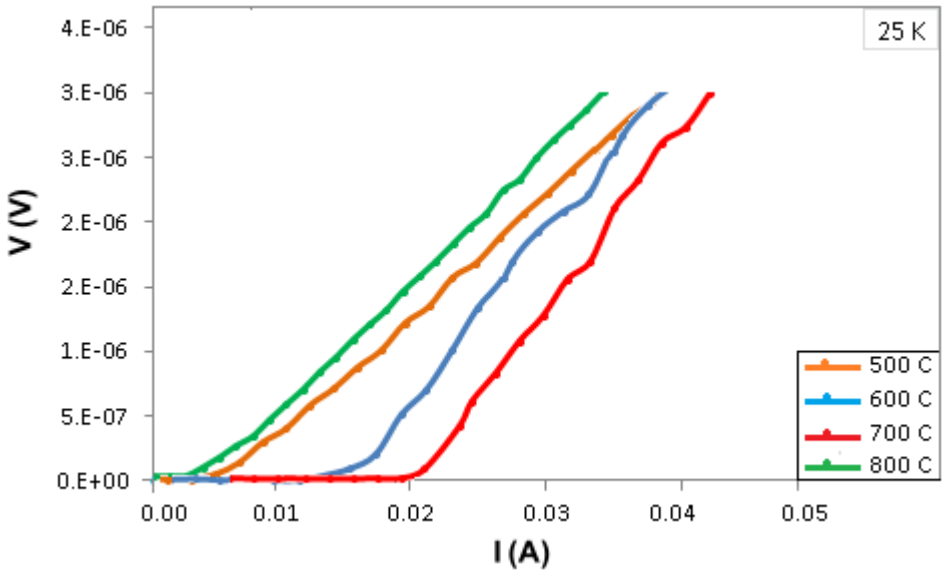

Figure 5.2.2.2: I-V measurement graph of the commercial MgB_2 powder monocore wire (at 25K).

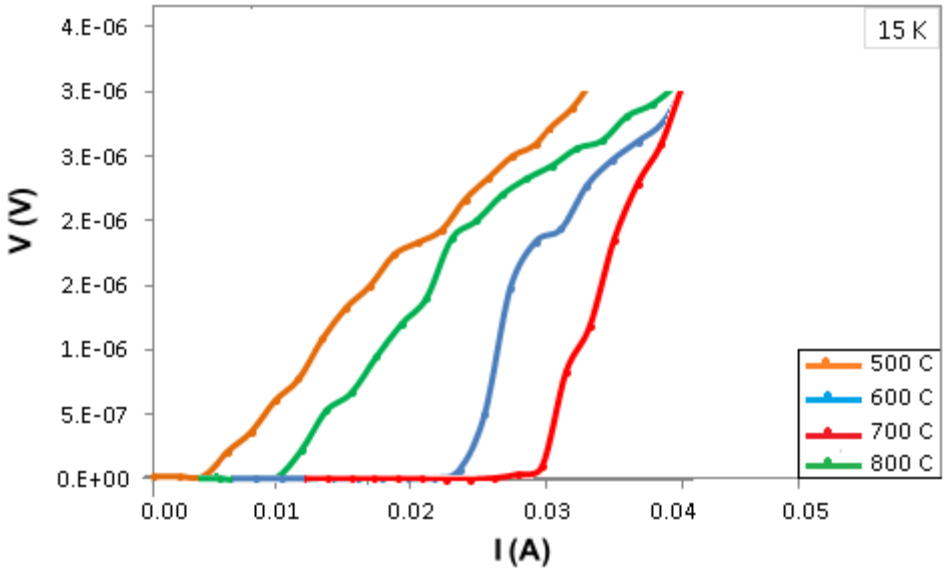

Figure 5.2.2.3: I-V measurement graph of the mechanical alloyed MgB_2 powder monocore wire (at 15K).

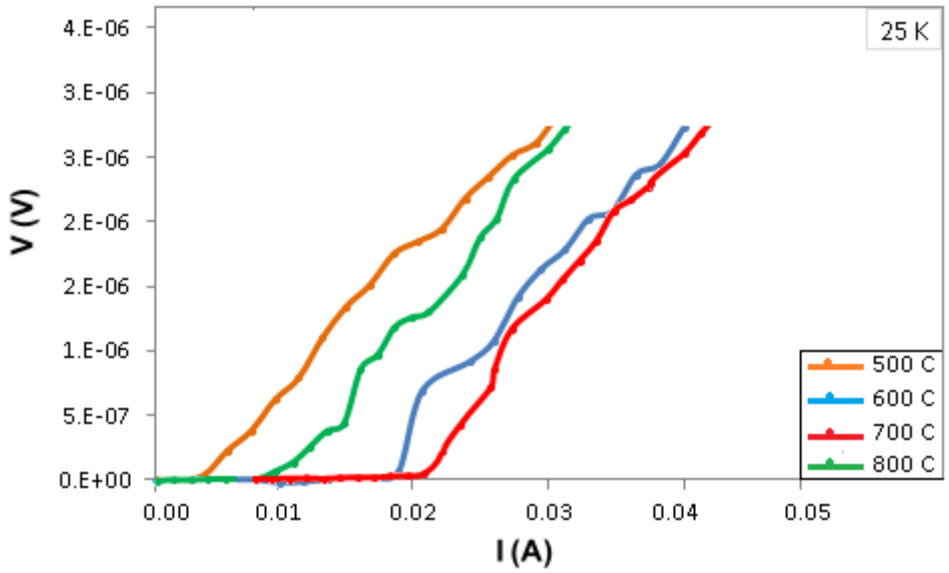

Figure 5.2.2.4: I-V measurement graph of the mechanical alloyed MgB_2 powder monocore wire (at 25K).

Since delta button is released as open while taking I-V values of the multicore wires, the initial values seems negative. However, the critical current values are read from the graphs obviously.

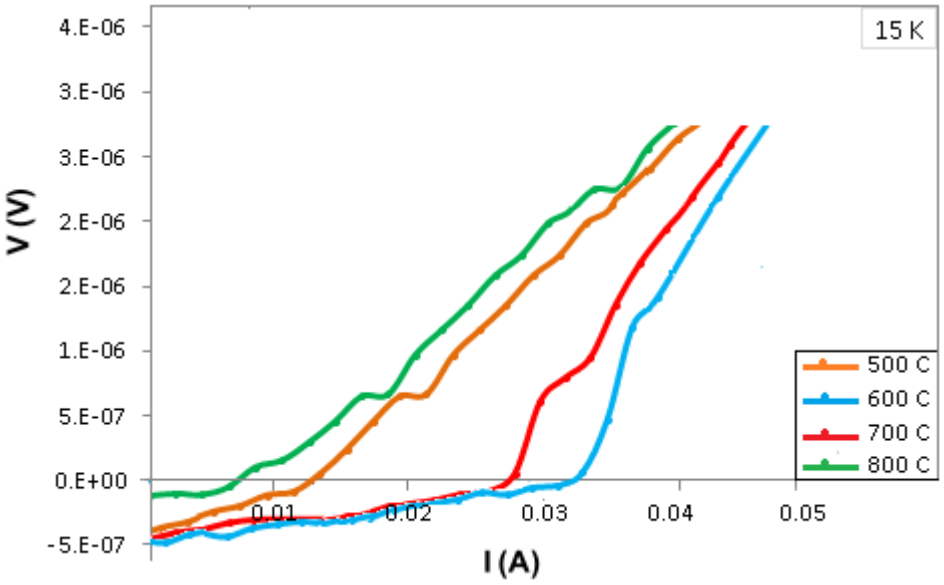

Figure 5.2.2.5: I-V measurement graph of the commercial MgB_2 powder multicore (7 cores) wire (at 15K).

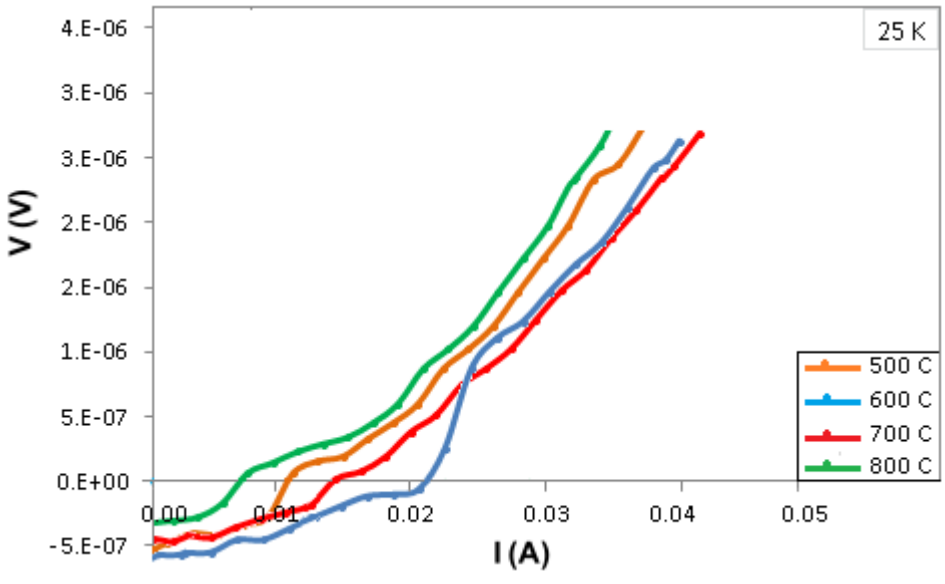

Figure 5.2.2.6: I-V measurement graph of the commercial MgB2 powder multicore (7 cores) wire (at 25K).

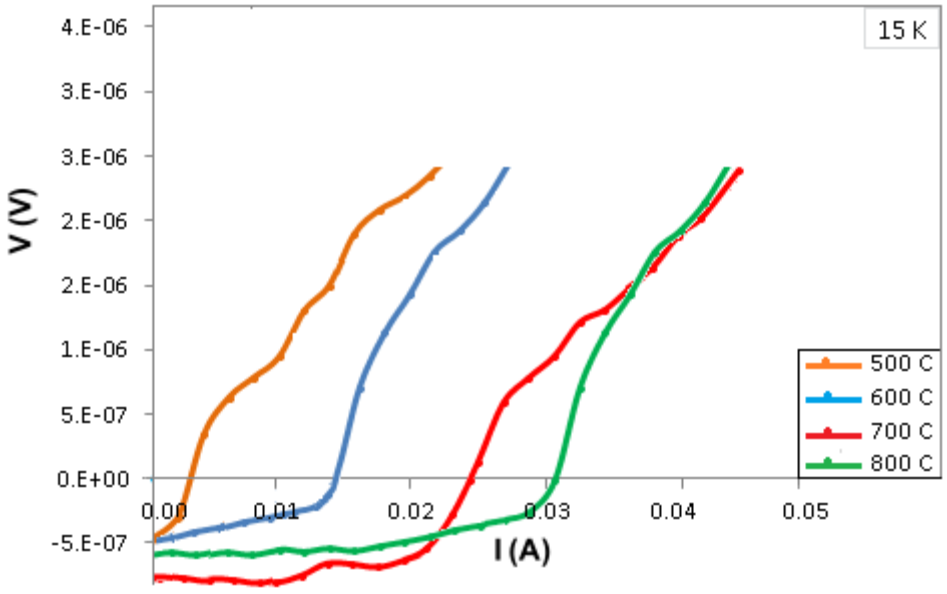

Figure 5.2.2.7: I-V measurement graph of the mechanical alloyed MgB_2 powder multicore (4 cores) wire (at 15K).

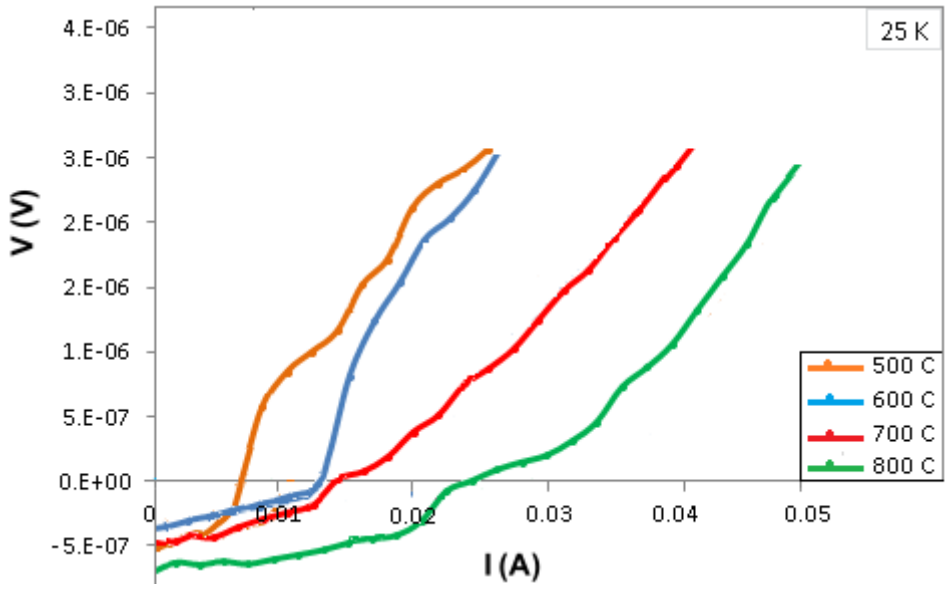

Figure 5.2.2.8: I-V measurement graph of the mechanical alloyed MgB_2 powder multicore (4 cores) wire (at 25K).

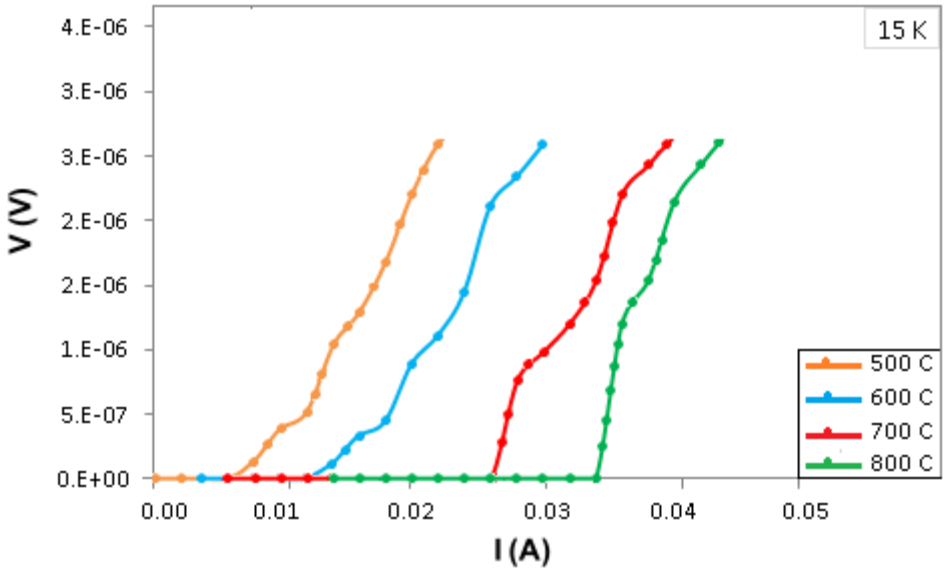

Figure 5.2.2.9: I-V measurement graph of the PIP method monocore wire at 15 K.

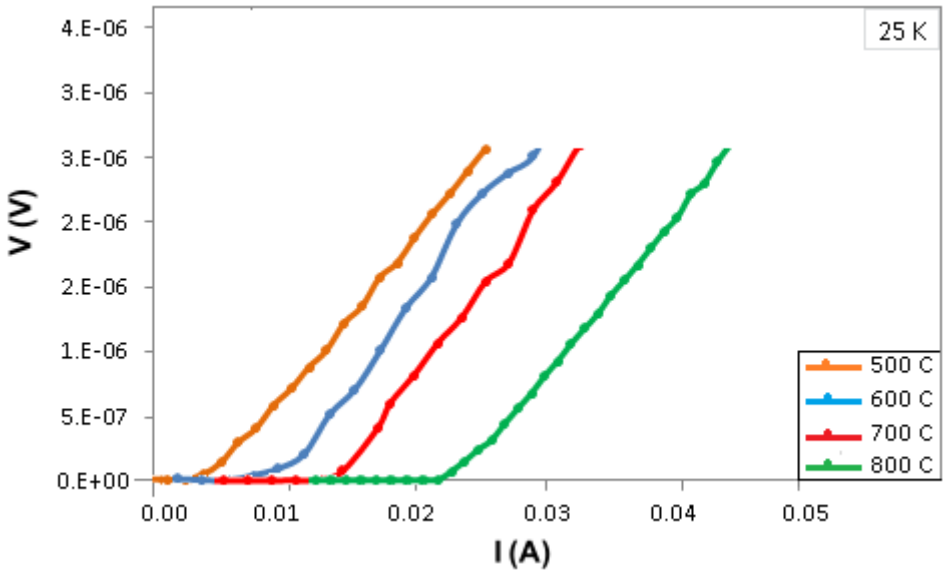

Figure 5.2.2.10: I-V measurement graph of the PIP method monocore wire at 25 K.

Electrical field vs. Critical Current Density graphs were consisted from I-V data. One of the most significant feature of a superconductor is the critical current density (J_c). The length of the superconductor sample wires were 30 cm which are used to obtain E-J_c graphs. Centimeter unit is used in graphs. Between the Figure 5.2.2.11 and Figure 5.2.2.20 are shown the E-J_c graphs.

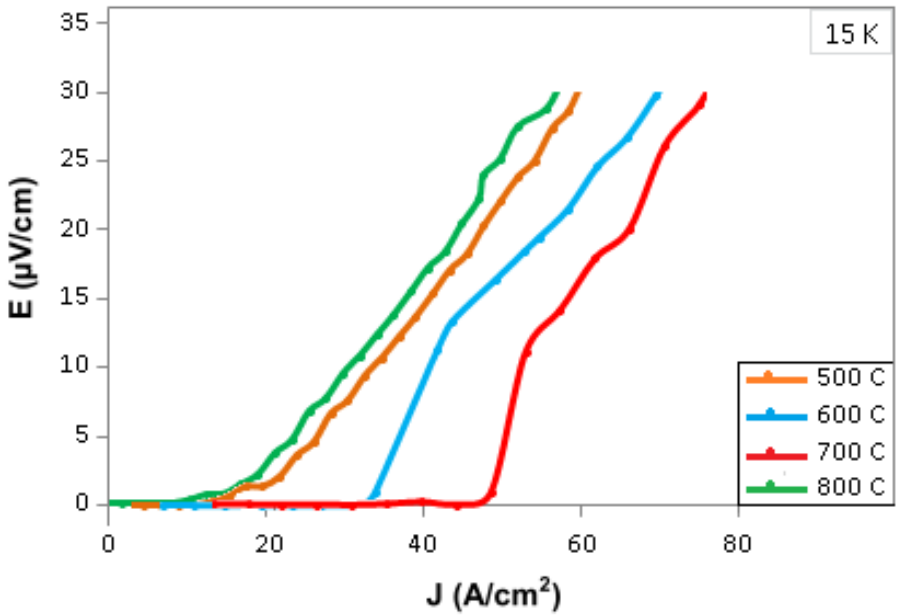

Figure 5.2.2.11: E-J_c measurement graph of the commercial MgB_2 powder monocore wire at 15K.

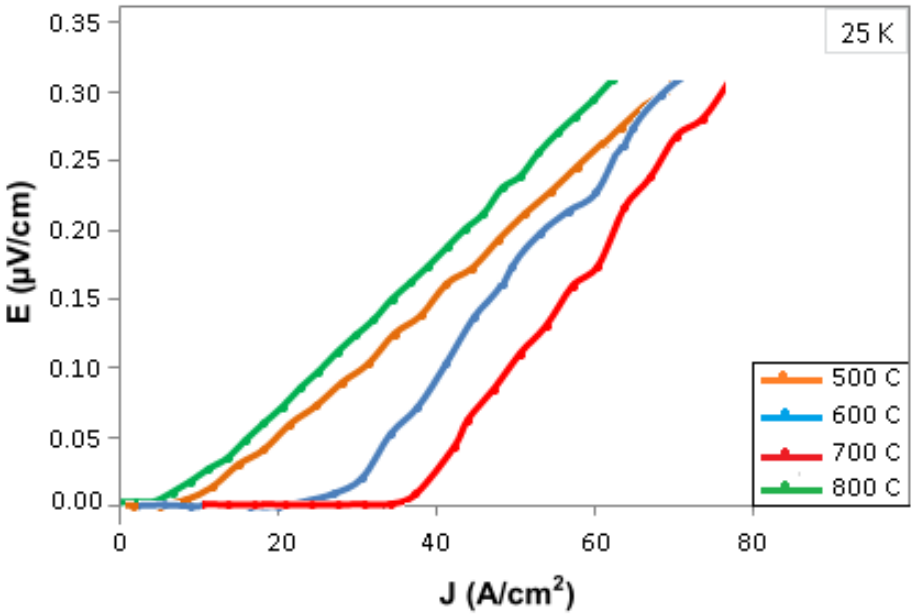

Figure 5.2.2.12: E-J_c measurement graph oh the commercial MgB_2 powder monocore wire at 25K.

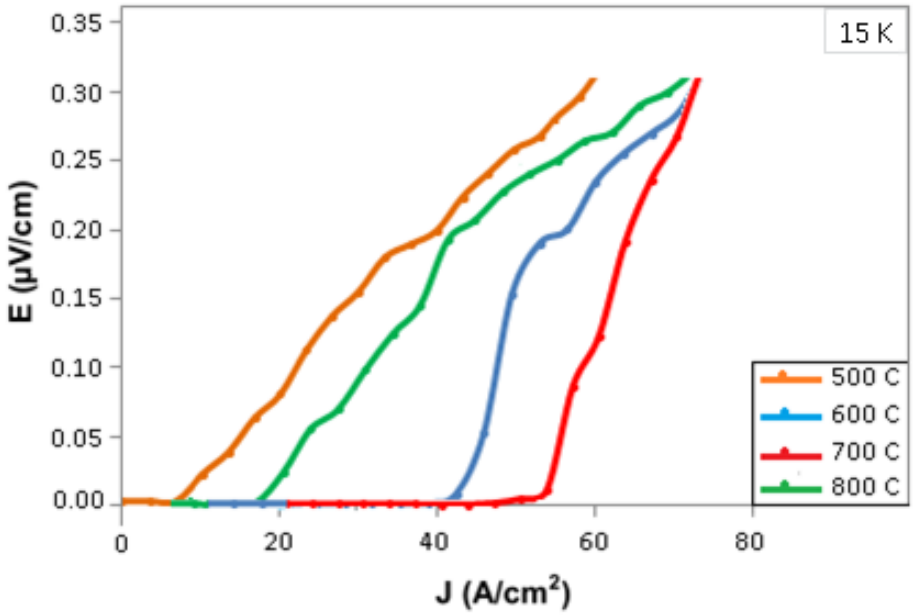

Figure 5.2.2.13: E-J_c measurement graph of the mechanical alloyed MgB_2 powder monocore wire at 15K.

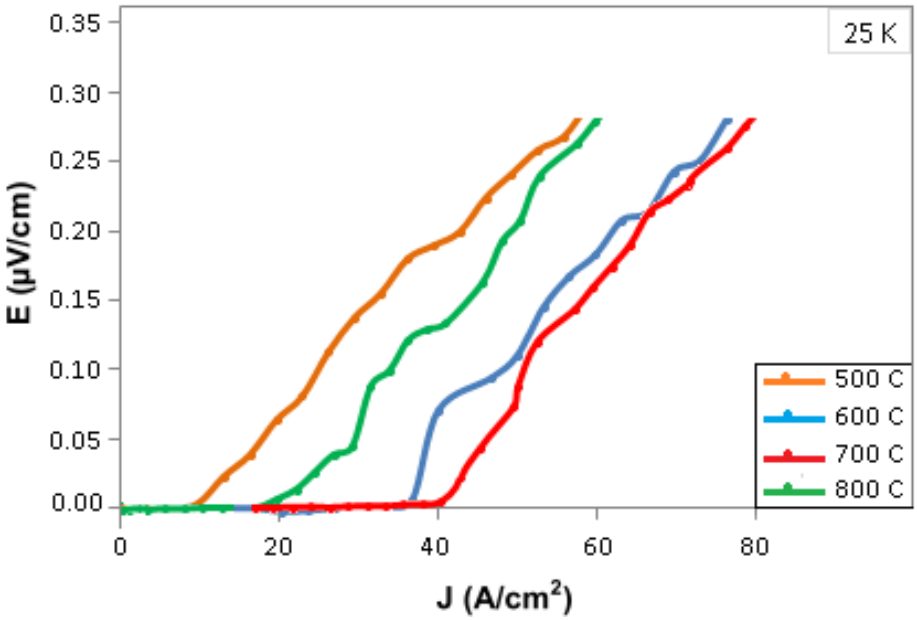

Figure 5.2.2.14: E-J_c measurement graph of the mechanical alloyed MgB_2 powder monocore wire at 25K.

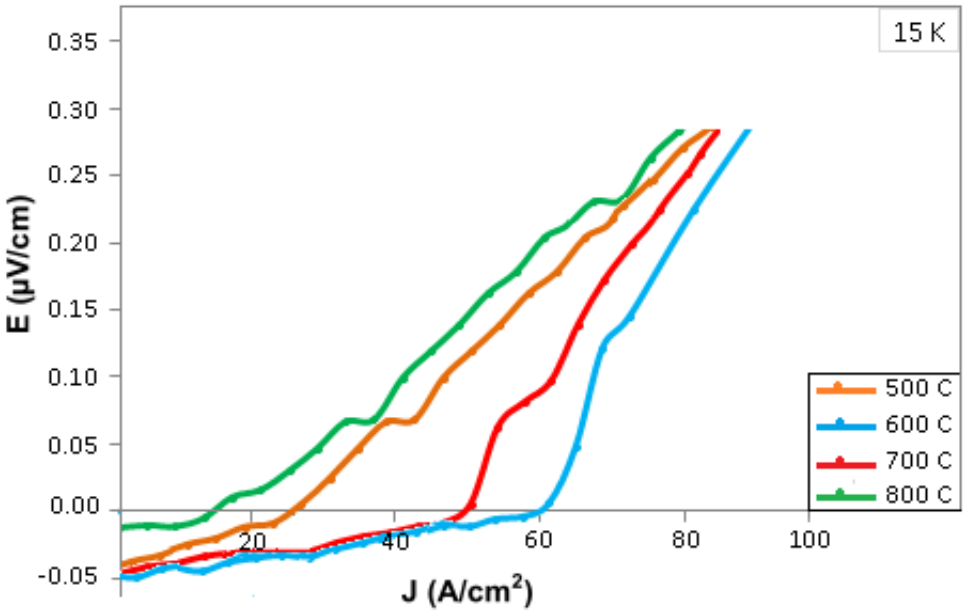

Figure 5.2.2.15: E-J_c measurement graph of the commercial MgB_2 powder multicore (7 cores) wire at 15K.

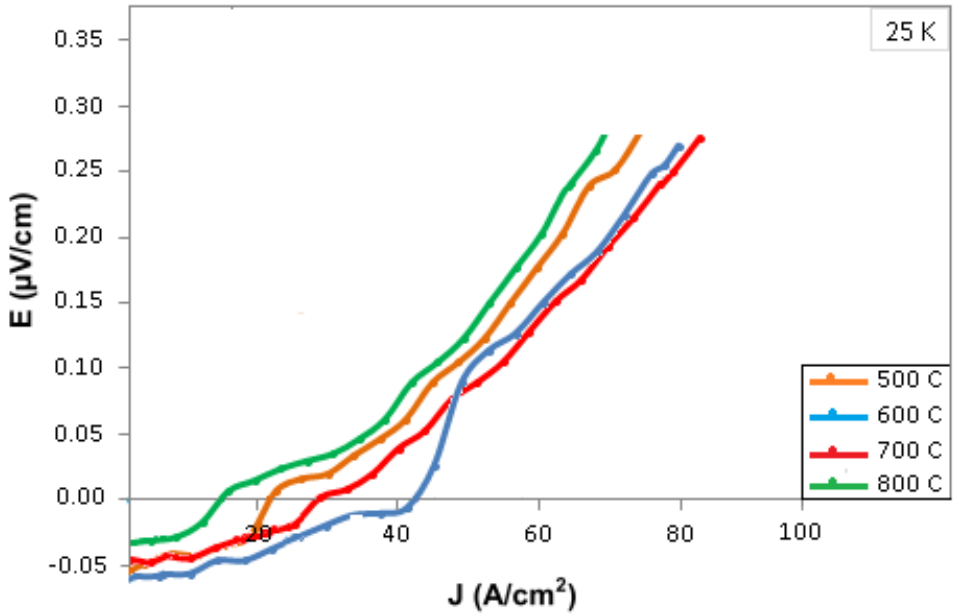

Figure 5.2.2.16: E-J_c measurement graph of the commercial MgB_2 powder multicore (7 cores) wire at 25K.

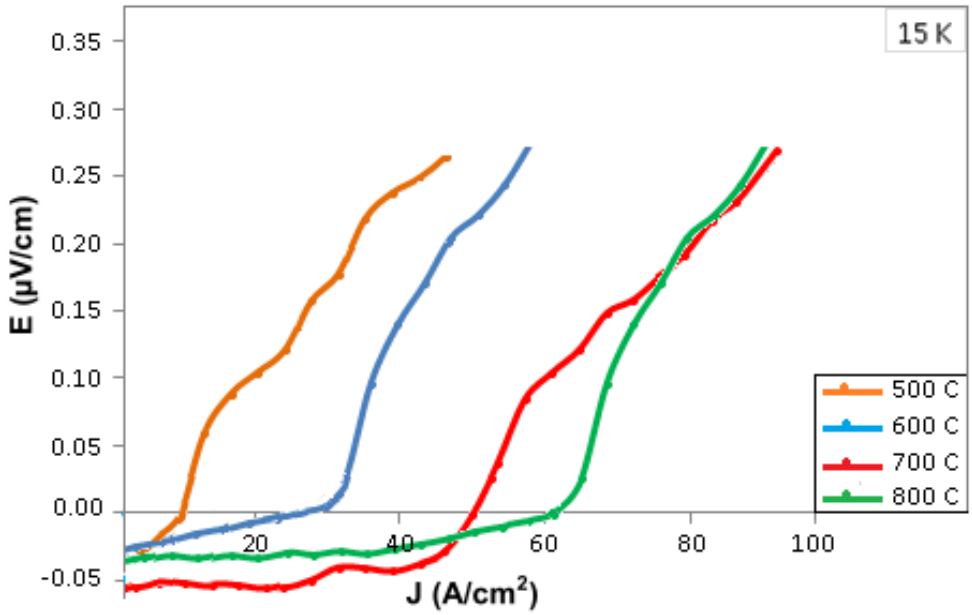

Figure 5.2.2.17: E-J_c measurement graph of the mechanical alloyed MgB_2 powder multicore (4 cores) wire at 15K.

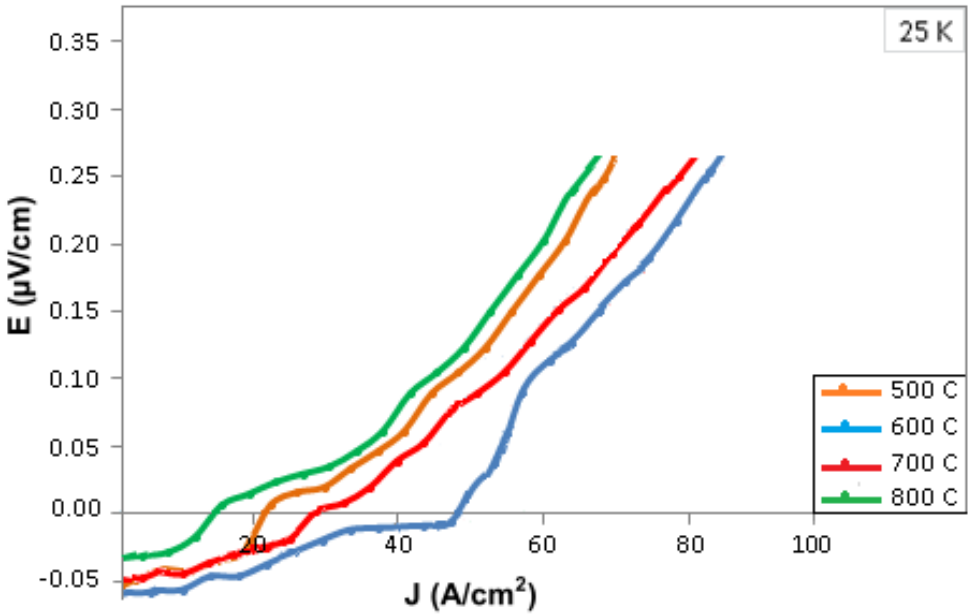

Figure 5.2.2.18: E-J_c measurement graph of the mechanical alloyed MgB_2 powder multicore (4 cores) wire at 25K

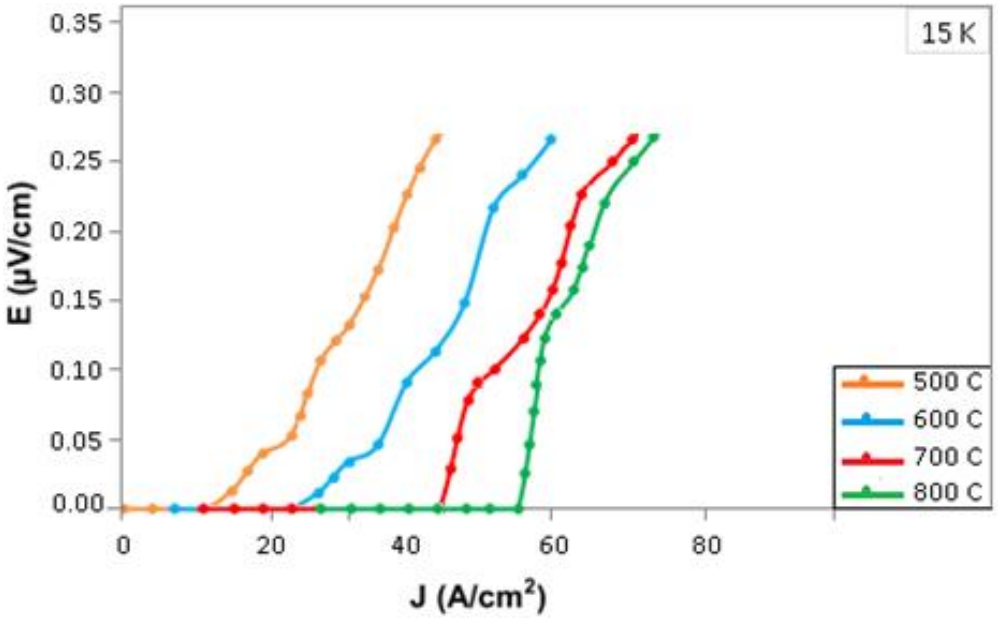

Figure 5.2.2.19: E-J_c measurement graph of the PIP method monocore wire at 15 K.

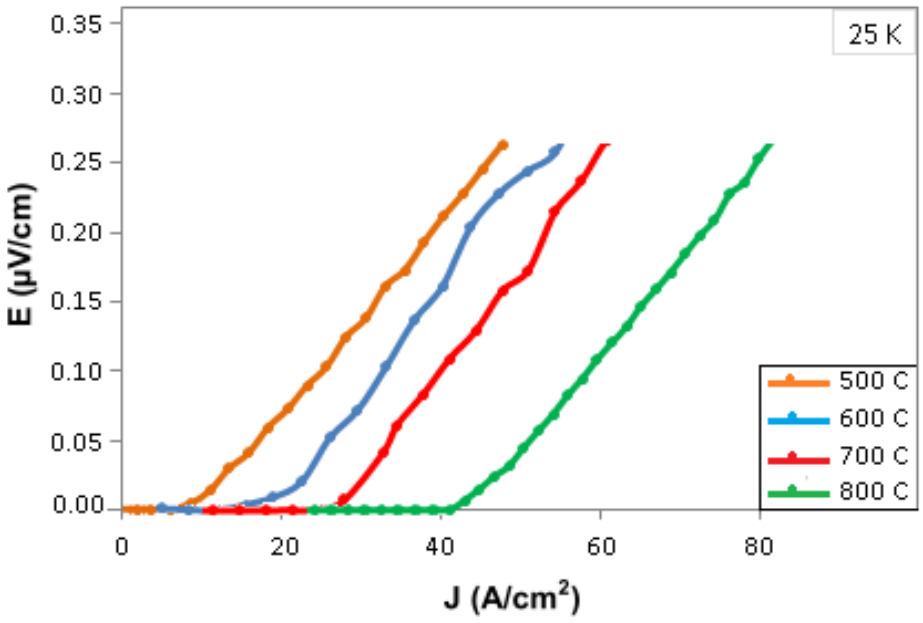

Figure 5.2.2.20: E-J_c measurement graph of the PIP method monocore wire at 25 K.

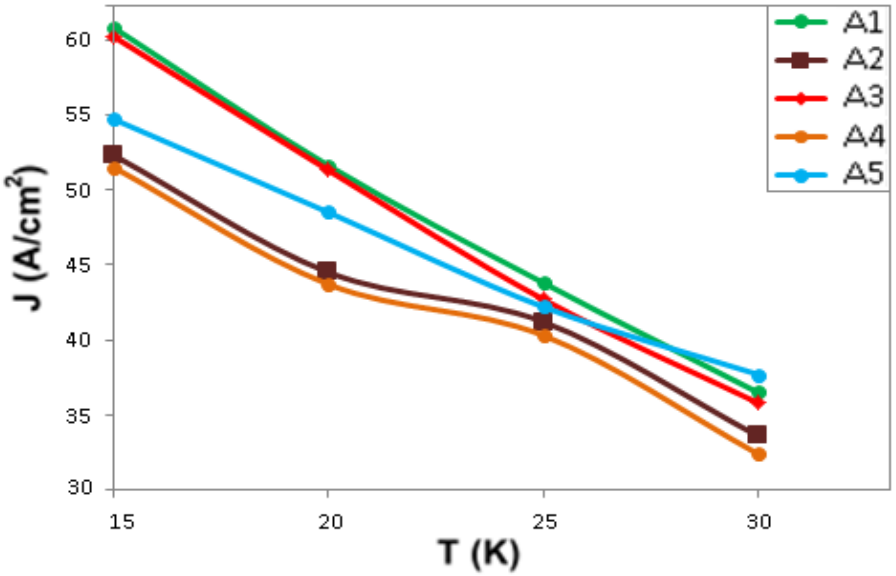

A1	Multicore (7 cores) wire made with commercial MgB_2 powder (annealed at 600 °C)
A2	Monocore wire made with commercial MgB_2 powder (annealed at 700 °C)
A3	Multicore (4 cores) wire made with mechanical alloyed MgB_2 powder (annealed at 800 °C)
A4	Monocore wire made with mechanical alloyed MgB_2 powder (annealed at 700 °C)
A5	Monocore wire made with Powder-in-Powder method (annealed at 800 °C)

Figure 5.2.2.21: Critical current density vs. temperature graph of some wire samples.

Table 5.2.2.1: Table of J_c values of the sample wires.

	J_c (A/cm^2)			
	15K	20K	25K	30K
A1	60.8	51.6	43.8	36.5
A2	52.3	44.5	41.2	33.6
A3	60.2	51.3	42.7	35.8
A4	51.5	43.7	40.3	32.4
A5	54.7	48.5	42.2	34.7

5.3 MAGNETORESISTIVITY MEASUREMENTS

The upper critical field measurements were performed between 1 Tesla and 4 Tesla applying external magnetic field. Over 4 Tesla magnetic fields could not be applied since the accuracy of the measurements were not valuable. Between the Figure 5.2.3.1 and Figure 5.2.3.8 are belong to the monocore wire made with commercial MgB_2 powder and monocore wire made with mechanical alloyed MgB_2 powder respectively.

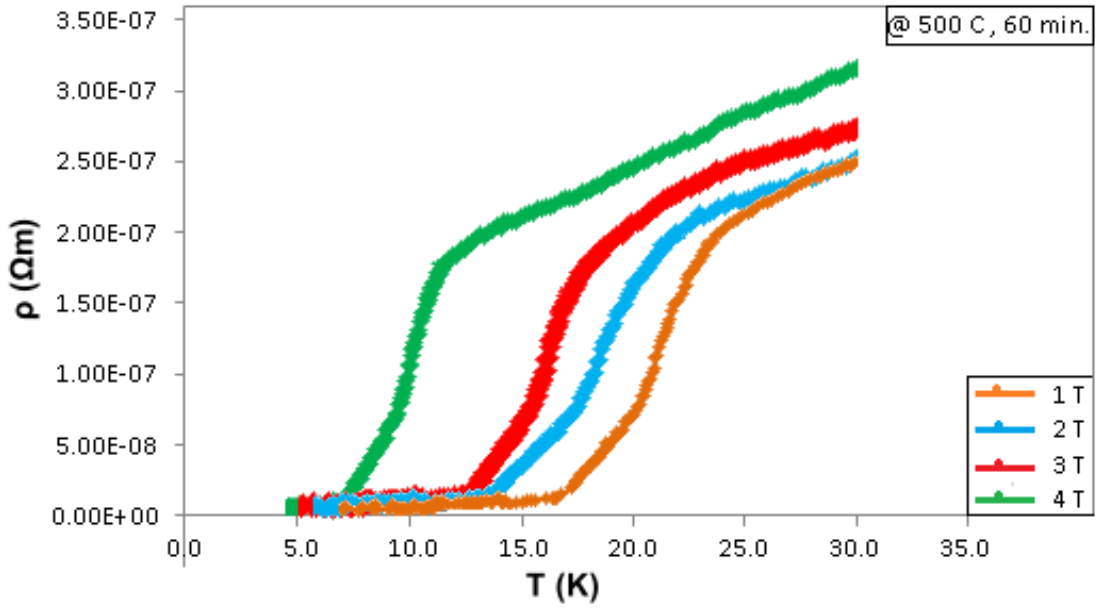

Figure 5.2.3.1: Resistivity vs. Temperature graph under the varied (1 – 4 Tesla) external magnetic field and 500 ^{o}C – 60 min. sintering value of the monocore wire made with commercial MgB_2 powder.

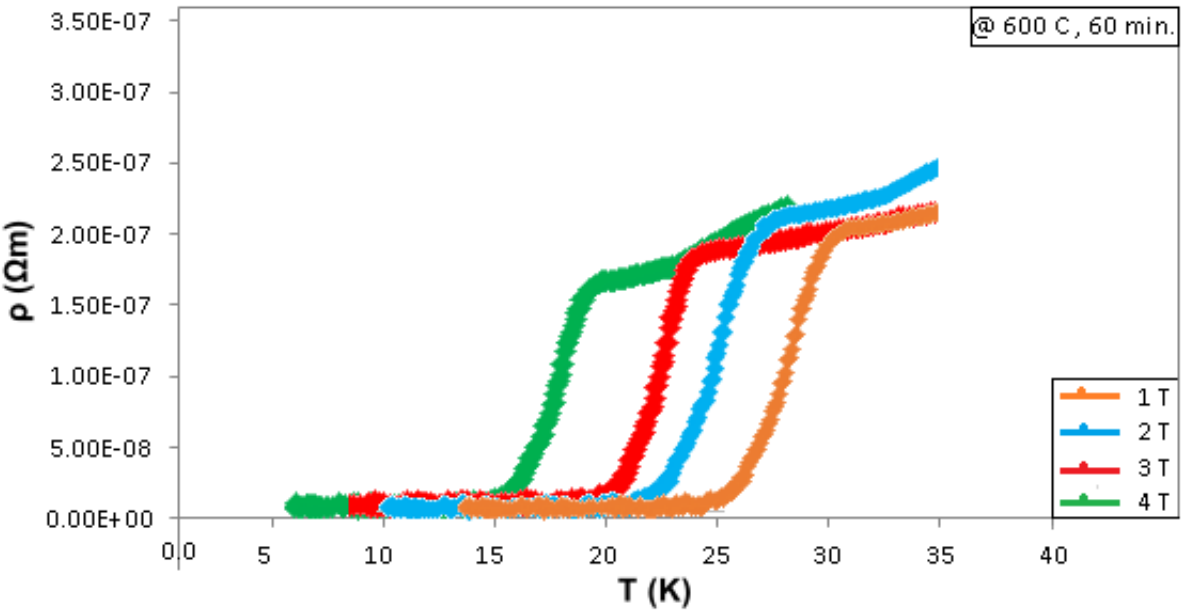

Figure 5.2.3.2: Resistivity vs.Ttemperature graph under the varied (1 – 4 Tesla) external magnetic field and 600 ^{o}C – 60 min. sintering value of the monocore wire made with commercial MgB_2 powder.

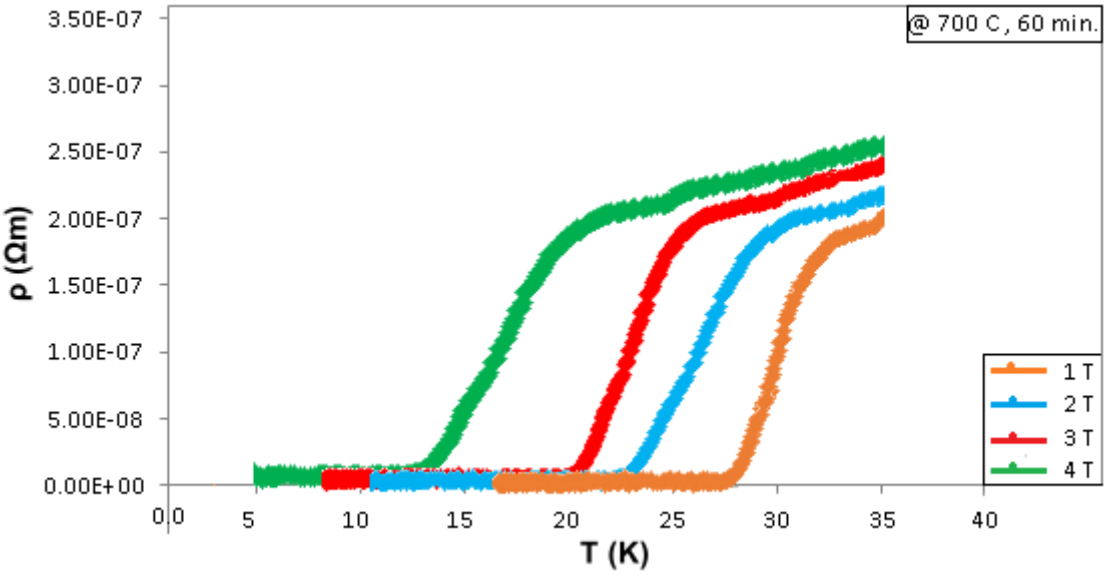

Figure 5.2.3.3: Resistivity vs. Temperature graph under the varied (1 – 4 Tesla) external magnetic field and 700 ^{o}C – 60 min. sintering value of the monocore wire made with commercial MgB_2 powder.

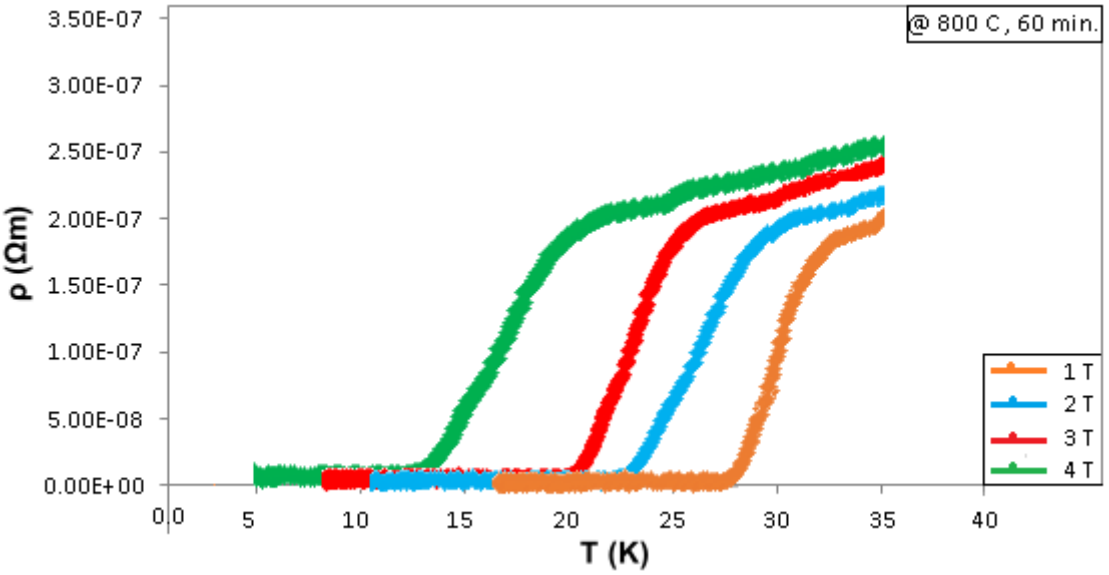

Figure 5.2.3.4: Resistivity vs. Temperature graph under the varied (1 – 4 Tesla) external magnetic field and 800 ^{o}C – 60 min. sintering value of the monocore wire made with commercial MgB_2 powder.

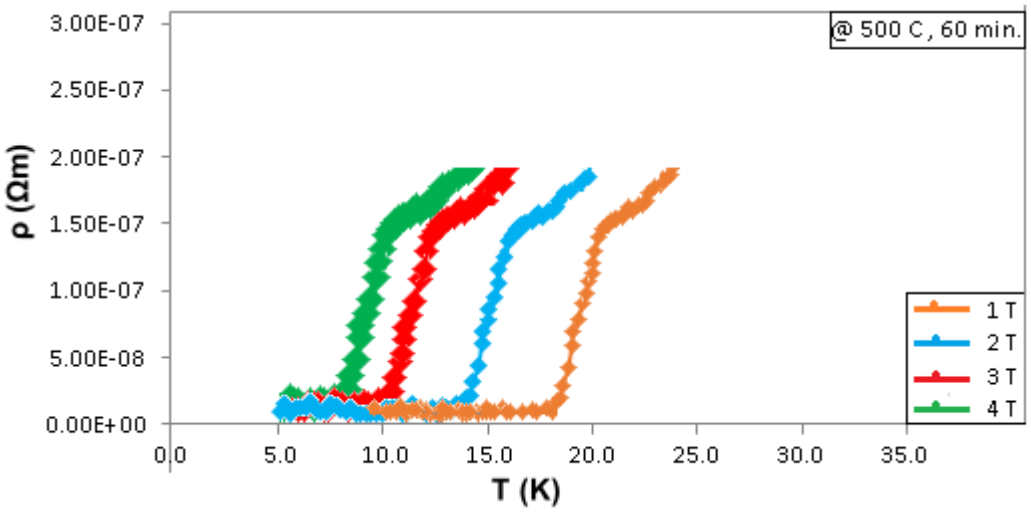

Figure 5.2.3.5: Resistivity vs. Temperature graph under the varied (1 – 4 Tesla) external magnetic field and 500 ^{o}C – 60 min. sintering value of the monocore wire made with mechanical alloyed MgB_2 powder (1st product).

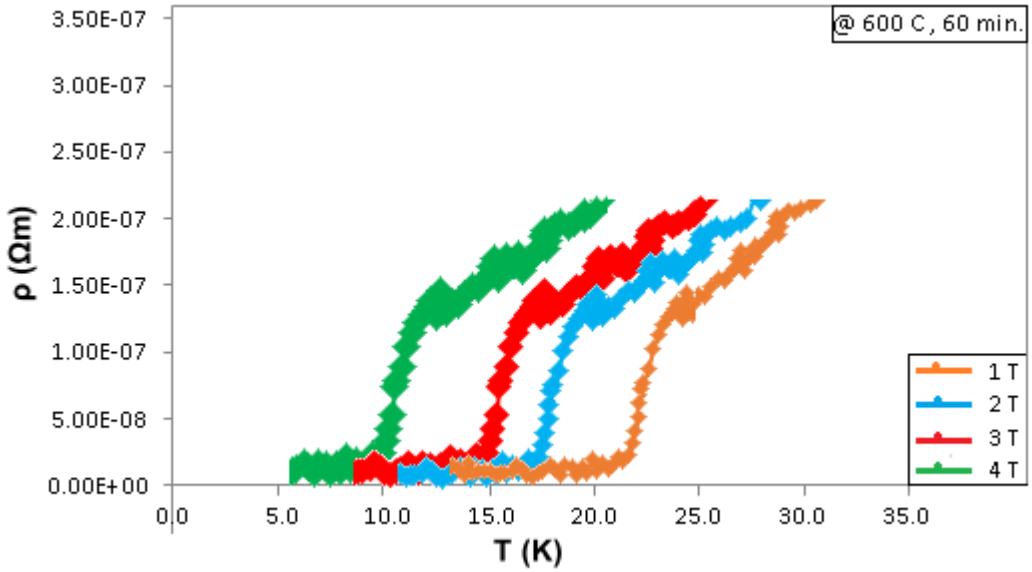

Figure 5.2.3.6: Resistivity vs. Temperature graph under the varied (1 – 4 Tesla) external magnetic field and 600 ^{o}C – 60 min. sintering value of the monocore wire made with mechanical alloyed MgB_2 powder (1st product).

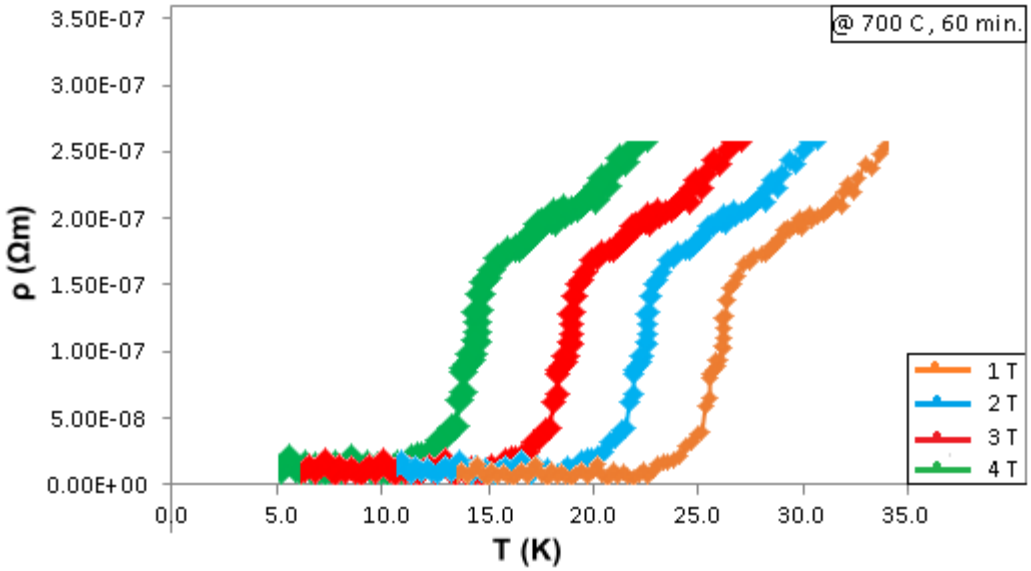

Figure 5.2.3.7: Resistivity vs. Temperature graph under the varied (1 – 4 Tesla) external magnetic field and 700 ^{o}C – 60 min. sintering value of the monocore wire made with mechanical alloyed MgB_2 powder (1st product).

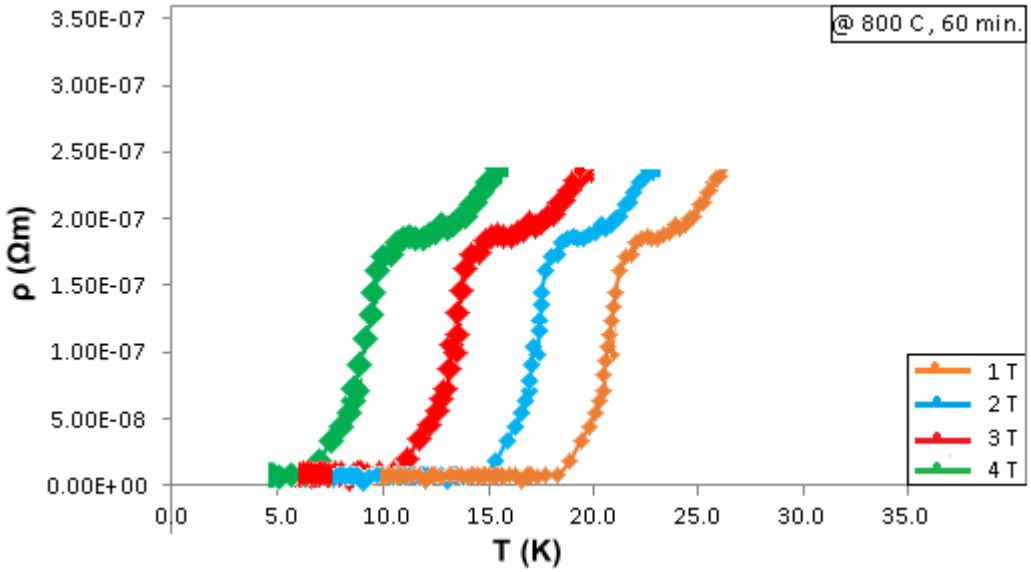

Figure 5.2.3.8: Resistivity vs.Ttemperature graph under the varied (1 – 4 Tesla) external magnetic field and 800 ^{o}C – 60 min. sintering value of the monocore wire made with mechanical alloyed MgB_2 powder (1st product).

Between the the Figure 5.2.3.5 and Figure 5.2.3.11 are shown the upper critical field graphs the MgB_2 wires.

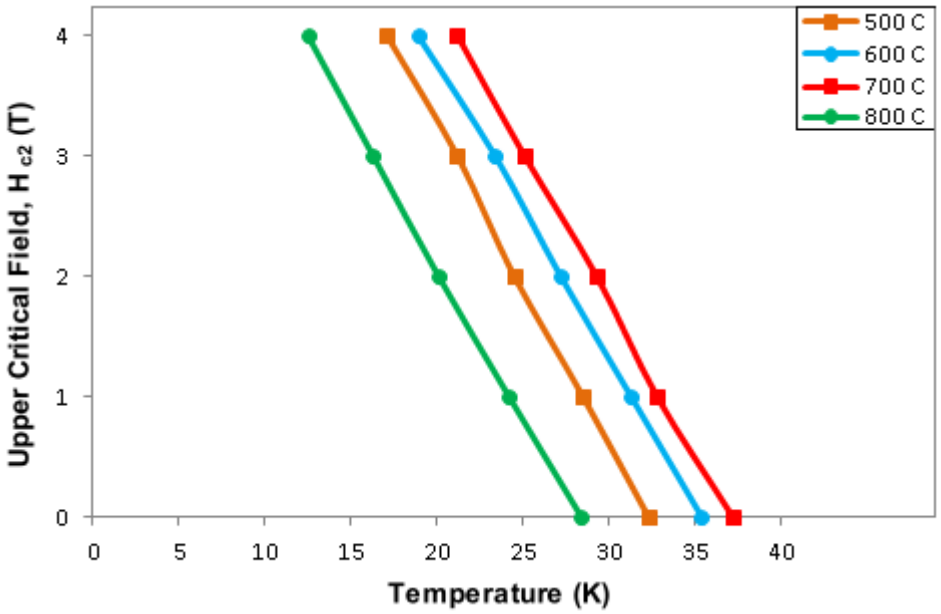

Figure 5.2.3.9: Upper Critical Field vs. Temperature graph for monocore wire made with commercial MgB_2 powder.

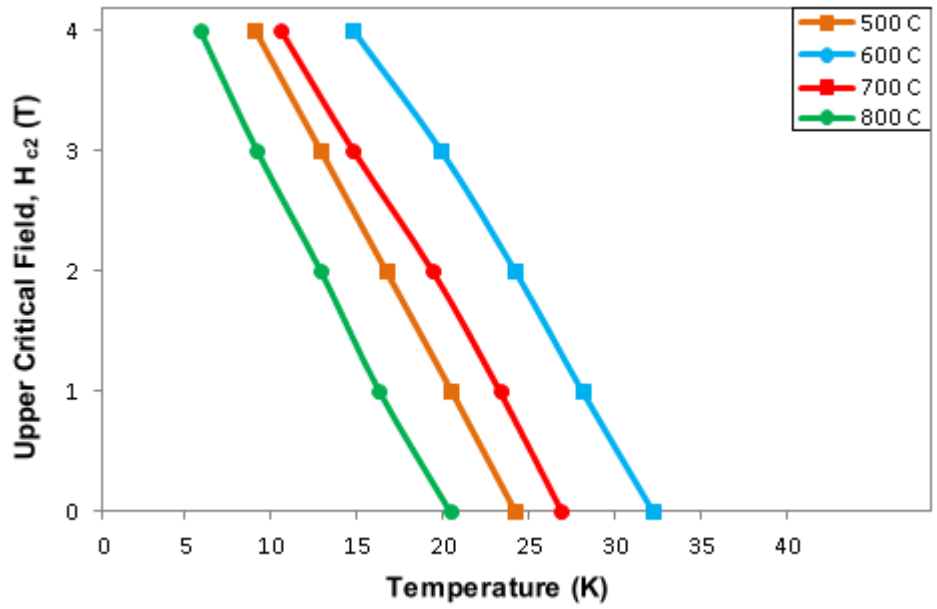

Figure 5.2.3.10: Upper Critical Field vs. Temperature graph for multicore (7 cores) wire made with commercial MgB_2 powder.

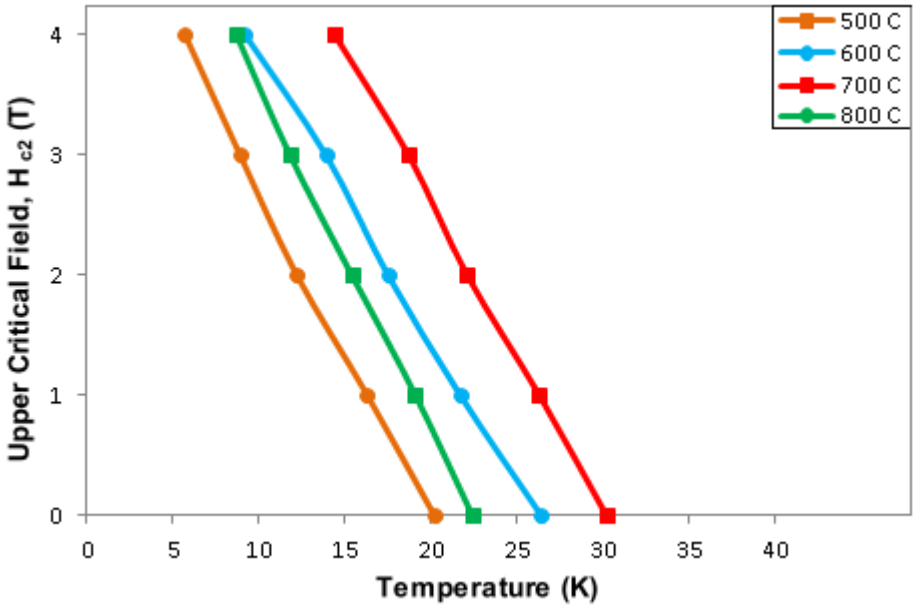

Figure 5.2.3.11: Upper Critical Field vs. Temperature graph for monocore wire made with mechanical alloyed MgB_2 (1^{st} product) powder.

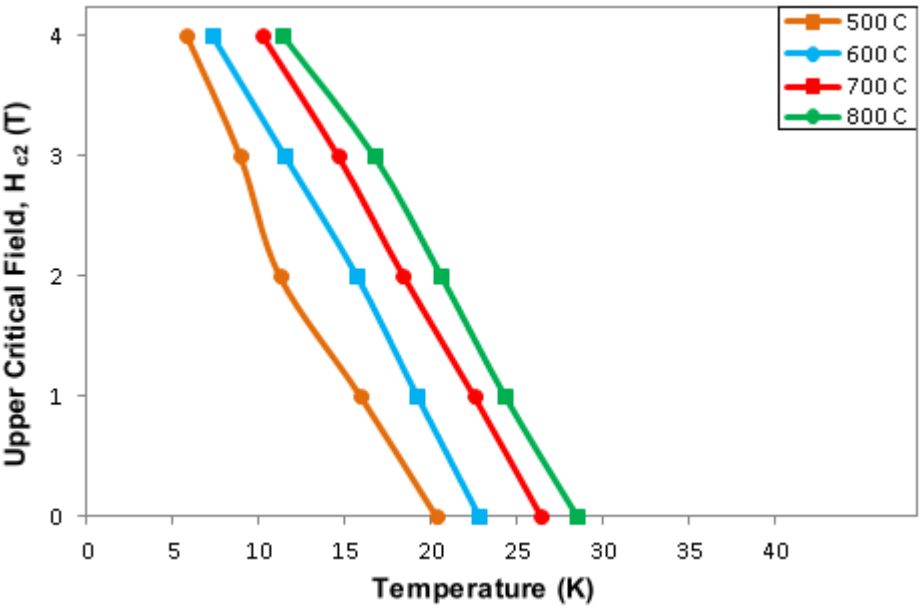

Figure 5.2.3.12: Upper Critical Field vs. Temperature graph for monocore wire made with mechanical alloyed MgB_2 (2^{nd} product) powder.

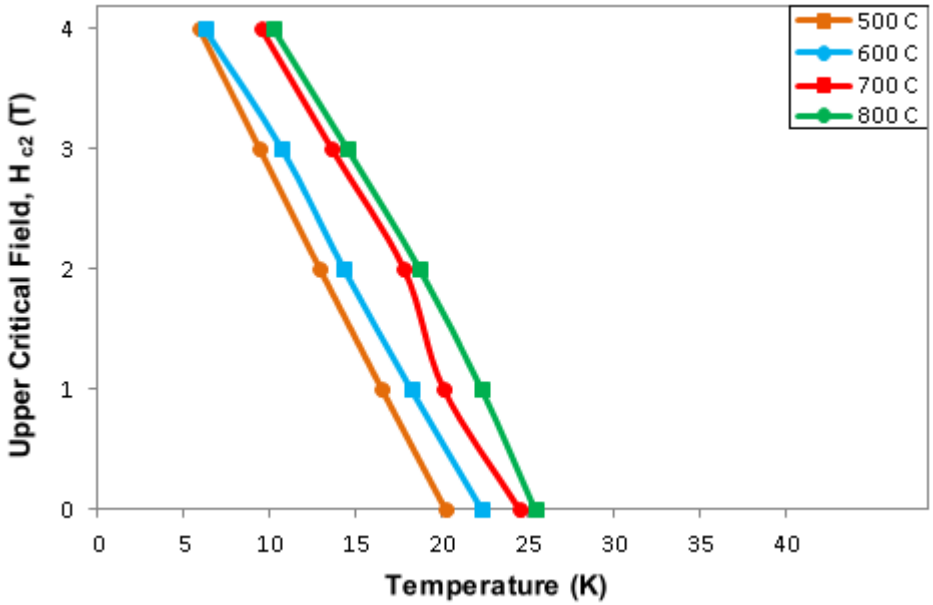

Figure 5.2.3.13: Upper Critical Field vs. Temperature graph for multicore (3 cores) wire made with mechanical alloyed MgB_2 (2^{nd} product) powder.

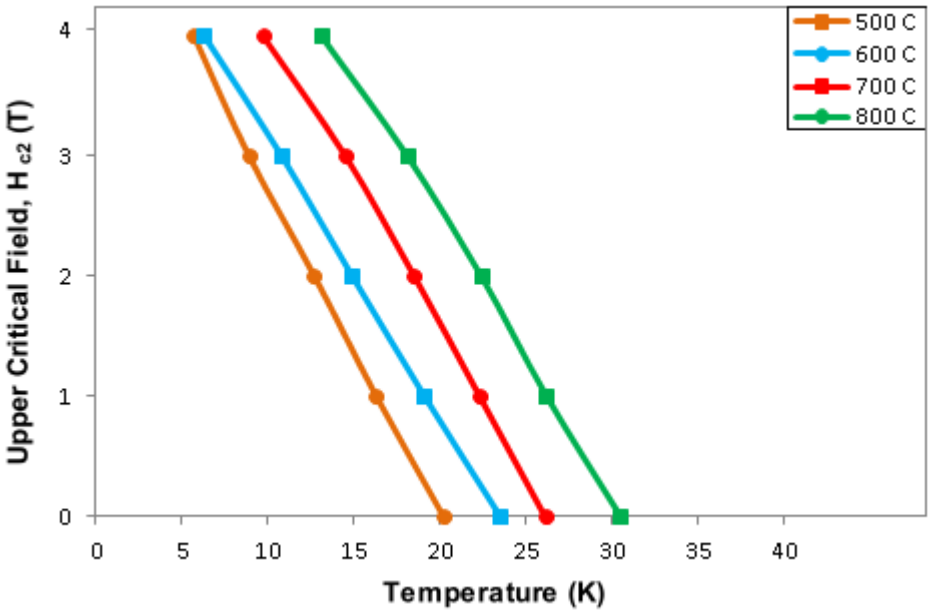

Figure 5.2.3.14: Upper Critical Field vs. Temperature graph for multicore (4 cores) wire made with mechanical alloyed MgB_2 (2^{nd} product) powder.

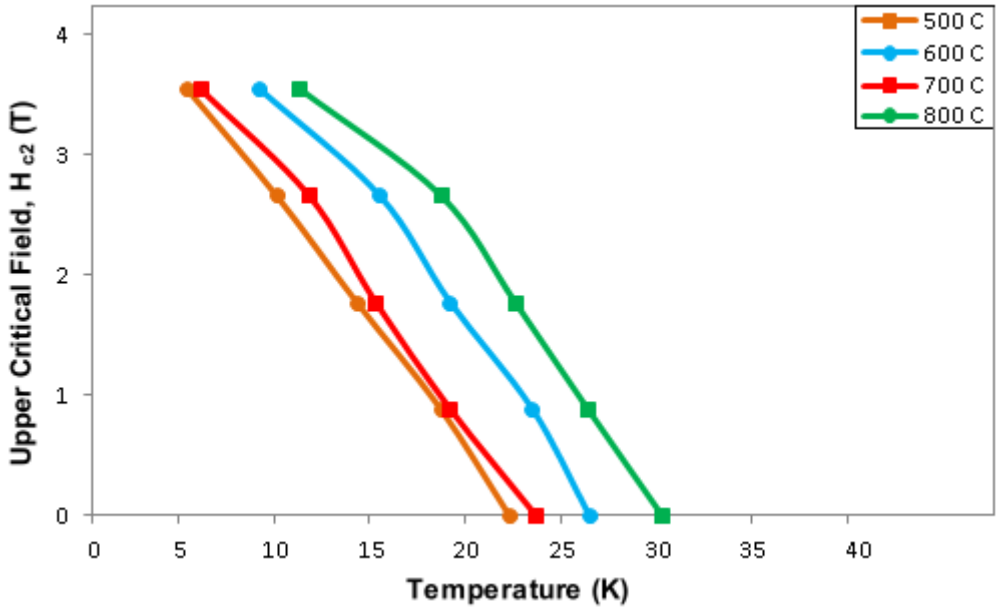

Figure 5.2.3.15: Upper Critical Field vs. Temperature graph for monocore wire made with powder-in-powder method.

5.4 EFFECT OF THE SHEATH MATERIAL

Many different sheath material uses in the superconducting wire fabrication. The most widely known elements : Cu, Ag, Ni, Ta, Fe and Nb can be mentioned. Easy plastic forming can be applied to these metals. The MgB_2 superconductor wires and tapes sheathed by copper demonstrate higher critical current densities than the Fe-sheathed wires if prepared at temperatures below 850 ^{o}C. On the other hand, the superconductor material composition and microstructure is better in the Fe-sheathed wires and tapes under all sintering conditions [104]. Ni, Nb and Ti metals were preferred in many different MgB_2 superconductor fabrication [105-106]. But to say that is not a scientific approach which is the best sheath metal for the construction of a superconducting wire. In some of the studies for the electrical characteristics come to the fore while in some others mechanical properties. Hence the scientists use different sheath materials for superconductor wire fabrication. In this study, copper rods and powders were preferred. Iron alloys were not selected as a sheath material because wire bending was a big issue to make coils.

5.5 SEM IMAGES OF WIRE CROSS-SECTIONAL AREA

After the mechanical and electromagnetic tests, wire samples were mounted in acrylic material by mounting press (in Figure 5.5.1). Then the pressed sample molds were grinded and polished by Metkon grinding device during 30 minutes (in Figure 5.5.2). Final sample product picture is given in Figure 5.5.3.

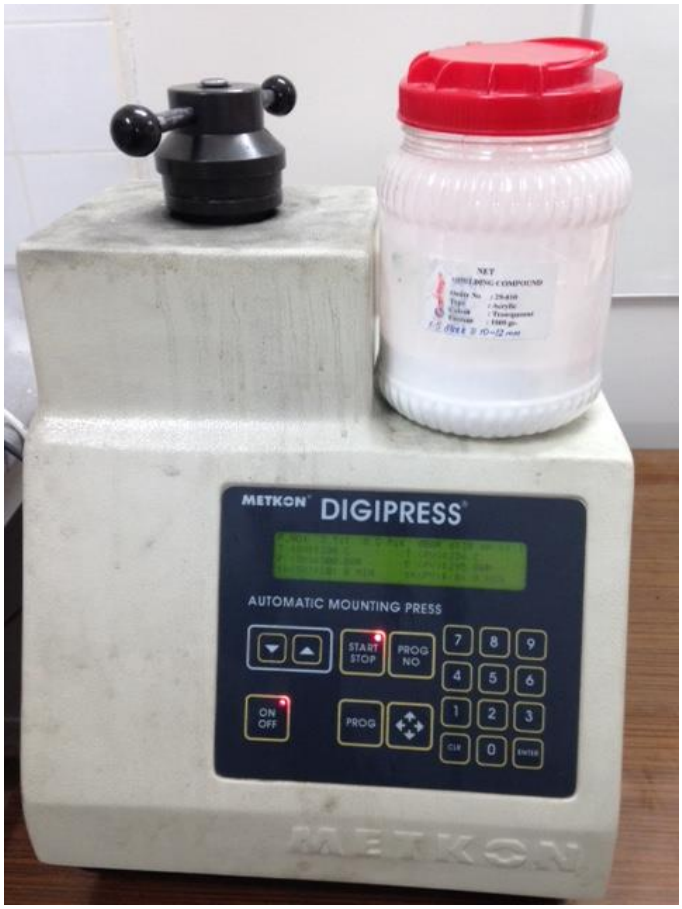

. Figure 5.5.1: Automatic Mounting Press and Acrylic Material.

Figure 5.5.2: Grinding and polishing device.

Figure 5.5.3: Acrylic pressed samples.

SEM images of wire samples were scanned by Zeiss Evo LS10 scanning elctron microscopy device in Erciyes Unv.-Tamu Research Center (in Figure 5.5.4). Cross sectional SEM images were taken at a resolution of 1 micron level in order to understand the grain size, intergranular bondings and the structure of the porosity.

Figure 5.5.4: SEM imaging system in Erciyes Unv. Ernam.

The SEM pictures of MgB_2 superconductor wire cross-sections were given between in Figure 5.5.5 and Figure 5.5.10.

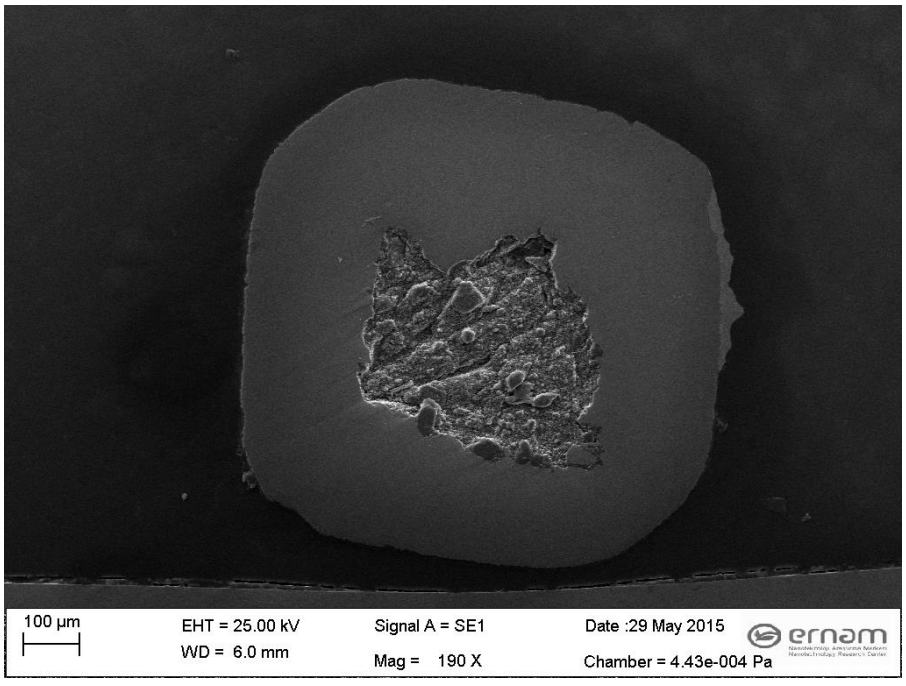

Figure 5.5.5: SEM pictures of MgB_2 superconductor wires by PIP method at 600 ^{o}C for 60 min.

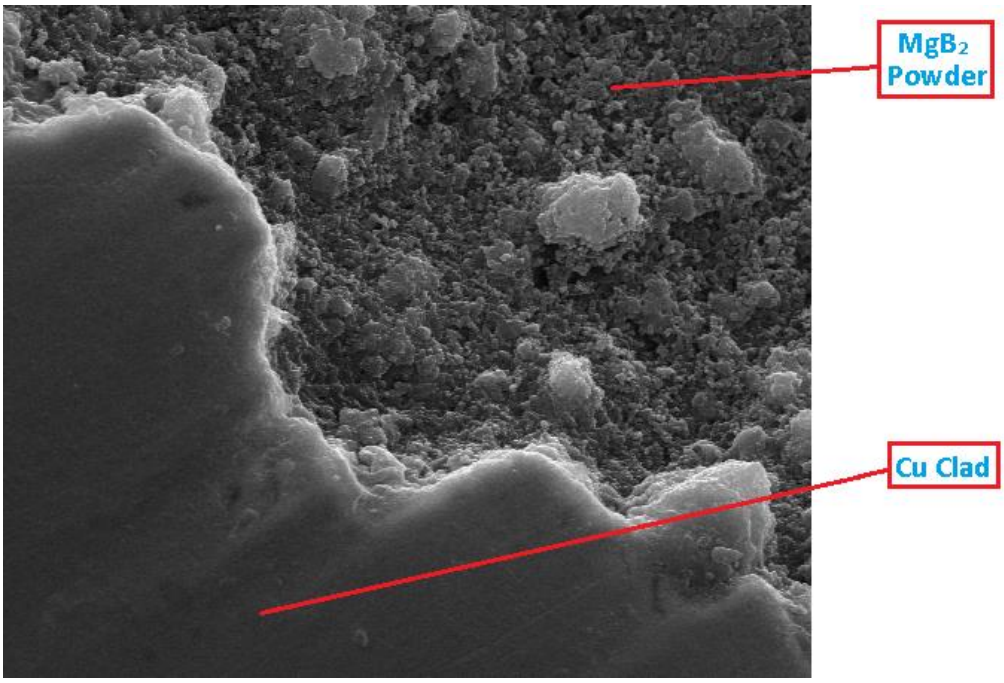

Figure 5.5.6: Cross sectional.SEM pictures of MgB_2 superconductor wires by PIP method

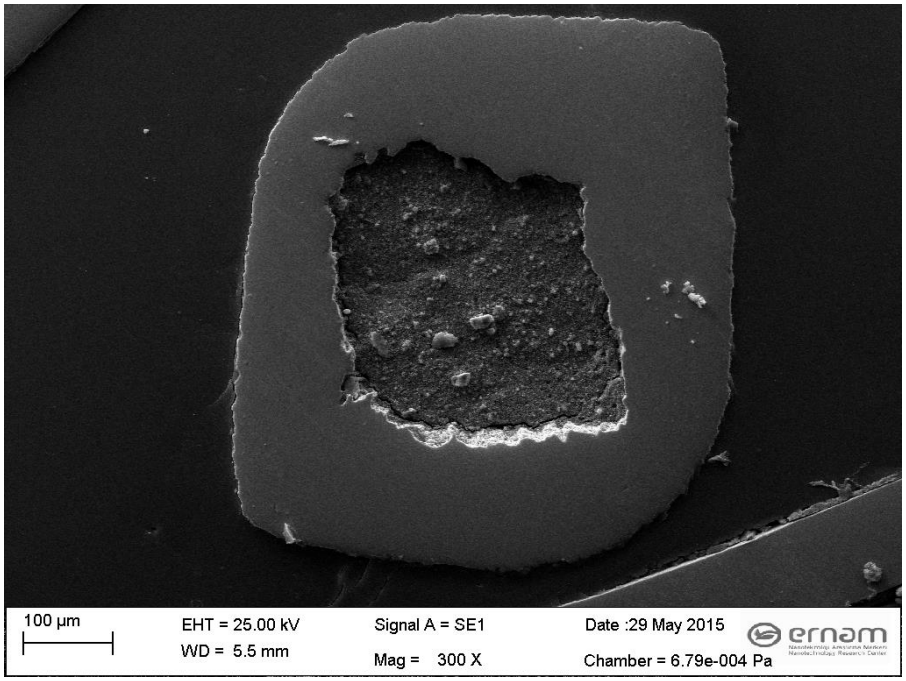

Figure 5.5.7: SEM pictures of MgB_2 superconductor monocore wire made with mechanical alloyed MgB_2 powder.

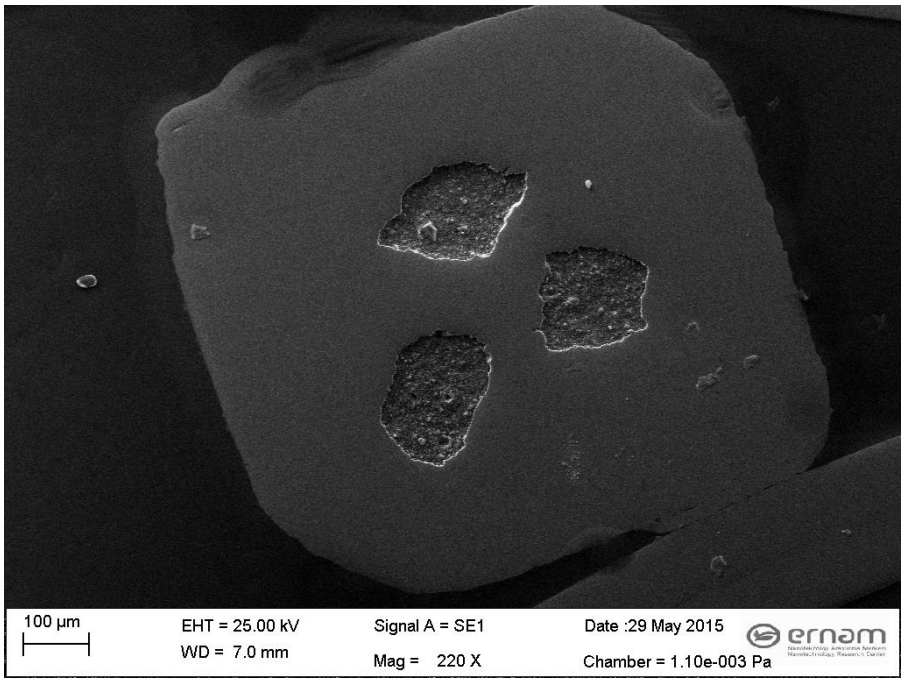

Figure 5.5.8: Cross Sectional SEM pictures of MgB_2 superconductor multicore (3 cores) wire made with mechanical alloyed MgB_2 powder.

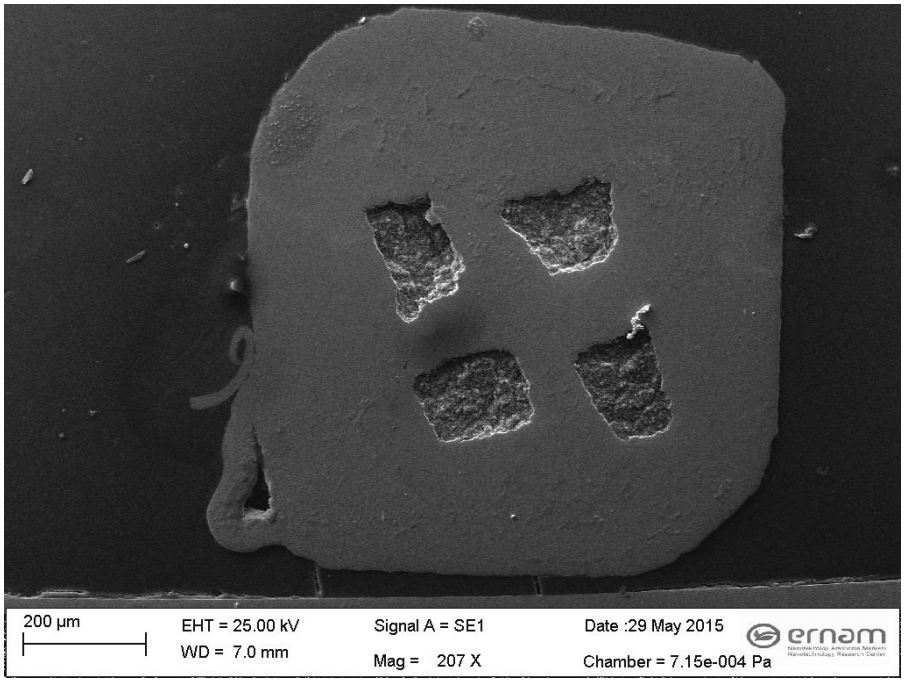

Figure 5.5.9: Cross Sectional SEM pictures of MgB_2 superconductor multicore (4 cores) wires made with mechanical alloyed MgB_2 powder.

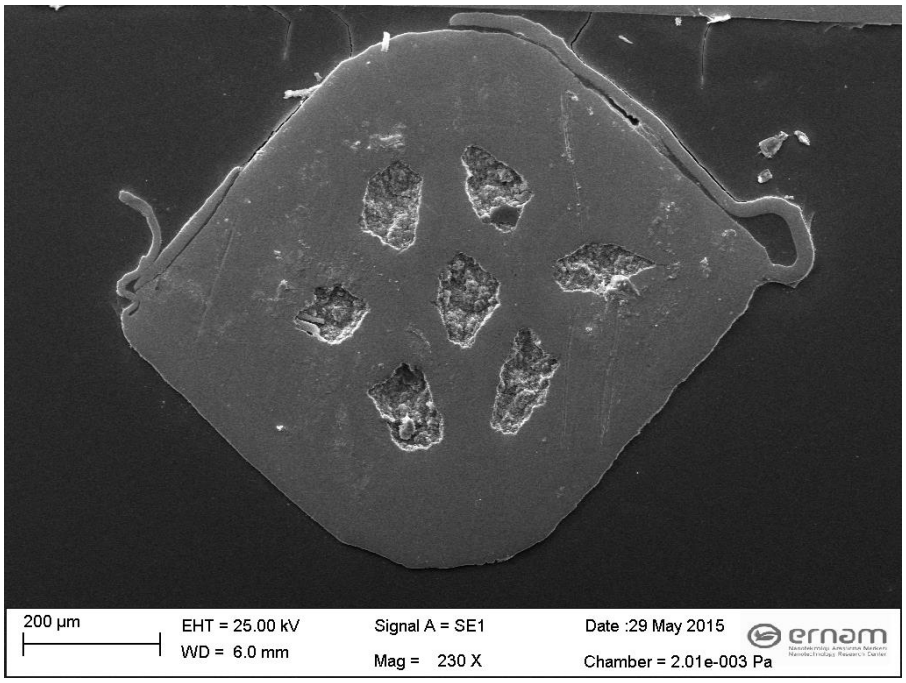

Figure 5.5.10: Cross Sectional SEM pictures of MgB_2 superconductor multicore (7 cores) wires made with mechanical alloyed MgB_2 powder.

The SEM pictures of different MgB_2 powders were given between in Figure 5.5.11 and Figure 5.5.13.

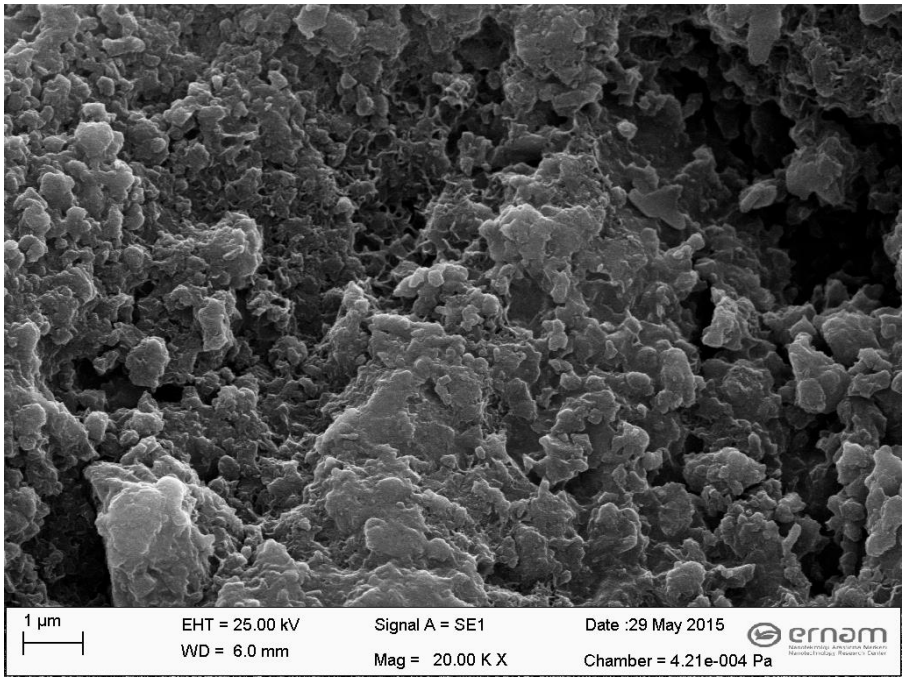

Figure 5.5.11: SEM pictures of MgB_2 superconductor wires (by PIP) cross-section at 600 ^{o}C sintering temperature for 90 min.

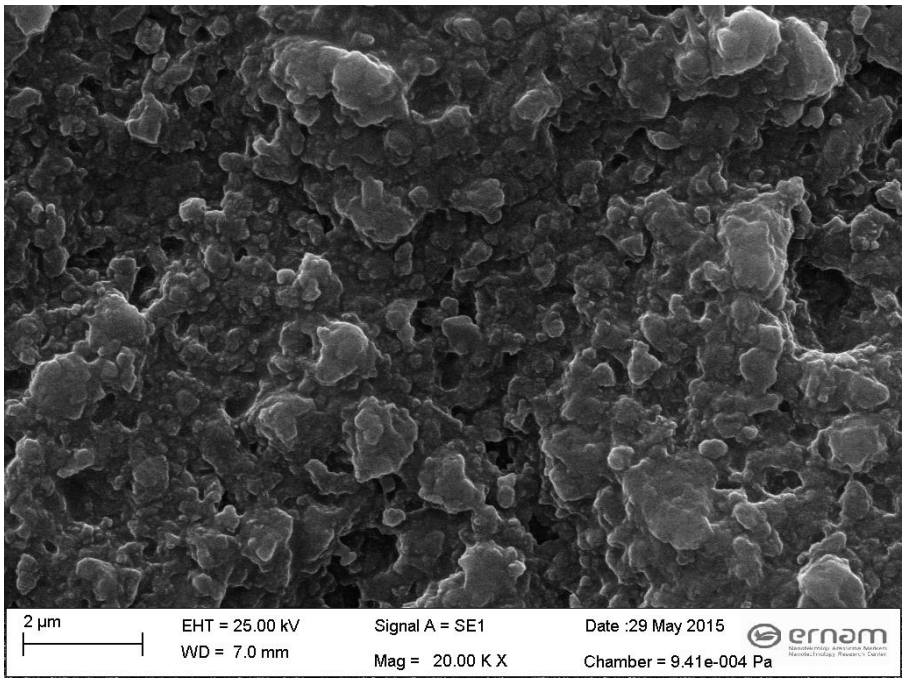

Figure 5.5.12: SEM picture of the (1st product group) mechanical alloyed MgB_2 powder at 600 ^{o}C sintering temperature for 60 min.

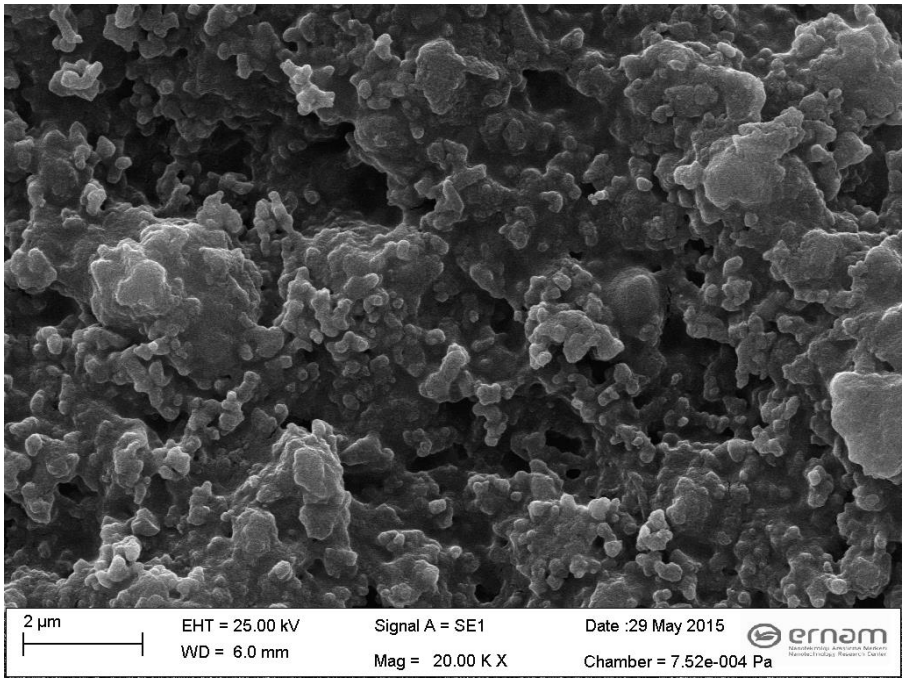

Figure 5.5.13: SEM picture of the (2nd product group) mechanical alloyed MgB_2 powder at 600 ^{o}C sintering temperature for 60 min.

CHAPTER 6

CONCLUSION

In this dissertation**,** have manufactured monocore and multicore superconductor wires in different core numbers (3,4,7 cores). Basic superconductor material was commercial and mechanical alloyed MgB_2. Copper was preferred as a sheath material of wires. Unlike many studies in this regard, after filling the powder, the tubes were not made wires immediately by PIT – PIP tecniques. just before the wire drawing transaction, an extrusion process was applied. Extrusion process provided the better compaction of MgB_2 powder inside the copper billet. Another benefit of extrusion is obtained much more longer copper rods. Eventually, the length of over 40 meters and in a single piece of superconducting wires could be manufactured. Insomuch that can be reach a length of 250 meters when needed.

Although not as much commercially produced MgB_2 powders, as can be seen in the SEM images, it could be reduced to micron level of the the intermetallic MgB_2 powders which is manufactured by mechanical alloying in this study. 1^{st} group product powder compared to 2^{nd} group one, although not emerged an accurate result about grain size, slightly better transition temperature values are obtained from the first group of powder.

Interesting results emerged in the electrical and magneto measurements of superconducting wires. In the heat treatment process, it would be considered very good results in a better granular bonds of powders at high-temperature but was not obtained at all. Even the lower heat treatment temperature results was better than higher in some measurements. Many different reasons are possible for this situation : The formation of the intermediate phase of copper could led to degradation of MgB_2 powder at 800 ^oC and higher temperatures, copper was preferred as a clad material and other metals (Fe, Ni, Nb etc.) were not used. Therefore, the effect of Fe or Nb were not tested as a sheath material.

One of the most important part was the powder-in-powder method of this experimental study. The copper powders used as a sheath material. The powders compacted under high pressure and thanks to this method, very long MgB_2 cored copper rods were obtained. In electrical measurements, the best ΔT_c values were found in samples which are manufactured by powder-in-powder method. Moreover, the 30.2 K transition temperature value was better than most of others. In addition, interesting mechanical tensile test results were obtained also. It is understood in this study results, powder-in-powder method is integrated with hot extrusion method and these two consecutive applicable instantaneously. It can be manufactured a much longer series and more continuity of superconducting wire than powder-in-tube method. Finally it may be preferred as a main method of series manufacturing.

Current carrying capacity is limited amount of our electronic measuring system. The actual value of the critical current density of a superconductor wire has not been fully tested since the 40 mA current was not sufficient for this experiment. but nevertheless were obtained satisfying results about of MgB_2 wire superconductivity in this dissertation study.

It is understood that the resulting of electrical and magnetic findings, it is possible to make a superconductor electromagnet of produced wires. Also a half millimeter diameter of wires to be used for electromagnets, it enables the electromagnet design in many different designs and geometries.

REFERENCES

[1] M. K. Wu, J. R. Ashburn, C. J. Torng, P. H. Hor, R. L. Meng, L. Gao, Z. J. Huang, Y. Q. Wang, and C. W. Chu, "Superconductivity at 93 K in a New Mixed-Phase Y-Ba-Cu-O Compound System at Ambient Pressure", *Physical Review Letters* **58** (9): 908-910, PhRvL,58-908W, 1987.

[2] http://www.crystallography.ru/MA/articles/benjamin-1974.pdf

[3] J. Nagamatsu, N. Nakagawa, T. Muranaka, Y. Zenitani, and J. Akimitsu, "Superconductivity at 39K in MgB_2", *Nature (London)* 410-63, 2001.

[4] M. Eisterer, "Magnetic properties and critical currents of MgB_2", *Superconductor Science and Technology* 20 (12): R47, 2007.

[5] Hossain, M S A et al., "Significant enhancement of H_{c2} and Hirr in MgB_2+$C_4H_6O_5$ bulks at a low sintering temperature of 600 °C", *Superconductor Science and Technology* 20 (8), doi:10.1088/0953-2048/20/8/L03, 2007.

[6] Yamada, H; Uchiyama, N; Matsumoto, A; Kitaguchi, H; Kumakura, H (2007). "The excellent superconducting properties of in situ powder-in-tube processed MgB_2 tapes with both ethyltoluene and SiC powder added".*Superconductor Science and Technology* 20 (6):L30, doi:10.1088/0953-048/20/6/L02, 2007.

[7] Jones, Morton E. and Marsh, Richard E. "The Preparation and Structure of Magnesium Boride, MgB_2".*Journal of the American Chemical Society* 76 (5): 1434.doi:10.1021/ja01634a089, 1954.

[8] Hinks DG, Claus H, Jorgensen JD, "The origin of the anomalous superconducting properties of MgB_2", *Nature* 411, 2001.

[9] D. C. Larbalestier et all, "Strongly linked current flow in polycrystalline forms of the new superconductor MgB2", *Nature (London)* 410, 186, 2001.

[10] P. C. Canfield, D. K. Finnemore, S. L. Bud'ko, J. E. Ostenson, G. Lapertot, C. E. Cunningham, and C. Petrovic, "Superconductivity in dense MgB_2 Wire", *Phys. Rev. Lett*. 86, 2423, 2001.

[11] D. K. Finnemore, J. E. Ostenson, S. L. Bud'ko, G. Lapertot, and P. C. Canfield, "Thermodynamic and Transport Properties of Superconducting MgB_2", *Phys. Rev. Lett*. 86, 2420, 2001.

[12] Y. Bugoslavsky, G. K. Perkins, X. Qi, L. F. Cohen, and A. D. Caplin, Vortex dynamics in superconducting MgB2 and prospects for applications", *Nature (London)* 410, 563, 2001.

[13] A.Gurevich, "Enhancement of the upper critical field by nonmagnetic impurities in dirty two-gap superconductors", *Phys. Rev. B*, 67 184515, 2003.

[14] R.M. Scanlan, A.P Malozemoff and D.C. Larbalestier, "Superconducting materials for large scale applications.", *Proc. IEEE*, 92-1639, 2004.

[15] M. D. Sumption, M. Bhatia, F. Buta, S. Bohnenstiehl, M. Tomsic, M. Rindfleisch, J. Yue, J. Phillips, S. Kawabata, and E. W. Collings, "Solenoidal coils made from monofilamentary and multifilamentary MgB strands", *Supercond. Sci. Technol*., vol. 18, no. 7, pp. 961–965, 2005.

[16] K. Tanaka, H. Kitaguchi, H. Kumakura, H. Yamada, M. Hirakawa, and M. Okada, "Fabrication and transport properties of an MgB solenoid coil", *Supercond. Sci. Technology*, vol. 18, no. 5, pp. 678–681, 2005.

[17] M. Modica, S. Angius, L. Bertora, D. Damiani, R. Marabotto, D. Nardelli, M. Perrella, M. Razeti, and M. Tassisto, "Construction and installation of cryogen free MgB2 magnets for open MRI systems," *IEEE Trans. Appl. Supercond.*, vol. 18, no. 2, pp. 882–886, 2008.

[18] http://www.docstoc.com/docs/28314809/ASG-Superconductors-Paramed-Medical-Systems-and-Columbus

[19] M. Suenaga and A.F. Clark , Filamentary A15 Superconductors, *Plenum Press*, New York, 1980.

[20] I. Hušek, P. Kováč and W. Pachla, "Microhardness profiles in BSCCO/Ag composites made by various technological steps", *Sup. Sci. and Technology 8*, 617, 1995.

[21] I. Hušek, P. Kováč, C.R.M. Grovenor and L. Goodrich, "Microhardness as a tool for the filament density and metal sheath analysis in MgB2/Fe/(Cu) wires", *Sup. Sci. and Technology 17*, 971, 2004.

[22] Malagoli A, Grasso G, Vignolo M, Tumino A, Braccini V, Bernini C, Tropeano M, Siri A S, Nardelli D and Modica M M, "Long Length MgB2 Conductors for Industrial Applications", *Adv. Sci. Technol*. 47 238–4, 2006.

[23] Tomsic M, Rindfleisch M, Yue J, McFadden K, Doll D, Phillips J, Sumption M D, Bhatia M, Bohnenstiehl S and E W Collings, "Development of magnesium diboride (MgB2) wires and magnets using in situ strand fabrication method", *Physica C*, 456 203-208, 2007.

[24] I.I. Akimov et al., "Multifilamentary composite MgB2 wires: preparation and testing", *IEEE Trans Appl. Supercond.*, vol. 14, no. 2, pp.1035–1038, 2004.

[25] P. C. Canfield, D. K. Finnemore, S. L. Bud'ko, J. E. Ostenson, G. Lapertot, C. E. Cunningham, and C. Petrovic, "Superconductivity in dense MgB_2 Wire.", *Phys. Rev. Lett.* 86, 2423, 2001.

[26] G. Giunchi et al., "High performance new MgB_2 superconducting hollow wires", *Supercond. Sci. Technol.*, vol. 16, no. 2, pp. 285–291, 2003.

[27] R. Musenich, P. Fabbricatore, S. Farinon, C. Ferdeghini, G. Grasso, M. Greco, A. Malagoli, R. Marabotto, M. Modica, D. Nardelli, A. S. Siri, M. Tassisto, and A. Tumino, "Behavior of MgB_2 react and wind coils above 10 K", *IEEE Transactions on Applied Superconductivity*, 15, 2, 2005.

[28] RMusenich, M Greco, M Razetiand G Tavilla, "Electrical characterization of a multi-strand MgB2 cable", *Supercond. Sci. Technology*. 20 235–238, 2007.

[29] P Kov´aˇc, I Huˇsek and T Meliˇsek, "MgB_2 cable made from two-axially rolled wires", *Supercond. Sci. Technology*, 21 125003 (4pp), 2008.

[30] V. Selvamanickam, Y. Chen, X. Xiong, Y. Xie, X. Zhang, A. Rar, M. Martchevskii, R. Schmidt, K. Lenseth, J. Herrin, "Progress in second-generation HTS wire development and manufacturing", *Physica C 468*, 1504-1509, 2008.

[31] T. Masuda et. al., "Verification tests of 100m HTS cable system for practical use", *IEEE Electric Power and Energy Convention*, 2002.

[32] P.J. Ford, " The Rise of the Superconductors", *CRC Press*, 2005.

[33] A. Schilling et al. "Superconductivity above 130 K in the Hg–Ba–Ca–Cu–O system", *Nature 363* (6424): 56, 1993.

[34] C. W. Chu et al. "Superconductivity above 150 K in HgBa2Ca2Cu3O8+δ at high pressures", *Nature 365* (6444): 323, 1993.

[35] D. Shi et al. "Origin of enhanced growth of the 110 K superconducting phase by Pb doping in the Bi-Sr-Ca-Cu-O system", *Applied Physics Letters* 55 (7): 699, 1989.

[36] A. Mann, "High-temperature superconductivity at 25: Still in suspense", *Nature 475*: 280–282, 2011.

[37] J. Zaanen, "A modern, but way too short history of the theory of superconductivity at a high temperature", ArXiv. [arXiv:1012.5461v2], 2010.

[38] Baskaran, Ganapathy "Five-fold way to new high Tc superconductors", *Pramana 73* (1): 61–112, 2009.

[39] T. Dombre, G. Kotliar, "Instability of the long-range resonating valence bond state in the mean-field approach", *Physical Review B* 39 (1): 855–857, 1989.

[40] H. Maeda, Y. Tanaka, M. Fukutumi, and T. Asano, "A New High-Tc Oxide Superconductor without a Rare Earth Element", *Jpn. J. Appl. Phys.* 27 (2): L209–L210, 1988.

[41] R. Hazen et al. "Superconductivity in the high-Tc Bi-Ca-Sr-Cu-O system: Phase identification", *Physical Review Letters* 60 (12): 1174, 1988.

[42] J. Tenbrink, M. Wilhelm", K. Heine, and H. Krauth, "Development of Technical Gigh-T_c Superconductor, Wires and Tapes", *Applied Superconductivity, IEEE Transactions* on (Volume:3 , Issue:1), 1051-8223 : 1123 – 1126, 1993.

[43] F. Sumiyoshi, R. Kinoshita and Y. Miyazono, "Proposal of new type Ag-BSCCO tapes and wires with low losses", *Applied Superconductivity, IEEE Transactions on Applied Superconductivity*, Vol.9 , No.2, ISBN.1051-8223, pp.2549 – 2552, 1999.

[44] D. Turrioni, E. Barzi, M. J. Lamm, R. Yamada, A. V. Zlobin, A. Kikuchi, "Study of HTS Wires at High Magnetic Fields", *IEEE Transactions on Applied Superconductivity*, Vol.19, No.3, 1051-8223, pp.3057-3060, 2009.

[45] Y.V. Cherpak, V.A. Komashko, S.A. Pozigun, A.V. Semenov, C.G. Tretiatchenko, E.A. Pashitskii, and V.M. Pan , "Critical Current Density of HTS Single Crystal YBCO Thin Films in Applied dc Field", *IEEE Transactions on Applied Superconductivity*, Vol.15, No.2, 2005.

[46] Y.Y. Xie, M. Marchevsky, X. Zhang, K. Lenseth, Y. Chen, X. Xiong, Y. Qiao, A. Rar, B. Gogia, R. Schmidt, A. Knoll, V. Selvamanickam, G. G. Pethuraja, and P. Dutta, "Second-generation HTS Conductor Design and Engineering for Electrical Power Applications" , *IEEE Transactions on Applied Superconductivity*, Vol.19, No.3, 2009.

[47] E. Oberg, F.D. Jones, L.H. Holbrook, H. Ryffel, "Machinery's Handbook", (26th ed.), *Industrial Press*, New York, ISBN.0-8311-2635-3, 2000.

[48] Liu, Y.B., Kwok, J.K.M., Lim, S.C., Lu, L. and Lai, M.A., "Fabrication of Al-4.5Cu/15SiCp composites: I. Processing using mechanical alloying", *Journal of Materials Processing Technology*, 37: 441-451, 1993.

[49] Lu, L., Kwok, J.K.M., Lai, M.O., Liu, Y.B. and Lim, S.C., "Fabrication of Al-4.5Cu/15SiC composite: II. Effects of the processing parameters on fracture properties", *Journal of Materials Processing Technology*, 37: 453-462, 1993.

[50] T. S. Chou and H. K. D. H. Bhadeshia, "Crystallographic texture in mechanically alloyed oxide dispersion-strengthened MA956 and MA957 steels", *Metallurgical Transactions A*, Vol.24, No.4, pp.773-779, 1993.

[51] J. S. Benjamin: *Met. Trans.*, Vol. l, pp. 2943-51, 1970.

[52] J.S. Benjamin, "*Dispersion-strengthened electrical heating alloys by powder metallurgy"*, US Patent #US3 660 049, 1972.

[53] J.S. Benjamin and P.S. Gilman, *Metals Handbook*, 9th Edition, Materials Park OH, ASM International, 1983.

[54] J.S. Benjamin, *New Materials by Mechanical Alloying Techniques*, DGM Confer., Calw-Hirsau (FRG), Ed. E. Arzt and L. Schultz, Informationsgesellschaft Publishing, 1988.

[55] C.Suryanarayana, E.Ivanov, V.V.Boldyrev, "The science and technology of mechanical alloying", *Material Science and Engineering A*, Vol.304-306, pp.151-158, 2001.

[56] G.E.Dieter, *Mechanical Metallurgy*, McGraw-Hill, London, 1988.

[57] L.Edwards, M.J.Endean, *Manufacturing with Materials*, Heinemann, 1990

[58] J.O.Willis, "Superconducting Transmission Cables", *IEEE Power Engineering Review*, vol.20, iss.8, pp.10-14, 2000.

[59] http://www.amsc.com/documents/hts-cable-systems-for-ac-networks/

[60] Snitchler, G. ; American Supercond., Devens, MA, USA ; Gamble, B. ; King, C. "10 MW Class Superconductor Wind Turbine Generators", *Applied Superconductivity, IEEE Transactions* on Volume:21, Iss: 3, Page(s): 1089 – 1092, ISSN : 1051-8223.

[61] P. N. Barnesa, Michael D. Sumptionb, Gregory L. Rhoadsa,"Review of high power density superconducting generators: Present state and prospects for incorporating YBCO windings**",** *Cryogenics* **,** Volume 45, Issues 10–11, October–November 2005, Pages 670–686.

[62] http://www.amsc.com/

[63] http://www.iec.ch/whitepaper/

[64] A. Badel, "Superconducting Magnetic Energy Storage Haute Temp´erature Critique comme Source Impulsionnelle", Thesis, Institut National Polytechnique de Grenoble - INPG, French, 2010.

[65] Z. Melhem, J. Brown, R. Wotherspoon, R. Viznichenko, J. Burgoyne, K. Lonergan, A. Twin, D. Warren, "Development of New High Field Superconducting Magnets for Research Applications", Oxford Instruments.

[66] M.A. Aksan, A. Guldeste, Y. Balcı, M.E. Yakıncı, "Degradation of superconducting properties in MgB_2 by Cu addition". *Solid State Communications* , 137:320–325, 2006.

[67] J.C. Hung, Chinghua Hung, "The design and development of a hydrostatic extrusion apparatus", Journal of Materials Processing Tech., 104.226-235, 2000.

[68] K. Osakada, P.B. Mellor, "Fundamentals of Hydrostatic Extrusion", *Springer*, 978-94-010-8696-7, pp 7-20, 1985.

[69] J. Beddoes and M.J. Bibbly, "Principles of metal manufacturing process", *Arnold*, 0-470-35241-8, 1999.

[70] S.S. Kalsi, "Applications of High Temperature Superconductors to Electric Power Equipment", *Wiley-IEEE Press*, 2011.

[71] P.J. Ford and G.A. Saunders, "The Rise of the Superconductors", *CRC Press*, 2004.

[72] K.H. Benneman and J. B. Ketterson, "History of Superconductivity: Conventional, High-Transition Temperature and Novel Superconductors", *Springer*, Volume:1, 978-3-540-73252-5, 2008.

[73] A.A. Abrikosov, "On the magnetic properties of superconductors of the second group", *Journal of Exptl. Theoret. Phys*., 32, U.S.S.R., 1957.

[74] J.G. Bednorz and K.A. Müller, "Possible highT_c superconductivity in the Ba−La−Cu−O system", *Zeitschrift für Physik B Condensed Matter*, Volume 64, Issue 2, pp 189-193, 1986.

[75] C. Zhou, "Intra Wire Resistance and Strain affecting the Transport Properties of Nb3Sn Strands in Cable-In-Conduit Conductors", *PhD thesis, University of Twente,* The Netherlands, ISBN: 978-90-365-3760-5, 2014.

[76] http://www.physics.usyd.edu.au/~khachan

[77] https://www.repository.cam.ac.uk/bitstream/handle/1810/34597

[78] M. Tomsic et all, "Development of magnesium diboride (MgB 2) wires and magnets using in situ strand fabrication method", *Physica C*, 456-203–208, 2007.

[79] T. Sheahen, "Introduction to High-Temperature Superconductivity", ISBN: 0-306-44793-2, NewYork, USA, 1994.

[80] http://www.nexans.com/

[81] http://www.eurekamagazine.co.uk/design-engineering-features/technology/super-

conducting-material-set-to-improve-performance-of-electric-motors/47910/,
J.Cunningham Published: February 2013.

[82] T. Masuda et all, "High-temperature Superconducting Cable Technology and Development Trends", SEI Technical Review, Number:59, 2005.

[83] S. Mukoyama et all, "Development of YBCO High-Tc Superconducting Power Cables", Furukawa Review, No. 35, 2009.

[84] Ken-ichi-Sato, "Present Status and Future Perspective of HTS", SEI Technical Review, Number:66, 2008.

[85] http://energy.gov/eere/office-energy-efficiency-renewable-energy.

[86] H. Kuhn, A. Lawley, "Powder Metallurg: The Techniques and Analyses", Academic Press, Inc., ISBN: 0-12-428450-7, 1978.

[87] V. Marinov, "Manufacturing Processes for Metal Products", *Kendall Hunt Publishing Comp*., 2008.

[88] M. Hill, "Effect of Change of Scale on Sintering Phenomena", *J. Applied Phys*., 21-301, 1950.

[89] F. Thümmler, W. Thomma, "Sintering Process", Vol.12, Iss.1, pp.69-108, 1967.

[90] A.S. Argon, "Strengthening Mechanisms in Crystal Plasticity", *Oxford Unv. Press*, New York, 2008.

[91] http://www.ams02.org/what-is-ams/tecnology/magnet/scmagnet/

[92] M.P. Groover, " Fundamentals of Modern Manufacturing Materials, Process and Systems", *Prentice Hall Int. Inc*., 1996.

[93] F.P. Leander, W.G. West, "*Fundamentals of Powder Metallurgy*", New Jersey, 2002.

[94] R.M. German, "Powder Matallurgy Science", *MPIF-Priceton*, New Jersey, 1984.

[95] http://nptel.ac.in/courses/112107144/

[96] http://www.htstriax.com/cabledesign.html.

[97] T. Nakane, K. Takahashi, H. Kitaguchi and H. Kumkura, "Fabrication of Cu-sheathed MgB_2 wire with high J c –B performance using a mixture of in situ and ex situ PIT techniques", *Physica C*, 469,1531-1535, 2009.

[98] M. Tomsic et all, "Overrview of MgB_2 Superconductor Applications", *Int. Journ. Appl. Ceramic. Tech*., 4(3), 250-259, 2007.

[99] S.I. Schlachter, W. Goldacker, "MgB_2 and BSCCO", *HTS Fusion Conductor Workshop*, Karlsruhe- Germ., 2011.

[100] G. Alecu, A. Cosac, S. Zamfir, "Superconductivity in MgB_2", *NIRD in Electrical Eng. Series*, INCDIE ICPE-CA, Unv. Of Craiova, Romania, 2006.

[101] J.M. Hur et all, "Fabrication of high performance MgB 2 wires by an internal Mg diffusion process", *Superconductor Science and Tech*., Vol.21, Num.3, 2008.

[102] M.Putti, R. Vaglio and J.M. Rowell, "Radiation effects on MgB_2: a review and a comparison with A15 superconductors", *Superconductor Science and Tech*., Vol.21, Num.4, 2008.

[103] E. Ciminli, "A Study for Manufacturability of Cu / MgB_2 Superconducting Wires by Powder-in-Powder Method", *Master Thesis*, Erciyes Unv., 2015.

[104] S. Zhou, A. Pan, M. Ionecu, H. Liu and S. Dou, "Influence of Ag, Cu and Fe sheaths on MgB_2 superconducting tapes", *Superconductor Science and Tech*., 15, 236-240, 2002.

[105] P Kováč, I Hušek, L Kopera, T Melišek, A Rosová and E Dobročka, "Properties of in situ made MgB2 in Nb or Ti sheath", *Superconductor Science and Tech*., 26-025007, 2012.

[106] P Kováč1, I Hušek, T Melišek, M Kulich and V Štrbík ,"MgB2 composite wires with Fe, Nb and Ta sheaths", *Superconductor Science and Tech*., 19-600, 2006.

[107] D. Sutanto and K.W.E. Cheng, "Superconducting Magnetic Energy Storage Systems for Power System Applications", *Proceedings of 2009 IEEE Int. Conf. on App.Superconductivity and Electromagnetic Devices*, Chengdu, China, Sep.25-27, 2009.

[108] E. Yucel, C. Terzioglu, A. Varilci, I. Belenli, "Fabrication and magnetoresistivity of ex-situ processed MgB_2/Fe monofilament tapes without any intermediate annealing", *Journal of Materials Science: Materials in Electronics*, Volume 22, Issue 8, pp 1143-1153, 2011.

[109] J.S. Colton, *Manufacturing Processes and Engineering*, Lec.Notes, Georgia Ins. of Tech., 2009.